Technische Universität München

Lehrstuhl für Biophysikalische Chemie

Fast Conformational Dynamics in Folded Peptides and Proteins Measured by Triplet-Triplet Energy Transfer

Sabine Neumaier

Vollständiger Abdruck der von der Fakultät für Chemie der Technischen Universität München zur Erlangung des akademischen Grades eines

Doktors der Naturwissenschaften

genehmigten Dissertation.

Vorsitzende:	Univ.-Prof. Dr. Sevil Weinkauf
Prüfer der Dissertation:	1. Univ.-Prof. Dr. Thomas Kiefhaber
	2. Univ.-Prof. Dr. Michael Groll
	3. Univ.-Prof. Dr. Wolfgang Zinth (Ludwig-Maximilians-Universität München)

Die Dissertation wurde am 07.11.2013 bei der Technischen Universität München eingereicht und durch die Fakultät für Chemie am 04.12.2013 angenommen.

Contents

1 Introduction

1.1 Protein Folding

Proteins are one of the major components in living cells and are involved in all processes within the cell and in multicellular organisms. They fulfill functions in catalysis, transcription and translation as well as in transport, signal transduction and structural stability. In the cell proteins are synthesized at the ribosome by translation and can be post-translationally modified. They consist of a linear sequence of 21 proteinogenic α-L-amino acids that are linked by peptide bonds. All amino acids have the same composition of the backbone but distinct side chains with different properties and reactivities. The sequence of amino acids determines the three-dimensional structure of the protein in solution[1]. The spontaneous process in which a linear poly-amino acid chain finds its structure is referred to as protein folding.

1.1.1 The unfolded and the native state

A polypeptide chain can only adopt certain angles within the backbone (Fig. 1.1 A). In the Ramachandran plot the axes represent the two dihedral angles Φ and Ψ of the protein backbone[2,3] (Fig. 1.1 B). Secondary structures are defined by the dihedral backbone angles Φ between C-N-C_α-C, and Ψ between N-C_α-C-N (Fig. 1.1 A). In this two-dimensional plot only a broad β-region and the α-regions are sterically allowed. In these regions no atomic clashes appear between neighboring residues. Recent work extents the requirements for allowed regions in the Ramachandran plot by taking into account that all backbone polar groups should form hydrogen bonds either intramolecularly or with the solvent[4].

The unfolded state (U) is generally defined as a unstructured random coil[6,7]. U is flexible and has no direct structural correlation to distant parts of the polypeptide chain. The restrictions in the conformational space that are shown in the Ramachandran plot reduce the conformational entropy in U. Usually the unfolded state is ex-

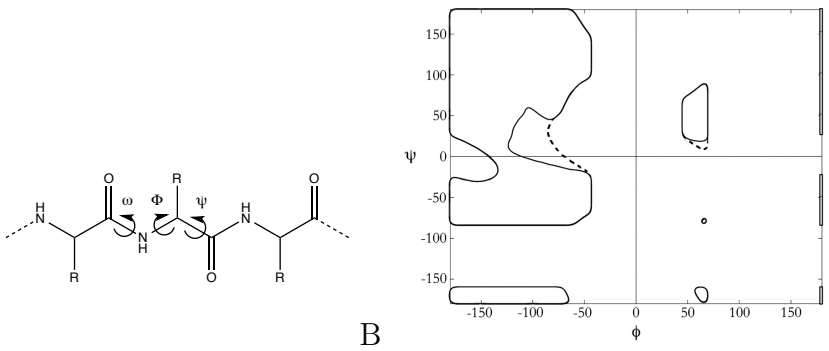

Figure 1.1: Structure of the protein backbone. (A) The dihedral angles Φ and Ψ as well as the angle of the peptide bond ω are shown. Figure adapted from[5]. (B) Ramachandran plot of a alanine dipeptide. The area within the dashed lines designate the allowed regions in the hard sphere model. In the top left corner is the β-region and connected over a bridge the α-region below. The bridge region is reduced if hydrogen-bonding constrains are included (solid line). Figure from[4]

amined under denaturing conditions, i.e. at high concentrations of denaturant, high temperature, pressure or extreme pH. However, the properties of the unfolded state under these conditions might differ from those under folding conditions. Recently, many intrinsically disordered proteins were found, which can serve as models for the unfolded state[8] under physiological conditions. There, the intrinsically disordered proteins were shown to occupy mainly a collapsed but a highly dynamic state. Also in the unfolded state of many proteins residual structure has been found that differs from the model of a complete random coil[9,10]. These residual structure elements can influence the protein folding reaction as already a bias to some secondary structures is present. However U resembles a highly dynamic ensemble of multiple states with low barriers between the conformations so they interchange rapidly.

Most proteins under physiological conditions are found to adopt a specific three-dimensional structure, the native state (N). In the native state optimal hydrogen bond saturation of the backbone amide groups can only be achieved in defined secondary structure elements such as α-helices, β-sheets and turns. These secondary structures form very fast and often in the absence of specific tertiary interactions.

The secondary structure elements assemble in defined spatial topology to the tertiary structure, which is mainly stabilized by side chain interactions such as electrostatic interactions[11], van-der-Waals interactions, hydrogen bonds[12] and the hydrophobic effect[13,14]. In most proteins the solvent is excluded from the interior thus eliminating unfavorable interactions of water with the hydrophobic side chains. Big-

ger proteins often consist of domains, which are typically about 100 amino acids in size and form stable folding units within the protein[15,16]. In some proteins quaternary structures are formed by association of several polypeptide chains into larger complexes. Many structures of proteins are known to atomic detail by X-ray crystallography or nuclear magnetic resonance (NMR) spectroscopy. Although the structures sometimes appear to have a rigid topology the dynamics in the native state are of fundamental importance for protein folding and function. These dynamics range from small thermal fluctuations to motions of whole domains. The function of the protein often is closely related to its dynamic properties as folding, binding and also enzymatic activity depend strongly on the dynamic properties.

There are three basic models that describe how the proteins find their folded structure from the ensemble of unfolded states. In the nucleation-growth-model secondary structure elements are assumed to nucleate locally from which the structure propagates until it reaches the native topology[15]. Similarly, in the diffusion-collision-model the secondary structures form first before they find and lock their tertiary structure by diffusion[17]. The third model, the hydrophobic-collapse-model, suggests a collapse of the protein so the hydrophobic amino acids agglomerate. This intermediate can then rearrange to the native state[18].

1.1.2 Thermodynamics in protein folding

In general, the protein folding reaction is cooperative and can be described as an equilibrium reaction, which also implies that the reaction is reversible[6,19]. In the simplest model, mainly valid in small, single domain proteins, only two states are involved in the reaction: the native (N) and the unfolded state (U) (Eq. 1.1, Fig. 1.2)[20].

$$\mathrm{N} \underset{k_\mathrm{f}}{\overset{k_\mathrm{u}}{\rightleftharpoons}} \mathrm{U} \tag{1.1}$$

N and U resemble thermodynamic states with a multitude of microscopic substates. The folding rate constant is k_f and the unfolding rate constant k_u. The equilibrium constant K_{eq}, the ratio of the equilibrium concentrations of the native (N) and the unfolded state (U), determines the free energy of the folding reaction ΔG^0 (Eq. 1.2).

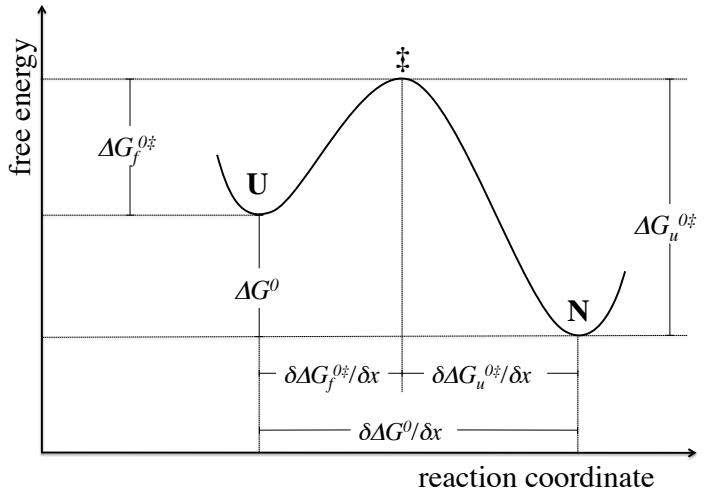

Figure 1.2: Free energy diagram of the unfolded (U) and the native state (N) in a two-state transition. The total free energy difference ΔG^0 is the energy difference of the states and the activation free energies $\Delta G_u^{0\ddagger}$ and $\Delta G_f^{0\ddagger}$ are the height of the barrier. Additionally the effect of a perturbation on the activation free energy $\delta\Delta G_{u,f}^{0\ddagger}/\delta x$ with respect to the effect on the total free energy $\delta\Delta G^0/\delta x$ is shown. Figure adapted from[21].

$$\Delta G^0 = -RT \cdot \ln K_{eq} = -RT \cdot \ln \frac{[N]}{[U]} \tag{1.2}$$

Usually the free energy for protein folding is in the range of -15 to -60 kJ/mol[20]. The stability of the folded state is small due to compensating effects, the loss of entropy and gain in enthalpy. The free energy is a function of pressure p, temperature T and the concentration of denaturants, $[D]$ (Eq. 1.3).

$$d\Delta G^0 = \Delta V^0 dp - \Delta S^0 dT + m\ d[D] \tag{1.3}$$

Each perturbation gives information on different thermodynamic parameters of the system. Pressure changes allow direct measurement of volume changes ΔV^0 and temperature transitions yield information on entropy ΔS^0 and enthalpy ΔH^0. The van′Hoff equation gives the effect of temperature on the reaction enthalpy:

$$\frac{\ln K_{eq}}{dT} = -\frac{dH^0}{RT^2} \tag{1.4}$$

The folded and the unfolded state have a different heat capacity C_p since buried parts of the folded protein are exposed to the solvent in U. Therefore, the thermody-

namic parameters ΔH and ΔS change with the temperature according to equation 1.5. Due to this dependency proteins unfold at high and low temperatures, known a heat and cold denaturation.

$$d\Delta H(T) = \Delta H(T_0) + \Delta C_p \cdot (T - T_0) \tag{1.5a}$$

$$d\Delta S(T) = \Delta S(T_0) + \Delta C_p \cdot ln\left(\frac{T}{T_0}\right) \tag{1.5b}$$

The change of ΔG^0 with the denaturant concentration is typically linear with the proportionality constant m. The m-value is defined in equation 1.3 to $m = \delta\Delta G^0/\delta[D]$. Addition of denaturants provides information on the change in solvent accessible surface area (SASA) (Eq. 1.3)[22]. The folding equilibrium is governed by interactions, solvent to backbone or backbone to backbone, depending on which hydrogen bonds are more favorable. In general, water is a poor solvent for proteins, not only for the hydrophobic side chains, but also for the protein backbone. Thus in water intramolecular hydrogen bonds are favored and the protein folds[23]. The effect of the solvent additives is therefore a function of the solvent quality. Denaturants such as urea or guanidinium chloride (GdmCl) are good solvents for the backbone[6]. The protein unfolds and extents into the solvent thereby more surface gets exposed. The m-value directly correlates with the change in SASA[24]. On the other hand, stabilizing additives such as trimethylamine N-oxide (TMAO) and sarcosin shift the equilibrium towards N as they are even worse solvents than water[23].

1.1.3 Kinetics of protein folding

Typical timescales for protein folding reactions range from microseconds[25] up to several seconds or hours[26,27]. Very different kinds of motions are required for protein folding. Side chain rotations already appear on the ps timescale, loop motions are usually within ns[28–30] and whole domain motions up to microseconds[31]. Reactions that are known to slow down protein folding significantly are proline isomerizations[32,33], disulfide bridge formation[34] and incorporation of cofactors.

In protein folding the unfolded and the native state are local minima in the free energy landscape that are separated by a free energy barrier (Eq. 1.1, Fig. 1.2).

Also the transition state and possible intermediates are energetically well-defined and separated from the other states[9]. To obtain information on transition states as well as minima in the free energy landscape thermodynamic and kinetic data have to be combined. In the two-state model (Fig. 1.1) the observable rate constant λ is the sum of the folding and the unfolding rate constants.

$$\lambda = k_f + k_u \tag{1.6}$$

The microscopic rate constants, k_f and k_u, can be determined in a chevron plot, where the logarithm of the observed rate constant is determined as a function of denaturant concentration. By extrapolation of the folding and the unfolding branch to zero denaturant, k_u and k_f are resolved. The equilibrium constant K_{eq} is given by by the ratio of the equilibrium concentrations of N and U as well as by the ratio of rate constants for folding and unfolding (Eq. 1.7). If thermodynamic and kinetic data yield the same results the apparent two-state mechanism is confirmed.

$$K_{eq} = \frac{[N]_{eq}}{[U]_{eq}} = \frac{k_f}{k_u} \tag{1.7}$$

In addition, the height of the barrier $\Delta G^{0\ddagger}$ can be determined by the temperature dependence of the rate constants k_u and k_f (Eq. 1.8)[32,35]. The pre-exponential factor k_0 is the maximum rate constant in the absence of a free energy barrier. The total free energy difference ΔG^0 is the difference between the activation energies for folding and unfolding, $\Delta G_f^{0\ddagger}$ and $\Delta G_u^{0\ddagger}$.

$$k = k_0 \cdot e^{(-\Delta G^{0\ddagger}/RT)} \tag{1.8}$$

Characterization of the transitions state is difficult as it is not populated. To gain information on the properties of the transition state the rate equilibrium free energy relationships (REFERs) can be used. The activation parameters are analogous to the Gibbs equation for protein folding (Eq. 1.3) given by:

$$d\Delta G^{0\ddagger} = \Delta V^{0\ddagger} dp - \Delta S^{0\ddagger} dT + m^{\ddagger}\, d[D] \tag{1.9}$$

With the REFERs the effect of perturbations on the kinetics are compared to the corresponding effects on thermodynamics (Eq. 1.10)[36]. The changes in the activation

free energy $\Delta G^{0\ddagger}$ due to the perturbation are linearly related to the change in free energy ΔG^0 by the α-value. The perturbation can be a change in pressure, temperature, denaturant concentration or structural changes by mutation[21].

$$\alpha_x = \frac{\delta \Delta G_i^{0\ddagger}/\delta x}{\delta \Delta G^0/\delta x} = \frac{\delta \ \ln k_i}{\delta \ \ln K_{eq}} \tag{1.10}$$

In the Lefflerplot[36] the logarithm of the rate constant is plotted against the logarithm of the equilibrium constant. The slope represents the α-value which it is usually between 0 and 1. For $\alpha = 1$ the perturbation acts on the transition state in the same way as in the folded state, whereas for values close to 0 the transition state is more like the unfolded state. If the perturbation is described by the reaction coordinate the α-value locates the transition state between U and N (Fig. 1.2). In the special case of mutational analysis the α-value is often referred to as Φ-value.

Variation of pressure gives information on volume changes between U and N (ΔV^0) and the transition state ($\Delta V^{0\ddagger}$). Temperature dependencies give the relative position of the transitions state with respect to the entropy as well as indirectly the enthalpy. The rate constants for folding and unfolding as well as the equilibrium constant are linearly related to the concentration of denaturant such as urea and GdmCl with the slope m. Denaturant induced REFERs therefore yield information on the change of SASA between the transition state and the ground states[24]. Mutational analysis determines if the probed interaction is already present in the transition state[21].

With help of this analysis tools it is possible to obtain information on the structural and thermodynamic properties of the transition state. It can be characterized with respect to interaction (ΔH^0), flexibility (ΔS^0), volume(ΔV^0) or solvation. The transition state can be located on the different reaction coordinates and this facilitates a better understanding of the energy landscape for protein folding.

1.1.4 Folding intermediates and the dry molten globule state

The two-state behavior is mainly valid in small proteins and even in these intermediates are often present[37,38]. Many larger proteins fold through partially folded intermediates[39]. Two models for the occurrence of intermediates during protein folding have been proposed. The first one assumes that sequential intermediates occur on-pathway during folding in a hierarchical manner. Stable equilibrium intermediates

observed under non-physiological conditions and the corresponding kinetic intermediates show up in multi-exponential folding kinetics[40,41]. According to the second model protein folding occurs on multiple pathways on a rough energy landscape with local minima. It accounts for the intermediates as kinetic traps in the energy landscape with partly misfolded structure elements[42,43].

Intermediates have been investigated by a multitude of experimental techniques, nonetheless they represent a major challenge in this field. Often intermediates are only transiently populated or their equilibrium concentrations are low compared to the ground state species. Some intermediates arise from slow steps in the protein folding mechanism, e.g. intermediates that have a native-like secondary structure but a proline residue still has to isomerize to form N[44]. Kinetic intermediates lead to complex kinetics with more than one observable rate constant. In general, the number of observable rate constants n corresponds to $n + 1$ kinetic species including N and U. In some cases a heterogeneous unfolded state, e.g. different proline isomers, cause multiple kinetic phases and have to be taken into account.

A special intermediate is the molten globule. The wet and the dry molten globule state was first proposed by Shaknovich and Finkelstein[45,46], who predicted it to be a high energy state that cannot be detected experimentally. In both the wet and the dry molten globule state secondary structure elements are formed and also the topology is close to the native state but not tightly packed. In the wet molten globule solvent is still present in the core whereas in the dry molten globule (DMG) solvent is precluded from the core. In both the side chains have not yet established all interactions and remain flexible. Compared to the native state the DMG state was proposed to be expanded. As the secondary structure stays intact and solvation does not change in the DMG compared to N, this intermediate is invisible for standard spectroscopic methods such as circular dichroism (CD) or fluorescence as well as most data evaluation methods of molecular dynamics (MD) simulations. However with NMR and energy transfer methods such as Förster resonance energy transfer (FRET) or triplet-triplet energy transfer (TTET) detection of the DMG was proposed[47]. With these methods distance distributions and contact formation are monitored, which are parameters that change between the fully folded state N and the DMG state.

Intermediates on the native side of the major unfolding barrier were detected in several proteins. The first hint was found in ribonuclease A (RNaseA) by NMR. In hydrogen-deuterium (H/D) exchange experiments no intermediate for unfolding could

be detected, but in real-time 1D ^{1}H NMR spectra during the unfolding of RNaseA, a rapidly formed intermediate was found that has increased side chain flexibility. The backbone NH groups are highly protected thus in the intermediate state the solvent accessibility stays native-like. This points to the proposed DMG state[48–50]. A similar intermediate was observed during unfolding of dihydrofolate reductase (DHFR). Unfolding of the ^{19}F-Trp labelled DHFR, measured by stopped flow mixing, showed that the ^{19}F-NMR resonance line of N disappeared but the line for U rose with some delay. The slow phase corresponds well with results from spectroscopic measurements. The protein rapidly forms an intermediate with flexible side chains that is not detectable in kinetics recorded with far-UV CD or fluorescence[51]. A further example for the existence of the DMG state was found in single chain monellin. In near-UV CD data an intermediate can be detected in which the Trp chromophore is not exposed to water as seen in fluorescence data. The unfolding kinetics monitored by FRET revealed changes in the distance between the labels suggesting an expansion of the protein[52]. Furthermore, the DMG intermediate was proposed in the villin headpiece subdomain. This will be discussed in detail in section 1.4[53].

1.1.5 The effect of pressure on stability and dynamics of proteins

Pressure perturbation in protein folding studies yields information on the fundamental principles of protein folding[54]. According to Le Chatelier′s principle with increasing pressure the equilibrium is shifted to the state with the smallest system volume. It was found that high pressure denatures proteins[55–58], but the exact origin of the volume increase upon folding is still under investigation. The volume change upon protein folding is very small, often only 0.5 % of the total volume[59] and typically ΔV_u^0 ranges between 5-180 ml/mol[57]. Hence proteins denature only at pressures above 300 MPa. Measurements under these high pressures are experimentally demanding and therefore only few data are available. In general, it is assumed that the native state stays unchanged under high pressure but the equilibrium is shifted to U. The pressure unfolded state often maintains secondary structure elements even at high pressures[59–62].

The pressure dependence of the equilibrium constant K_{eq} yields information on the reaction volume ΔV^0 according to the Planck equation:

$$\frac{\delta \ln K_{eq}}{\delta p} = -\frac{dV^0}{RT} \tag{1.11}$$

The pressure-temperature phase diagram for a two-state system is elliptically shaped [63]. The change of Gibbs free energy with respect to standard conditions p_0 and T_0 is described by[64]

$$\begin{aligned}\Delta G =& \frac{\Delta\beta}{2}(p-p_0)^2 + \Delta\alpha(p-p_0)(T-T_0) - \Delta C_p\left(T\left(\ln\frac{T}{T_0}-1\right)+T_0\right) \\ &+ \Delta V_0(p-p_0) - \Delta S_0(T-T_0) + \Delta G_0\end{aligned} \tag{1.12}$$

with the compressibility factor β and the thermal expansivity α. $\Delta G = 0$ represents the transition line in the phase diagram. This diagram includes pressure denaturation as well as heat- and cold denaturation. Due to its elliptical shape it is possible to start from a denatured ensemble at high temperature and enter the native area with increasing pressure. At even higher pressure the denatured regime is re-entered again. Two assumptions are made for this theory: first, it is a two state transition without intermediates and second, the transitions is completely reversible[64].

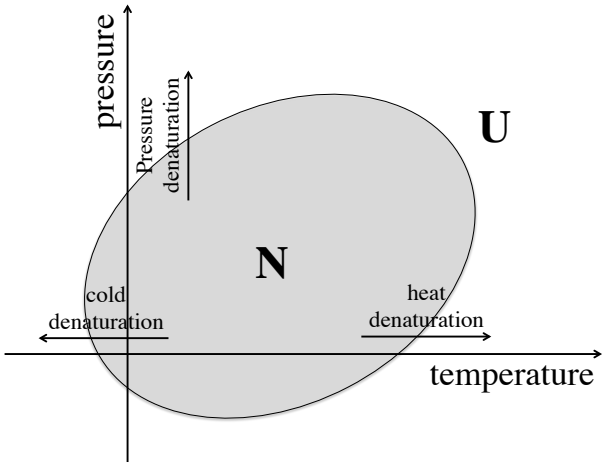

Figure 1.3: Elliptic pressure-temperature phase diagram of proteins. The area with a higher stability for the folded state is shown in grey, the denaturing regime in white and the line represents the transition from the native to the unfolded state with $K_{eq} = 1$. Figure adapted from[64].

Many opposing contributions were found to cause changes in the system volume upon folding. Newer studies suggest that the voids and cavities within the native structure are the main cause of the volume increase upon folding[65]. On the other hand the presence of intramolecular hydrogen bonds and van-der-Waals interactions in the native state reduce the atomic volumes in the folded state[66]. As not only the protein itself determines the system volume but also changes in the solvent contribute to it, the increase of the water volume around exposed hydrophobic groups results in a negative volume change upon folding[67,68]. Electrostriction around charged groups[69] and solvation of the peptide backbone contribute to a positive volume change upon folding[68].

Information on volume changes in the transition state of the protein folding reaction can be obtained by kinetic measurements. The pressure-dependence of the rate constant for folding and unfolding is proportional to the activation volume $dV^{0\ddagger}$ (see also Eq. 1.9):

$$\frac{\delta \ln k}{\delta p} = -\frac{dV^{0\ddagger}}{RT} \tag{1.13}$$

Only few studies on the effect of pressure on folding kinetics are available. In Tendamistat chevron plots in the pressure range from 1 to 1000 bar were recorded by high-pressure stopped flow measurements[70]. At higher pressures tendamistat is destabilized indicating that the folding reaction is accompanied by a increase in volume by 41.4 cm^3/mol. The kinetic measurements revealed that the volume of the transition state is 60 % native-like. At high concentrations of denaturant the volume of the transition state even exceeds the volume of the native state. It was argued that the protein folds in denaturant via a transition state that is already dehydrated but still not well-packed[21,70]. In cold-shock protein CspB kinetic folding and unfolding studies were done by pressure-jump relaxation experiments[71,72]. The feasible pressure jumps up to 16 MPa are very small compared to those needed for complete unfolding transition. Therefore, the effect on the equilibrium constant is small and very small signal changes have to be detected. For staphylococcal nuclease a high activation volume for the transition state was found showing the the transition state has a larger volume than either of the folded or the unfolded state[73]. Also in some variants of the ankyrin repeat domain of the Notch receptor a transition state with higher volume than in either ground state was found[74].

The protein folding reaction includes the formation of intramolecular hydrogen bonds as well as packing and the formation of the hydrophobic core. How each of these contribute to the volume change upon folding is still under debate. The effect of pressure on the dynamics of secondary structure elements like α-helices, β-sheets and hairpins are not yet known.

1.2 Triplet-Triplet Energy Transfer as a Tool to Monitor Peptide and Protein Dynamics

Detailed knowledge of the dynamics of polypeptide chains in the unfolded state gives information on the early steps of protein folding. Loop formation within polypeptide chains is important for the search of the conformational space and for the formation of specific interactions between distant parts of the polypeptide. Intrachain diffusion might even limit the protein folding reaction [75]. The fast electron transfer reaction triplet-triplet energy transfer (TTET) monitors the contact formation between two labels. With the two labels within one polypeptide chain, it is a valuable method to study loop formation within the peptide and also in proteins. Therefore, the donor 9-oxoxanthene-2 carboxylic acid (xanthone, Xan) to the acceptor naphthalene (Nal) are introduced in peptides and proteins and TTET is monitored over time. TTET can also be coupled to the conformational equilibrium to study folded systems. This will yield information on local folding and unfolding rate constants.

1.2.1 Triplet-triplet energy transfer (TTET)

For TTET the donor xanthone is exited to the S_1 state by a short laser pulse at 355 nm and undergoes intersystem crossing to the triplet state efficiently ($\sim 99\%$) in less than 2 ps [76,77]. The intrinsic lifetime of the triplet state in absence of oxygen is up to 80 µs in folded peptides which determines the upper time limit for observation [78].

The transfer of the triplet state from xanthone to the acceptor naphthalene through space has a strong distance dependence. The energy transfer only occurs at distances of up to 5Å [79], which basically implies the formation of van-der-Waals contact. Energy transfer through chemical bonds is only possible at a donor-acceptor separation below 9 bonds [80,81], which is much shorter than in all peptides used in this study. The

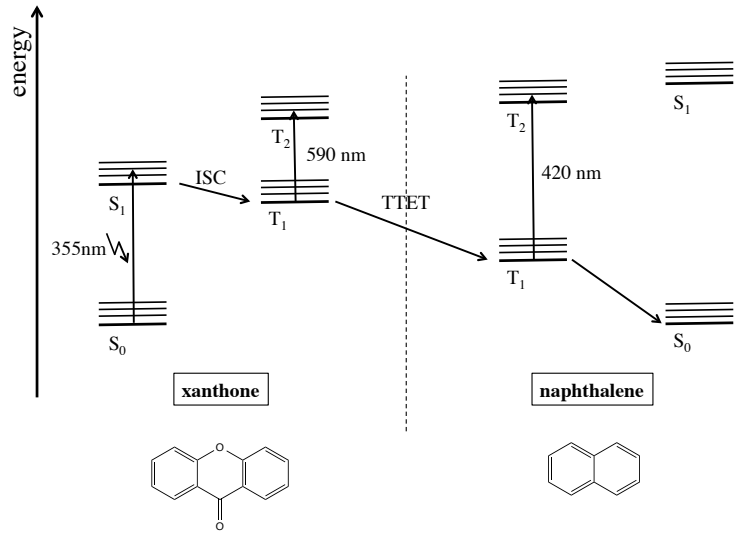

Figure 1.4: Jablonski diagram for triplet-triplet energy transfer between xanthone and naphthalene. Figure adapted from[5].

energy transfer to the acceptor occurs radiationless through a two electron exchange reaction (Dexter mechanism) within 2 ps (Fig. 1.4)[79]. The triplet states of the donor and the acceptor can be monitored by time resolved absorbance spectroscopy. The decay of the xanthone triplet state can be followed at 590 nm ($\epsilon^T_{590} \approx 10000$ M^{-1} cm^{-1}) and the corresponding increase of the acceptor triplet state at 420 nm. Contributions from intermolecular energy transfer can be neglected below peptide concentration of 50 μM[28,29]. In contrast to the Förster resonance energy transfer (FRET), TTET measures the actual contact formation between the labels and not a distance distribution of the labels.

Experiments under pseudo first order conditions with the labels free in solution show that the energy transfer reaction is diffusion controlled. The second order rate constant is $4 \cdot 10^9$ M^{-1} s^{-1}[29,76] in agreement with the prediction from the Smolochowski equation. The rate constant in inversely viscosity-dependent ($k \sim \frac{1}{\eta}$) and the activation energy for the energy transfer is zero ($E_a = 0$)[29,82] in accordance with a diffusion-controlled reaction[83]. Due to the diffusion-controlled mechanism and the

extremely fast photo physics of excitation and energy transfer, the contact formation rate constant can be directly measured for processes slower than 20 ps[5].

Some natural amino acids such as trypophane, tyrosine, methionine, histidin and cystein quench the triplet state of xanthone or perform TTET themselves. For TTET experiments these amino acids should not be present within the protein of interest[75].

1.2.2 TTET in unfolded polypeptides

In unfolded model peptides, e.g. in poly-serine and poly-glycine-serine peptide (GS), loop formation rate constants have been studied in great detail with TTET. The labels were introduced within one peptide. Upon loop formation the labels get into contact and the triplet state is transferred. The data of the unfolded polypeptides show single exponential absorbance decays at 590 nm and the loop formation rate constant can be directly accessed as the rate constant of the decay. Thereby, many details on the dynamics of intrachain diffusion and chain flexibility with varying chain length and sequence could be obtained[5,28–30,82–84]. Figure 1.5 shows representative traces from GS-peptides with varying loop sizes and their corresponding single exponential fits[29].

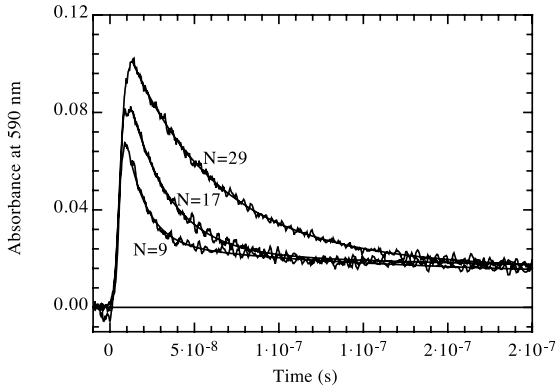

Figure 1.5: Triplet decay curves of xanthone monitored by the change in absorbance at 590 nm of Xan-$(GS)_N$-Nal-SG peptides of different lengths with the corresponding single exponential fit. Figure from[29].

Also the effect of solvent properties and thermodynamic parameter have been determined[83]. In less flexible peptides, the viscosity dependence is affecting the contact formation not to the full amount[85]. The temperature dependence of the viscosity

corrected contact formation rate constant follows the Arrhenius law[85] with activation energies between 5 and 20 kJ/mol. Addition of denaturant (D) has linear effect on the logarithm of the contact formation rate constant k_c with the proportionality constant m[83].

$$\ln k_c = \ln k_c^0 - \frac{m_c \cdot [\mathrm{D}]}{RT} \tag{1.14}$$

1.2.3 TTET in folded peptides and proteins

TTET can also be applied to study folded systems. By coupling the irreversible energy transfer reaction to a conformational equilibrium local dynamics in folded peptides and proteins become accessible. For TTET the labels are inserted in a sequence such as to prevent contact formation in the folded state. The local structure between the labels has to unfold to facilitate the energy transfer reaction. By this method protein folding can be probed in equilibrium, in contrast to relaxation methods, such as temperature jump (T-jump) spectroscopy, which are also used to investigate reactions in the nanosecond to microsecond time range[86–89].

$$N \underset{k_\mathrm{f}}{\overset{k_\mathrm{u}}{\rightleftharpoons}} \mathrm{U} \xrightarrow{k_\mathrm{c}} \mathrm{U}^* \tag{1.15}$$

The three-state system can be described by equation 1.15. N represents a folded structure with the labels separated. In this scheme U represents a partially unfolded conformation in which the region between the labels is flexible and loop formation can occur. In U* the irreversible energy transfer from xanthone to naphthalene has taken place. TTET can be followed spectroscopically (Fig. 1.5).

This mechanism is similar to the one in hydrogen-deuterium exchange experiments, where the irreversible exchange reaction of an amide deuterium to a hydrogen from the solvent is monitored. Exchange can only occur in non-hydrogen bonded and solvent accessible regions and consequently the protection depends on the folding and unfolding rate constant of the protein. The time scale of the probing reaction (k_c) determines the time resolution of the experiment. For the TTET experiments in fast folding proteins all three rate constants k_f, k_u and k_c are in the same order of magnitude. If both N and U are populated, k_f, k_u and k_c can be directly calculated

from the two apparent rate constants $\lambda_{1/2}$ and their corresponding amplitudes $A_{1,2}$[90] (Eq. 1.16).

$$\lambda_{1/2} = \frac{k_u + k_f + k_c \pm \sqrt{(k_u + k_f + k_c)^2 - 4k_u k_c}}{2} \tag{1.16a}$$

$$A_1 = \frac{1}{\lambda_1(\lambda_1 - \lambda_2)}([U]_0 \cdot k_c \cdot (k_u - \lambda_1) + [N]_0 \cdot k_u \cdot k_c) \tag{1.16b}$$

$$A_2 = \frac{1}{\lambda_2(\lambda_1 - \lambda_2)}([U]_0 \cdot k_c \cdot (\lambda_2 - k_u) + [N]_0 \cdot k_u \cdot k_c) \tag{1.16c}$$

1.3 α-Helices

α-Helices[91] are the most abundant secondary structure motif in proteins. About 30% of all amino acids in natural proteins participate in α-helices[92] and α-helix formation is suggested to be one of the first steps in protein folding as only local interactions have to be established. The average length of an α-helix within a protein is 10 amino acids[92]. The α-helix is a right handed twisted structure with a linear translation of 5.4 Å and 3.6 residues per turn (Fig. 1.6), i.e. 1.5 Å per amino acid. The helix shows very defined Φ and Ψ angles in the backbone of the polypeptide chain (Fig. 1.1) and is stabilized by consecutive hydrogen bonds between the backbone amide and carbonyl groups in i,i+4 spacing with nearly optimal distance between donor and acceptor of 2.8 Å [93,94]. The side chains of the amino acids point tangentially outward from the helix.

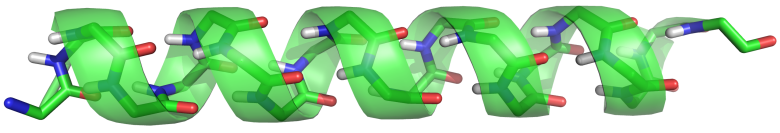

Figure 1.6: Structure of an α-helix. The figure was prepared with the program MacPyMOL.

The narrow 3_{10}-helix with a i,i+3 hydrogen bonding pattern is also found frequently in crystal structures often in stretches of 3-4 amino acids at the termini of α-helices[95]. The π-helix with i,i+5 hydrogen bonds is energetically unfavorable and thus only rarely found[94].

1.3.1 Stability of α-helices

Except glycine and proline all natural amino acids are found in α-helices. Nevertheless, the amino acids exhibit different helix propensities. Alanine was shown to be the best helix forming amino acid. Alanine-based helical peptides are helical even in isolation without stabilizing tertiary interaction[96]. To solubilize these peptides, charged amino acids were introduced in i,i+5 spacing. With this system it was possible to study α-helix formation extensively and the helix propensities for all amino acids were obtained (Tab. 1.2)[97–101]. Besides the helix propensities of the amino acids the effect of salt[97], denaturants[102,103] and 2,2,2-trifluorethanol (TFE)[104] was studied extensively in these alanine-based helical peptides. Addition of TFE to the peptide solution induces α-helix formation significantly even in sequences with low helix propensities[105,106]. It is unclear wether this is due to shielding of hydrogen bonds from backbone to water in the unfolded state[107] or the disruption of the solvent shell in the α-helix[108]. The helix propensity of all amino acids increases in TFE compared to water[94].

In proteins secondary and tertiary structures fold cooperatively. Tertiary interactions with other parts of the protein stabilize and enhance helix formation and lock in the final structure. In isolation helices have been found to be highly dynamic systems with multiple states and hence the two-state model is not valid. The helix can extend and abridge at both termini in one amino acid steps.

For the first turn in the helix four amino acids need to be in the right conformation to form one hydrogen bond (Fig. 1.7). This results in three amide NH groups at the N-terminal end of the helix that cannot form intramolecular hydrogen bonds but still have the unfavorable entropic restrictions. The same is true for three amide CO groups at the C-terminal end of a helix. Consequently nucleation of the helix is less likely than elongation where every residue contributes one hydrogen bond to the stability.

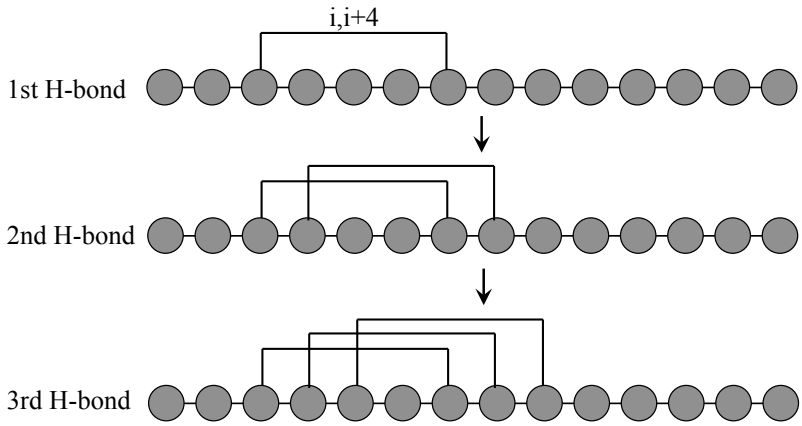

Figure 1.7: α-helix formation. For the first turn the angles of four peptide bonds have to be restricted to gain one hydrogen bond (H-bond), for helix elongation each peptide bond restriction gains one hydrogen bond.

Stabilizing side chain interactions within α-helices

Helices can additionally be stabilized by side chain interactions. The side chains of residues in i,i+3 or i,i+4 spacing are in close vicinity and can interact with each other. The typical side chain interactions in proteins, such as salt bridges, hydrogen bonds, hydrophobic interactions, basic/aromatic interactions and polar/nonpolar interactions were also found to stabilize helices. It was possible to quantify the stabilizing energies[94]. The alanine-based model systems even allowed the characterization of the mechanism for the less known interactions, such as the Phe-His interaction that was first found in the C-peptide[109,110]. Also specific interactions between the non-polar side chains tyrosine and leucine or valine[111] as well as tyrosine and the non-natural non-polar amino acids norleucine and norvaline[112] were determined. The strength of a Gln-Asp hydrogen bond was quantified to 1 kcal/mol for a charged aspartate in the defined system of the helices and the findings were used to screen protein sequences, where this interaction is quite frequent[113,114]. With 1.6 kcal/mol the phosphoserine-lysine salt bridge is the strongest side-chain interaction found so far[115].

Although strong stabilizing effects of salt bridges and hydrogen bonds had been found by CD spectroscopy the results could not be reproduced by TTET experiments[78]. One reason is the destabilization of the helix by replacing an alanine, the best helix builder, with an amino acid that contributes to the interaction. The interaction could only counteract this effect and could not be quantified. The reference

peptide without the studied interaction had a hydrophobic norvaline next to the label and was therefore stabilized as well by side chain interactions[78].

The helix dipole and helix capping

The successive hydrogen bonds in the helix arrange all peptide bonds equably perpendicular to the helix axis and the dipole moments adds up over the complete length to the helix dipole. The helix has an apparent positive partial charge at the N-terminus and a negative partial charge at the C-terminus. Both effects destabilize the helix and therefore have a high impact on amino acid preferences at the termini[94]. The first amino acid at the N-terminus without α-helical dihedral angles is the N-cap, at the C-terminus its the C-cap. Helix capping includes the N- and C-cap as well as the following amino acids denoted N1, N2, N3, N4 and C1, C2, C3, C4. These caps are able to contribute to helix stability either by counteracting the helix dipole with a charge or by providing favorable side chain to backbone or side chain-side chain interactions.

For example, the side chain of asparagine as N-capping residue can form a hydrogen bond with the amide NH of the third helical residue (N3) and counteract the dipole with the negative charge of the side chain[116]. Capping boxes have been found in protein sequences at the N-terminal end of helices[117] as well as the C-terminal end[118–120]. In artificial peptides such as the alanine-based peptides, an acetylated[121,122], or even a succinylated[123] N-terminus is the most favorable N-cap. It removes the positive charge, succinyl even counteracts with a negative charge and the carbonyl group can serve as a hydrogen bond acceptor for the unsaturated backbone NH groups of N3. At the C-terminus amidation acts in a similar way on helix stability and is a relatively good capping motif[116]. Favorable and destabilizing capping motifs[117] were introduced and characterized extensively[101,116] in alanine-based helical peptides and the N- and C-capping propensities are listed in table 1.2.

1.3.2 Helix-coil theory

Two models have been developed to describe the helix-coil transition, the Zimm-Bragg model[124] and the Lifson-Roig model[125]. In the Zimm -Bragg model[124] a peptide group is considered helical if the NH group forms a i,i+4 hydrogen bond. The code 1 denotes a helical and 0 a coiled state (Tab. 1.1). The statistical weight of helix

nucleation is σs, the elongation of an existing helix has the weight s. Peptide groups with no hydrogen bond of the NH group, state 0, are assigned a statistical weight of 1. By this we have basically the initiation parameter σ and the propagation parameter s that govern helix stability[94]. Two further limitations are set, first helices shorter than three segments are neglected and second the first three units are kept non helical as they cannot form a hydrogen bond. The s-values were determined experimentally for all proteinogenic amino acids (Tab. 1.2)[99,100].

In the Lifson-Roig model[125] the basic unit is one amino acid residue which is accounted for as helical (h) or coil (c) depending on the Φ and Ψ dihedral angles (Tab. 1.1). Statistical weights are assigned to the middle residue of a triplet. This is related to that of a coil residue between two other coil residues in the triplet ccc, which is defined as having a weight of 1. By this the actual state and the states of the nearest neighbors contribute to the statistical weigh. A helical residue in a helical region, such as in the triplet hhh, has the weight ω, the last helical residue in chh or hhc is referred to as ν. To gain the statistical weight of a helix with N residues the weights of the residues are multiplied and yield $\nu^2\omega^{N-2}$. N- and C-caps are taken in consideration by assignment of the statistical weights n and c to the coil residue in front and behind the helix as in cch and hcc. In the same manner preferences in the N1, N2 or N3 as well as the C-terminal helical residues can be included[94]. It is even possible to consider side chain interactions with the i, i + 4 interaction parameter, p, and an i,i + 3 interaction parameter, q[126].

Zimm-Bragg code	0	0	0	1	1	1	1	1	1	0	0	0	0
Zimm Bragg statistical weight	1	1	1	σs	s	s	s	s	σs	1	1	1	1
Lifson-Roig code	c	c	c	h	h	h	h	h	h	c	c	c	c
Lifson-Roig statistical weight	1	1	n	ν	ω	ω	ω	ω	ν	c	1	1	1

Table 1.1: Table of notation and statistical weights for the Zimm-Bragg and the Lifson-Roig model[94]

The sum of the weights of all possible conformations determines the partition function. The population of one conformation can be calculated by dividing its statistical weight by the partition function. Is the weight >1, the conformation has a higher probability than the all coil reference, is it <1, it has a lower probability. By this the overall helix-coil equilibrium can be retrieved[94]. The algorithm AGADIR is based on the Lifson-Roig model and gives reliable predictions on the helix-coil equilibrium for a given sequence[127,128].

The statistical weights of the two models can be converted into each other by[129]:

$$s = \frac{\omega}{1+\nu} \tag{1.17a}$$

$$\sigma = \frac{\nu^2}{(1+\nu)^4} \tag{1.17b}$$

This model has often been used in combination with experimental work[98,130,131] where the experimentally obtained helix content is used to parametrize the Zimm-Bragg model. Equation 1.18 gives the theoretical helix probability for a sequence of the length N and specific s- and σ-values[124].

$$p = \frac{(n-3)(s-1) - 2 + ((n-3)(s-1) + 2s) \cdot s^{-n+2}}{(n-3)(s-1)[1 + (s-2)^2 \cdot s^{-n+1}\frac{1}{\sigma} - ((n-3)(s-1) + s) \cdot s^{-n+2}]} \tag{1.18}$$

The Zimm-Bragg model was used to interpret the thermal unfolding curves of alanine-based peptides of different lengths yielding the propagation parameter s of about 1.35 for alanine and the nucleation penalty σ of about 0.003[131]. Here side chain interaction between glutamate and lysine were present in i,i+4 spacing. In further studies these could be eliminated and only lysine served to assist solubilization. With host-guest studies in these peptides the s-values of all natural amino acids could be obtained (Tab. 1.2)[99,100]. Furthermore, the Lifson-Roig model, which also accounts for capping effects, was used to reproduce the helix content from CD measurements. A propagation parameter ω was assigned to all amino acids (Tab. 1.2) and also converted to the s-value of the Zimm-Bragg model[129]. N- and C-capping preferences were included by the parameters n and c (Tab. 1.2).

With NMR H/D exchange and CD spectroscopy the length dependence of helix-coil transitions in alanine-based helical peptides has been investigated and the results were reproduced with the Lifson-Roig theory. The theory already infers length independent propagation and nucleation parameters and the experiment was able to confirm this[132]. Contrary to this a time resolved T-Jump infrared spectroscopy (IR) study suggested length dependent s-values, but here a two-state model was invoked

to model the relaxation kinetics[133]. However, the two-state model cannot describe the non-cooperative helix-coil transition in alanine-based helical peptides.

The kinetic linear Ising model is suitable for calculation of the helix-coil dynamics using the Zimm-Bragg model. As described before, each position is assigned one of two possible states and the transition between the states depends on the actual state and the nearest neighbors[134]. This is then expressed in statistical weights by addressing the transitions of the middle residue in a triplet. There are three possible scenarios:

1. Helix elongation:

$$hcc \underset{k_{-1}}{\overset{k_1}{\rightleftharpoons}} hhc \quad cch \underset{k_{-1}}{\overset{k_1}{\rightleftharpoons}} chh \qquad \frac{k_1}{k_{-1}} = s \tag{1.19}$$

2. Helix nucleation:

$$ccc \underset{k_{-2}}{\overset{k_2}{\rightleftharpoons}} chc \qquad \frac{k_2}{k_{-2}} = \sigma s \tag{1.20}$$

3. Coil nucleation:

$$hhh \underset{k_{-3}}{\overset{k_3}{\rightleftharpoons}} hch \qquad \frac{k_3}{k_{-3}} = \frac{\sigma}{s} \tag{1.21}$$

The s-value is the equilibrium constant of the elementary helix folding and unfolding reactions. Residues with a s-value bigger than 1 are more likely to be in a helix than in a coil state, s-value smaller than 1 indicate poor helix propensities. As described before, helix nucleation is unfavorable and σ, the nucleation penalty, is close to 0. For coil nucleation within a helix at least one turn has to unwind to open the helix and also has a low probability in this model. In addition the model can be extended to include kinetic effects by[135] ($1 \leq \gamma \ll \frac{1}{\sqrt{\sigma}}$):

$$\begin{aligned} k_2 &= \gamma_h \cdot \sigma \cdot k_1 \qquad & k_{-2} &= \gamma_h \cdot k_{-1} \\ k_3 &= \gamma_c \cdot \sigma \cdot k_{-1} \qquad & k_{-3} &= \gamma_c \cdot k_1 \end{aligned} \tag{1.22}$$

With the parameters s and σ as well as γ_h and γ_c the helix-coil dynamics are fully described and can be calculated with reference to k_1 which is arbitrarily set to 1. The models suggests that only one helical sequence is present at a time, because the nucleation is unlikely compared to helix propagation. Generally, this is referred to as

the single sequence approximation[129]. The second consequence for helices in general is, that at the termini the helix tends to open, known as helix fraying. This effect was also confirmed experimentally[97].

amino acid	s-value	ω-value	n-value	c-value
Ala	1.54	1.61	1	1
Arg^+	1.04	1.09	1.3	2.1
Leu	0.92	0.96	3.4	1.2
Lys^+	0.78	0.82	0.78	1.1
Glu	0.63	0.66	-	2.2
Met	0.60	0.63	1.8	1.6
Gln	0.53	.56	0.01	2.4
Glu^-	0.43	0.45	3.3	0.41
Ile	0.42	0.44	2.4	<0
Tyr	0.37-0.50	0.39-0.53	12	63
His	0.36	0.38	3.4	-
Ser	0.36	0.38	8.3	0.21
Cys	0.33	0.35	-	0.72
Asn	0.29	0.31	22	0.78
Asp^-	0.29	0.31	20	<0
Asp	0.29	0.31	-	0.66
Trp	0.29-0.36	0.30-0.38	7.3	<0
Phe	0.28	0.29	3.4	<0
Val	0.22	0.23	1.2	0.21
Thr	0.13	0.14	3.7	<0
His^+	0.06	0.06	-	1.4
Gly	0.05	0.05	8.9	0.88
Pro	$\sim$0.001	$\sim$0.001	1.9	<0
Cys^-	-	-	14	-
acetyl	-	-	12	-
amide	-	-	-	1.3

Table 1.2: Helix propensities of the Zimm-Bragg model, the s-value, for all natural amino acids derived from host-guest studies in alanine-based helical peptides with CD spectroscopy[99,100]. The error of the tryptophan and the tyrosine is due to the contribution of the aromatic side chain on the CD signal. The s-values are converted to the corresponding ω-value of the Lifson-Roig model. N- and C-capping propensities are given as n-values and c-values[116]

1.3.3 Kinetic studies in alanine-based helical peptides

Experimentally, the dynamics of the helix formation and unfolding in alanine-based helical peptides were mainly investigated by perturbation methods and were found to be on the time scale of the hundreds nanoseconds.

At first helical polymers, not on the basis of alanine, were investigated by dielectric relaxation[136] and ultrasonic relaxation methods[130]. In temperature-jump measurements[89,137] fluorescent probes, that change quantum yield upon helix formation, were introduced in alanine-based peptides. These experiments claimed to yield a helix propagation rate constants of approximately 10^8 s^{-1} but actually only fluctuations at the N-terminal fluorescent probe are visible by this method. Also time-resolved infrared spectroscopy measurements in alanine-based peptides revealed rate constants in a similar range[138]. With ^{13}C labeled samples these experiments facilitated even site-specific measurements[139]. However, the data from the IR experiments were evaluated on the basis of a two-state model. Data evaluation is a major challenge as experimental data from alanine-based peptides cannot be explained by a two-state model. The helix-coil transition is a highly dynamic multi-state system. The coupling of a irreversible reaction to the equilibrium could resolve the folding and unfolding rate constants. In a first approach triplet quenching of tryptophan by a disulfide was applied to the system and found dynamics in the time range of μs[140]. But here the quenching mechanism is not diffusion controlled and does not allow direct determination of folding and unfolding rate constants.

Fierz et.al[90] used TTET to examine the helix-coil transitions at different positions within a 21-amino acid alanine-based model peptide. Here the donor xanthone and naphthalene were attached to the peptide in i,i+6 spacing so as to be on opposing sides in the folded structure. Upon unfolding a loop can form and by van-der Waals contact between the donor and the acceptor moiety the energy is transferred. As energy transfer is an irreversible reaction the unfolding and the refolding reaction of the conformational equilibrium can be studied using the analytical solution of the three-state system (section 1.2.3).

Measurements of local dynamics at different positions within the peptide showed a position independent time constants for folding of 400 ns whereas the helix unfolding was faster at the termini (250 ns) compared to the center (1.4 μs)[90]. This behavior could be reproduced in Monte Carlo simulations using a kinetic linear Ising (section

1.3.2) with constant elementary steps of 50 ns for helix elongation and 65 ns for helix shrinking. The dynamics were described well by a one-dimensional diffusing boundary mechanism[90]. The boundary of the helical conformation moves along the sequence, but nucleation events both of the helix and coil are unlikely. This model as well as earlier experiments[98] suggest that for stable helix forming peptides the helix boundary resides in the terminal regions. Helix folding is only dependent on the helix propensity of the sequence whereas helix unfolding at a certain position also depends on the distance to the helix boundary. In central region the boundary has to diffuse over a longer distance and helix unfolding is slowed down in the center compared to the peptide termini.

1.3.4 Pressure effects on isolated α-helices

In proteins pressure denaturation is due to various effects. It has been shown that cavities and void in the core contribute but also solvent effects are important. The effect of pressure on secondary structure elements has not been studied yet. The alanine-based helical peptides are well suited to study the effect of high pressure on isolated α-helices. Contributions on the volume change upon exposure of side chains to the solvent or packing of the hydrophobic core are absent in this system and therefore the volume change for α-helix formation can directly be measured.

The amide-I band of a Fourier transform infrared spectroscopy (FTIR) spectrum of a poly-alanine peptide was used to determine the fraction of helix and coil in equilibrium under various pressures[141]. A positive volume change of 10.3 cm^3/mol was assigned to helix unfolding. But here the multi-state behavior of this system is not taken into account. Imamura and Kato[142] used alanine-based model peptides to gain information on the effect of pressure and temperature on the helix-coil transition. In for this propose they correlated the change in the CD signal over temperature with IR parameters from FTIR spectra. Thus the IR signal change of the pressure dependence could be evaluated with the Zimm-Bragg model[124]. A positive volume change of 0.98 cm^3/(mol res) was obtained for helix unfolding indicating the helix is stabilized under high pressure.

The volume change of an alanine-based peptide was also calculated by MD simulations[143]. In contrast to the experimental results a small but negative volume change of -2.3 cm^3/mol was found. However, this data was evaluated by a two-state model,

that is not very well suited to describe the helix-coil equilibrium. In addition, the amide-I band of the IR spectrum was calculated from the simulations and a red shift of the peak with pressure was found. For this reason the amide-I IR band might not be the best probe to determine pressure effects on the helix-coil equilibrium.

1.4 Villin headpiece subdomain

Villin is an actin-binding protein in the intestinal brush border and facilitates the formation of microvilli by bundling of F-actin[144]. The villin headpiece subdomain (HP35) is the C-terminal domain of villin. It consists of 35 amino acid and is stably folded in isolation[145]. The wild-type sequence is LSDEDFKAVFGMTRSAFANLPLWKQQNLKKEKGLF.

The structure of HP35 has been solved by NMR spectroscopy[146] as well as Xray crystallography[147] and showed a three helix bundle with a hydrophobic core (Fig. 1.8). The three helices are termed helix 1,2 and 3 starting from the N-terminus. Three phenylalanines at positions 6, 10 and 17 form the hydrophobic core[148,149] and also the Leu20 is essential[150]. The Trp23 is highly conserved and the PXWK motif is suggested to be involved in Trp-Pro stacking that determines the fold[151]. The overall stability is small with $\sim$12 kJ/mol[152], nevertheless the structure is well defined. Equilibrium measurements showed a two-state behavior in GdmCl and temperature induced unfolding experiments[145].

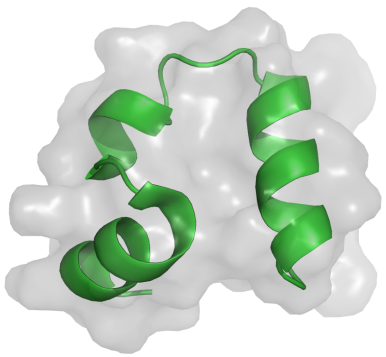

Figure 1.8: Structure of the villin headpiece subdomain based on the X-ray crystal structure[147]. The helices are shown as cartoon and the surface is outlined.The figure was prepared with the program MacPyMOL.

The folding kinetics of the villin headpiece subdomain have been subject to numerous experiments. In different T-jump studies with fluorescence quenching of tryptophan either by histidine[153] or by cysteine[154] very fast rate constants of a few µs have been found. The folding was highly cooperative, however the T-jump kinetics were not as expected single exponential but showed biphasic behavior. The experiments showed a transient unfolding intermediate[25,152,153]. More studies with T-jump spectroscopy[155] and NMR line shape analysis[156] confirmed the fast folding rate constant. By rational design an even faster folding time constant of 0.7 µs was observed in the mutant Lys24Nle/Lys29Nle[25]. Thus HP35 is the fastest folding protein known. In computational studies[157] as well as in NMR and IR experiments[155,158,159] native-like secondary structure elements in the unfolded state were suggested which could be an explanation for the rapid folding. Furthermore experiments showed that even the fragment consisting only of helix 1 and 2 is structured in isolation[158,160].

Due to the small size, the simple topology and the fast folding kinetics the villin headpiece subdomain is a perfect model for computational studies. It was the first protein, for which all-atom MD simulations with explicit solvent up to µs could be performed[161]. The experimental folding kinetics of some µs were reproduced well in further simulations[157]. The simulations found a rapid collapse of the molecule with subsequent rearrangement to the native state[157]. In replica exchange MD simulations Lei *et. al.* identified two intermediate states, one of which they suggested to be an obligatory on-pathway intermediate[162]. Also Ensign *et al.*[163] found in their simulations complex kinetics in folding of HP35.

Dynamics in the villin headpiece subdomain HP35 has been investigated by TTET[53]. The labels have been introduced in the protein at different, well-separated positions. Energy transfer thus only occurs after partial or global unfolding (Fig. 1.9) (section 1.2.3). The data suggest two native states on the native side of the major unfolding barrier, the locked (N) and the unlocked native state (N′). In both states the secondary structure elements are intact but in N′ the side chain interactions are loosened and the structure is more flexible.

Four variants of HP35 with the TTET labels in different positions were used to study equilibrium and kinetic properties in the probed regions (Fig. 1.10). The variant probing helix 1 and 2 (Fig. 1.10 A) and also the one probing the central region (Fig. 1.10 B) only showed kinetics on the timescale of the global unfolding reaction that cannot be resolved by TTET measurements. The first hint for conformational

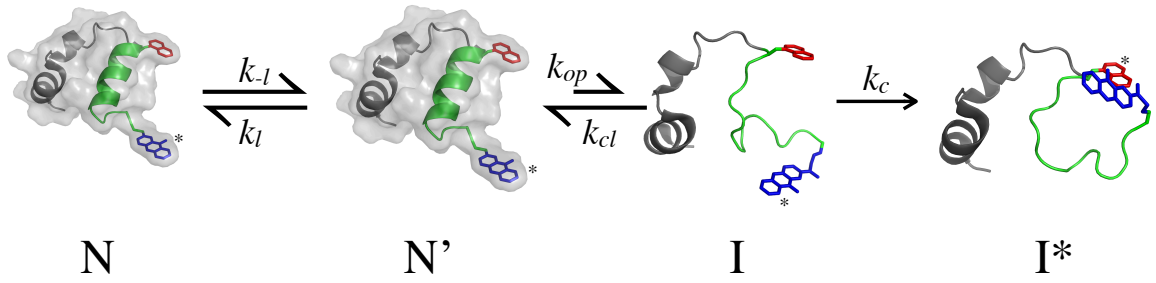

Figure 1.9: Schematic representation of TTET experiments to investigate native-state dynamics of HP35. The locked (N) and unlocked (N′) native state are in equilibrium. Local unfolding of helix 3 to a partially unfolded intermediate (I) only occurs from N′. The TTET labels xanthone (blue) and naphthylalanine (red) were placed at the N- and C-terminal ends of helix 3, respectively. After unfolding of helix 3 loop formation can occur which leads to TTET from xanthone to naphthylalanine. These experiments yield the rate constants for unlocking and unfolding of helix 3 as well as information on the populations of N and N′ in equilibrium.

heterogeneity was found in the variant with the labels at the N- and the C-termini (Fig. 1.10 C). The labels should be in close contact in the folded state thus TTET occurs in the dead-time of the instrument. An additional kinetic phase was detected that originates from a native state fluctuation. In the native state ensemble there was one population of about 70 % with the termini in close contact and a second population of 30% with a fast rate constant for loop formation[53].

In the variant probing helix 3 (Fig. 1.10 D) the alternative state, the unlocked native state (N′), could be further characterized. The two native states show different dynamics in the TTET experiments[53]. The slower process arises from the locked state with about 80% of the amplitude and has a low denaturant dependence. The fast process originating from the unlocked state with about 20% of the amplitude has a large m-value. This indicates no change in the solvent accessible surface area (SASA) in the rate limiting step in the locked state but a big change in SASA that corresponds to about 50% of global unfolding from the unlocked state. Kinetics from the locked state showed a large activation energy, which indicates a high enthalpic barrier that has to be overcome to allow loop formation. But from the unlocked state loop formation has a low activation energy although big structural changes, i.e. partial unfolding of helix 3, take place[53].

The locked state N is consistent with the X-ray and NMR structures with the termini close to each other and large scale fluctuations cannot occur unless the protein unlocks to N′. From N′ helix 3 can unfold and TTET is fast. The rate-limiting step

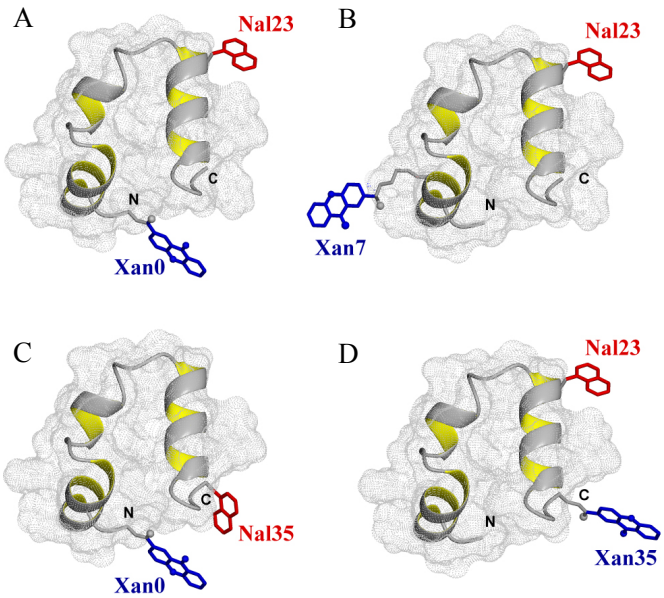

Figure 1.10: Variants of the HP35 studied by TTET[53]. The TTET labels xanthone (blue) and naphthylalanine (red) were introduced at the indicated positions. Figure from[53].

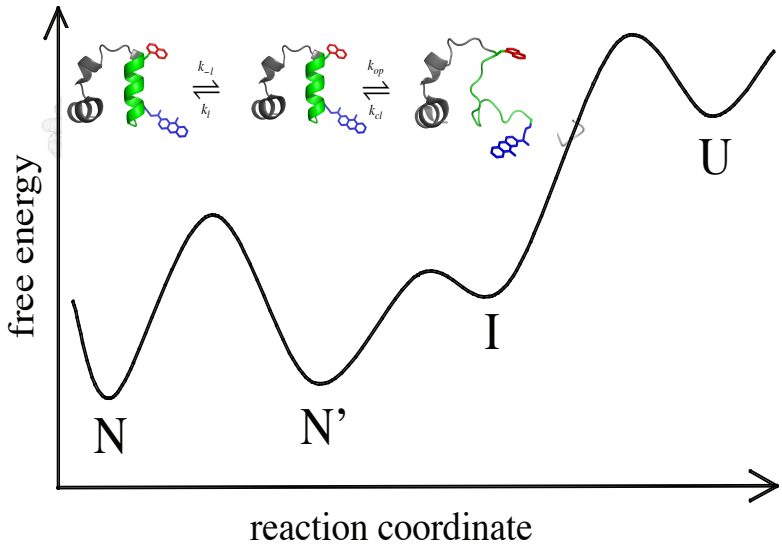

Figure 1.11: Free energy diagram for HP35 folding showing the two alternative native states separated by a free energy barrier. From N′ helix 3 can unfold to the high energy intermediate I prior to global unfolding. Figure from[53].

in N is the unlocking reaction characterized by a the low m-value. The temperature dependence revealed a positive ΔH of 35 kJ/mol and also a positive ΔS of 112 J/(mol K) for unlocking, suggesting a higher flexibility but weakened interactions in N′. The loop formation then occurred in an high energy intermediate state I with only helix 3 unfolded but intact helices 1 and 2[53]. The loop formation rate constant in U agrees with the rate constant that is expected for fully unfolded polypeptide chains. This result contradicts the assumption of residual structure in U at high concentrations of denaturant.

Beauchamp *et al.*[164] were able to reproduce TTET results with MD simulation and Markov state models by simulation of contact formation times[165] and could also monitor the two native conformations. Later on the alternative native state has been found by others in MD-simulation studies as well as in experiment. Serrano *et al.*[166] could monitor native state conformational heterogeneity by time resolved FRET measurements. The donor p-cyanophenylalanine is excited and FRET to the intrinsic Trp residue monitors the distance distribution between the labels.

2 Aim of Research

To gain insight into the fundamental principles of protein folding and function, it is essential to characterize the structural and dynamic properties of the native and unfolded state as well as of intermediate and transition states. Triplet-triplet energy transfer (TTET) coupled to a conformational equilibrium yields information on conformational dynamics in proteins and peptides on the nanosecond to microsecond time scale. A time range, which is difficult to access with other experimental methods.

Folding and unfolding dynamics in the helix-coil transition

The formation of secondary structure elements is one of the earliest steps in protein folding. Ala-based peptides form α-helical structures in isolation[96] and thus are a good model system for the investigation of structural and dynamic properties of α-helices in the absence of tertiary interactions. Previously, TTET labels were attached to Ala-based helical peptides and the local folding and unfolding rate constants between the labels were determined[90]. The measurements yielded a position-independent helix folding rate constant ($1/k_f$=400 ns) and a position-dependent helix unfolding rate constant with faster unfolding at the termini ($1/k_u$ = 250 ns) compared to the center ($1/k_u$ = 1.4 μs). The dynamics in these peptides were well described by a kinetic linear Ising model[124,125] which yielded thermodynamics as well as the kinetic properties of Ala-based helical peptides[90]. The mechanism of helix elongation and unfolding is governed by boundary diffusion during which the helix-coil boundary moves along the polypeptide chain. Due to this boundary diffusion mechanism the length of helical peptides should effect the unfolding rate constant while the folding rate constant should remain unaffected. It is the aim of this investigation to test this model by measuring the dynamics in the center of helical peptides of different lengths and investigate wether the dynamics can be described by an Einstein-type, one-dimensional diffusion process.

Helix capping motifs are known to influence helix stability to a great extent by interaction with the helix dipole or contribution of favorable interactions[119]. I intent to examine the origin of this effect by measuring the helix dynamics in the center of helical peptides with different N- and C-terminal caps and investigate whether these act on the diffusion of the helix-coil boundary. Locally, helix dynamics will be characterized by the variation of helix stability in between the TTET labels. I aim to introduce different N-caps and measure TTET dynamics at the N-terminus and additionally to replace amino acid in the center between the labels in a host-guest study.

To characterize the transition state and the ground state of the helix-coil transition I intend the use of high pressure TTET in Ala-based helical peptides. With increasing pressure most proteins unfold as the native state has a larger volume than the unfolded state[57]. The individual contributions of volume changes due to differences between the native and the unfolded state and solvation effects are still under debate. In Ala-based helical peptides the contribution of volume changes due to secondary structure formation can be characterized individually as all side chains remain solvent accessible and no void volumes are formed. Therefore, the TTET setup will be equipped with a high pressure cell system to measure TTET kinetics under pressure. I aim to investigate TTET kinetics of helical peptides under different pressures and compare the results to simulations with the kinetic linear Ising model in order to gain information on the reaction and the activation volume of adding and removing a single helical residue to and from a preexisting helix.

Dynamics in the villin headpiece subdomain

The villin headpiece subdomain (HP35) is the smallest known independently folding protein domain and its folding and dynamics have been extensively studied both experimentally and by simulations. In previous measurements the conformational equilibrium fluctuations in the folded state of the villin headpiece subdomain (HP35) were investigated by TTET coupled to the conformational equilibrium in HP35[53]. In addition to global folding and unfolding, a structural unlocking reaction has been found. The unlocked state (N′) is on the native side of the major folding/unfolding barrier and N′ exhibits weakened interactions and increased structural flexibility compared with the locked state (N). These are properties of a dry molten globule state

that was predicted before[45]. If this is the case the weakening of the interactions should result in a volume increase from the locked to the unlocked state. Therefore, I want to apply high pressure TTET to detect the reaction and the activation volume, ΔV^0 and $\Delta V^{0\ddagger}$, between between N and N′ and thus gain more information on the ground and transition states.

Furthermore, I want to characterize in more detail the N′/N equilibrium and its dynamics as well as the dynamics of partial unfolding in HP35 mainly focussing on the following questions: What are the effects of the solvent on the unlocking/relocking reaction? How do mutations influence the unlocking/relocking reaction and the unfolding of helix 3? Can also helix 1 unfold from the unlocked state N′ and form a high energy intermediate? Is it possible to obtain an even smaller cooperative folding unit than HP35? For this purpose I will measure TTET under different solvent conditions and synthesize HP35 variants to test the effect on the N′/N equilibrium and its dynamics. In addition, I plan to place the TTET labels at different positions within HP35 to characterize local dynamics in different parts of HP35.

3 Material and Methods

3.1 Synthesis and purification of peptides and proteins

All poly-alanine helical peptides were synthesized on an Applied Biosystems 433A peptide synthesizer (Foster City, CA, USA) with standard fluorenylmethoxycarbonyl (Fmoc) chemistry. Synthesis was performed either on TentraGel S Ram resin or TentaGel R PHB-Ala Fmoc (Rapp Polymer, Tübingen, Germany) in a 0.1 mmol scale. In the *FastMoc* 0.10 mmol chemistry standard amino acids with Fmoc protected amino group were deployed in 10 fold excess, naphthylalanine and α,β-diaminopropionic acid (Dpr) in 5 fold excess. As activation reagent 0.45 M O-(benzotriazol-1-yl)-N,N,N′,N′-tetramethyluronium hexafluorophosphate (HBTU) in dimethylformamid (DMF) was used for all helical peptides. The coupling agent was 2M N,N-diisopropylethylamine (DIPEA) in NMP and deprotection was done in 20% (v/v) piperidin in 1-methyl-2-pyrrolidinone (NMP). By UV feedback monitoring the Fmoc deprotection was controlled at 301 nm and deprotection was repeated when the following value was more than 5% of the one before.

The villin headpiece subdomain varianta were synthesized on TentaGel R PHB-Gly Fmoc resin. In the *FastMoc* 0.10 mmol chemistry prolonged coupling times were introduced. The activation was done by 0.45 M O-(7-azabenzotriazol-1-yl)-N,N,N′,N′-tetramethyluronium hexafluorophosphate (HATU) in DMF and as coupling agent also 2M DIPEA in NMP was used. In addition to deprotection in 20% (v/v) piperidin in NMP also 48 % (v/v) DMF, 48 % (v/v) dimethylsulfoxid (DMSO), 2 % (v/v) piperidin, 2 % (v/v) 1,8-diazabicyclo[5.4.0]undec-7-en (DBU) was used to deprotect.

Introduction of the TTET acceptor naphthalene was done by incorporation of the non-natural amino acid 1-(L)-naphthylalanine by solid-phase peptide synthesis. If necessary acetylation of the N-terminus was achieved with shaking the resin four times for 10 min in 10 % (v/v) acetic anhydride, 10% (v/v) DIPEA in DMF. Succinylation

was done four times 30 min with 2mg succinylanhydrid, 3 µl 4-methylmorpholine (NMM) in 1,2 ml DMF.

The TTET donor 9-oxoxanthen-2-carboxylic acid was synthesized as described[167]. After selective deprotection of the Dpr side chain with 2 % (v/v) trifluoroacetic acid (TFA), 2% (v/v) triethylsilan (TES) in dichlormethan (DCM) coupling of xanthonic acid to the β-amino group of Dpr was done in threefold excess by benzotriazol-1-yloxy)tripyrrolidinophosphonium hexafluorophosphate (PyBOP) activation in presence of 5 equivalents NMM in DMF for 40 minutes. Under the same conditions the xanthonic acid was coupled to the N-terminus.

If necessary any remaining Fmoc group was cleaved four times 10 min in 20 % (v/v) piperidin in DMF and additionally three times 10 min in 48 % (v/v) DMF, 48 % (v/v) DMSO, 2 % (v/v) piperidin, 2 % (v/v) DBU. Cleavage of the peptide from the resin was done in 2.5 % (v/v) TES, 2.5 % (v/v) water in TFA for 2 h while stirring. The product was precipitated in ice-cold methyl tert-butyl ether, centrifuged and the pellet was lyophilized.

Prior to purification the pellet was resolubilized in TFA and diluted to approximately 15 % TFA, 15% acetonitrile in water. All peptides and proteins were purified from the resolubilized pellet by high-performance liquid chromatography (HPLC) on a 1200 series from Agilent Technologies in a acetonitrile/water gradient (0.1% TFA) on one of the following columns: Merck RP-8 (LiChrosopher 100, 250 x 25.0 mm, 4 µm), Phenomenex Jupiter Proteo (C12, 250 x 30 mm, 10 µm) or Phenomenex Kinetex (XB-C18, 250 x 21 mm, 5 µm). Purity to more than 98 % was checked by analytical HPLC on Phenomenex Jupiter Proteo (C12, 150x4.6 µm, 4 µm) or Phenomenex Kinetex (XB-C18, 250x4.6 µm, 5 µm) columns. All masses were verified by matrix-assisted laser desorption/ionization time of flight mass spectrometry (MALDI-TOF-MS). The protein was lyophilized and stored for further usage at -20°C.

3.2 Sample preparation

Measurements on helical peptides were done either in 5 mM cacodylic acid, pH7 or 10 mM potassium phosphate, pH 7 as indicated. For HP35 all measurements were performed in 10 mM potassium phosphate buffer, pH 7 at 5°C. All buffers and samples were filtrated prior usage with 0.2 µm pore size filters. Protein concentrations were

determined by absorbance spectroscopy on a diode array absorbance spectrometer 8453 from Agilent Technologies (Santa Clara, CA, USA) with the molar absorption coefficient of $\epsilon = 3900\ \mathrm{cm}^{-1}\ \mathrm{M}^{-1}$ of xanthonic acid.

Urea and GdmCl concentrations were checked by the refractive index measured on a automatic refractometer AR7 Series of Reichert (Depew, NY, USA). Calculation of the concentrations followed equation 3.1 with n being the refractive index with (n_D) and without (n_0) denaturant[168].

$$\mathrm{c_{urea}} = (n_\mathrm{D} - n_0) \cdot 117.66\frac{mol}{l} + (n_\mathrm{D} - n_0)^2 \cdot 29.753\frac{mol}{l} + (n_\mathrm{D} - n_0)^3 \cdot 185.56\frac{mol}{l} \tag{3.1a}$$

$$\mathrm{c_{GdmCl}} = (n_\mathrm{D} - n_0) \cdot 57.147\frac{mol}{l} + (n_\mathrm{D} - n_0)^2 \cdot 38.68\frac{mol}{l} + (n_\mathrm{D} - n_0)^3 \cdot 91.60\frac{mol}{l} \tag{3.1b}$$

Viscosities were determined with a HAAKE falling-ball viscometer Type C from Thermo Scientific (Waltham, MA, USA). The solution was temperated in a water bath (F20-HC) from Julabo Labortechnik GmbH (Seelbach, Germany). Temperature equilibration was allowed for 10 min prior measurement.

3.3 Spectroscopic measurements

CD spectra were recorded on a circular dichroism spectrometer Model 410 of Aviv biomedical, Inc. (Lakewood, NJ, USA). For wavelength scans a 1 mm cuvettes with 50 µM sample was used. If possible spectra were recorded from 180 nm to 250 nm in 1 nm steps over either four or eight scans with 5 s averaging time. Temperature transitions were measured in a 10 mm cuvette with 5 µM sample at 222 nm while stirring in 1°C steps with 60 s signal averaging after 2 min of temperature equilibration. Denaturant transitions were recorded in a 10 mm cuvette with 5 µM sample at 222 nm with 60 s signal averaging. The samples for denaturant transitions were prepared from a stock solution and measured. For all measurements the buffer signal was recorded under the same conditions and subtracted.

TTET was measured on a Laser Flash Photolysis Reaction Analyzer (LKS.60) from Applied Photophysics (Surrey, UK). Excitation was achieved by a Nd:YAG

laser (Brilliant from Quantel, Les Ulis France) with a 4 ns pulse length at 355 nm. Transient absorbance changes at 420 nm and 590 nm were recorded on an Agilent infiniium oscilloscope with 600 MHz and 4GSa/s over at least 5 half-life periods on a logarithmic time base. Four to eight traces were recorded for each measurement and averaged. As reference a sample of 50 μM xanthonic acid was measured at each day and all trace were normalized in relation to the amplitude.

For high pressure TTET experiments the setup was modified with a high-pressure cell system from ISS (Urbana-Champaign, IL,USA). The cell was equipped with Sapphire windows and a high pressure was generated by a manual pump using ethanol for pressure transmission. The high-pressure cell was installed in a home-built construction, which allows alignment of the cell in the light path of the instrument.

The sample concentrations for all TTET measurements were between 30 and 60 µM and all samples were degassed three times prior measurement.

3.4 Data evaluation with the three-state model

Data evaluation in helical peptides

In helical peptides the three-state model for local helix-coil dynamics coupled to TTET can be described by equation 3.2

$$H \underset{k_\mathrm{f}}{\overset{k_\mathrm{u}}{\rightleftharpoons}} C \xrightarrow{k_\mathrm{c}} C^* \tag{3.2}$$

which results in two observable rate constants (λ_1 and λ_2) and their corresponding amplitudes (A_1 and A_2). From these experimental parameters all rate constants (k_i) can be determined using the following equations[90,169]:

$$\lambda_{1/2} = \frac{k_u + k_f + k_c \pm \sqrt{(k_u + k_f + k_c)^2 - 4k_u k_c}}{2} \tag{3.3a}$$

$$A_1 = \frac{1}{\lambda_1(\lambda_1 - \lambda_2)}([C]_0 \cdot k_c \cdot (k_u - \lambda_1) + [H]_0 \cdot k_u \cdot k_c) \tag{3.3b}$$

$$A_2 = \frac{1}{\lambda_2(\lambda_1 - \lambda_2)}([C]_0 \cdot k_c \cdot (\lambda_2 - k_u) + [H]_0 \cdot k_u \cdot k_c) \tag{3.3c}$$

The urea-dependencies of the TTET kinetics were fitted globally using equations 3.2 and 3.3 and assuming a linear effect of urea on the logarithm of the rate constants for helix formation and unfolding[90] and on the rate constant for loop formation in unfolded polypeptide chains (Eq. 3.4)[83].

$$\ln k_i = \ln k_i^0 - \frac{m[urea]}{RT} \tag{3.4}$$

Pressure dependencies of the TTET kinetics were also fitted globally using equations 3.2 and 3.3 with the pressure-dependencies of the rate constants yielding the activation volumes $dV^{0\ddagger}$:

$$\frac{\delta \ln k}{\delta p} = -\frac{dV^{0\ddagger}}{RT} \tag{3.5}$$

All helical peptides, especially the strongly destabilized ones, show reduced amplitudes of the observable TTET kinetics compared to the traces of donor-only peptides, due to rapid loop formation in the unfolded state during the dead time of the instrument[82]. This effect is taken into account in the global fit by addition of the missing amplitude to the amplitude of the fast TTET process (A_2), which mainly represents TTET from the coil state[90].

In the absence of acceptor the intrinsic lifetime of the triplet state of a xanthonic acid is about 30 µs. In some traces an additional phase with less than 5 % amplitude and a lifetime corresponding to the donor-only protein is observed. This phase is not considered in further analysis as it is probably due to small amounts of aggregated peptides.

All data from TTET and CD experiments were evaluated using the program ProFit (QuantumSoft, Zurich, Switzerland).

Data evaluation in HP35

In HP35 the locked (N) and unlocked (N′) native state are in equilibrium. Local unfolding to a partially unfolded intermediate (I) only occurs from N′. After partial unfolding loop formation can occur and lead to TTET from xanthone to naphthylalanine (I*) (Eq.3.6).

$$N \underset{k_{\mathrm{l}}}{\overset{k_{\text{-l}}}{\rightleftharpoons}} \mathrm{N}' \underset{k_{\mathrm{cl}}}{\overset{k_{\mathrm{op}}}{\rightleftharpoons}} I \xrightarrow{k_{\mathrm{c}}} I^* \tag{3.6}$$

The intermediate I is a high energy intermediate that is only populated to small amounts. Thus a single rate constant k_T describes the energy transfer reaction from N′ (Eq. 3.7).

$$k_T = \frac{k_{op} \cdot k_c}{k_{cl} + k_c} \tag{3.7}$$

The experimental data exhibits two observable rate constants (λ_1 and λ_2) and their corresponding amplitudes (A_1 and A_2) and from these all rate constants (k_i) can be determined (Eq. 3.8).

$$\lambda_{1/2} = \frac{k_{-1} + k_1 + k_T \pm \sqrt{(k_{-1} + k_1 + k_T)^2 - 4k_{-1}k_T}}{2} \tag{3.8a}$$

$$A_1 = \frac{1}{\lambda_1(\lambda_1 - \lambda_2)}([\mathrm{N}']_0 \cdot k_T \cdot (k_{-1} - \lambda_1) + [N]_0 \cdot k_{-1} \cdot k_T) \tag{3.8b}$$

$$A_2 = \frac{1}{\lambda_2(\lambda_1 - \lambda_2)}([\mathrm{N}']_0 \cdot k_T \cdot (\lambda_2 - k_{-1}) + [N]_0 \cdot k_{-1} \cdot k_T) \tag{3.8c}$$

The pressure dependencewas fitted globally using equations 3.6 to 3.8 and equation 3.5.

A minor slow kinetic phase with less than 10 % amplitude is observed in the triplet decay curves, which corresponds to the intrinsic triplet lifetime of the donor-only protein and probably is due a small fraction of aggregated protein.

3.5 Monte Carlo Simulations based on a Linear Ising Model

All simulations were done in collaboration with Maren Bütter.

Simulations for the Test of the Diffusing Boundary Model for the Helix-Coil Transition in Peptides.

Monte Carlo simulations based on a linear Ising model were performed as described[90]. According to helix-coil theory, the helix is thus represented by a linear

sequence of 21 amino acid residues , which can be either in the helical (h) or a coiled state (c):

$$\mathbf{ccccchhhhhhhhhhhcccc} \tag{3.9}$$

We applied the Zimm-Bragg model[124], which accounts only for nearest neighbor interactions and used the kinetic extension of the model introduced by Schwarz[135]. This model describes helix elongation/shrinking, helix nucleation and coil nucleation by the following equations:

- Helix elongation:

$$hcc \underset{k_{-1}}{\overset{k_1}{\rightleftharpoons}} hhc \quad cch \underset{k_{-1}}{\overset{k_1}{\rightleftharpoons}} chh \qquad \frac{k_1}{k_{-1}} = s \tag{3.10}$$

- Helix nucleation:

$$ccc \underset{k_{-2}}{\overset{k_2}{\rightleftharpoons}} chc \qquad \frac{k_2}{k_{-2}} = \sigma s \tag{3.11}$$

- Coil nucleation:

$$hhh \underset{k_{-3}}{\overset{k_3}{\rightleftharpoons}} hch \qquad \frac{k_3}{k_{-3}} = \frac{\sigma}{s} \tag{3.12}$$

- Kinetic parameters:

$$\begin{aligned} k_2 &= \gamma_h \cdot \sigma \cdot k_1 \qquad & k_{-2} &= \gamma_h \cdot k_{-1} \\ k_3 &= \gamma_c \cdot \sigma \cdot k_{-1} \qquad & k_{-3} &= \gamma_c \cdot k_1 \end{aligned} \tag{3.13}$$

For all peptides 10^7 steps with $\Delta t' = 0.05$ were simulated and k_1 was set to 1. Values of s =1.31 or s =1.17 were used for analysis at the N-terminus and in the centre, respectively. The nucleation parameter σ was set to 0.003 and the kinetic parameters to $\gamma_h = \gamma_c$ =2. The start conformations were taken from an equilibrated ensemble of helices. The folding and unfolding dynamics were analyzed by computing first-passage-times (FPTs). Since the experiments probe a region of five residues between the labels we adapted the simulation procedure to monitor the dynamics of larger segments instead of single site fluctuations. A segment of five residues was counted as helical if at least four of its residues were helical at a certain time. In contrast

to previous work[90], we constrained the start conformations by the condition, that at least 1 residue of the peptide should be in the H state. This constraint reduces the number of simulations, in which the peptide has to nucleate before helix growth and shrinking occur and thus improves the statistics of the boundary diffusion process. Helix nucleation will also not be observed in TTET experiments, since loop formation in the all-coil state is presumably much faster than helix nucleation. For each event and position, 10^5 FPTs were collected and stored in 100 bins, adjusted to the longest observed FPT. The distribution of the FPTs were fitted by single-exponential functions yielding the reduced rate constants of local helix folding and unfolding k_f/k_1 and k_u/k_1. Ten simulations were averaged to obtain a more accurate determination of the reduced rate constants. The best agreement between simulations and experiment for the length-dependence was obtained by scaling with $k_1 = 1.2 \cdot 10^7$ and s-values of 1.17 for centrally labeled peptides and 1.31 for N-terminally labeled peptides. The difference in s-values between N-terminally and centrally labeled peptides is probably due to the different location of the labels in the peptide. The TTET labels destabilize the helix more strongly in the center compared to the ends[98], which decreases the average s-value, used in our simulations. The best agreement between simulations and experimental data for the effect of N-capping on helix dynamics in the center was obtained with $k_1 = 7.6 \cdot 10^6$ and s=1.17. In simulations addressing the capping effects the s-value at positions 1 to 4 was varied between 0.1 and 2 by varying k_u. Since the first residue always remains in the coil state no adjustment is needed for this residue.

All simulations were performed using the framework of Matlab R2011 and R2012 (Math-Works) in combination with compiled C code for time-consuming iterations.

Simulations on effect of pressure on the elementary rate constants

The Monte Carlo simulations to reveal the effect of pressure on the elementary rate constants for helix elongation and shrinking was done as described before with some changes. As we used a helical peptide with a destabilizing N-cap, we distinguished the general s-value of the positions 5 to 21 from the s-value for the N-terminal cap assigned to positions 2 to 4 as before. To determine optimal s-values, we applied an optimization method using the Matlab *fminsearch* algorithm[170]. In contrast the procedure discribed before, the time step $\Delta t' =$ is 10-fold smaller to resolve the capping effects in simulations with s-values close to 1.

We introduced an optimization method to estimate the s-values from a given set of experimentally determined equilibrium constants at different pressures using the Matlab *fminsearch* algorithm. The simulation generates a pair of reduced rate constants k_f/k_1 and k_u/k_1, which allows to compute the equilibrium constant K_{eq}. The procedure was repeated 10 times and the output k_f/k_1, k_u/k_1 and K_{eq} were averaged each. Then, the difference in the logarithms of simulated and experimentally determined K_{eq}-values was minimized using *fminsearch* by varying the general s-value. The s-value of the N-cap was fixed at 0.1 since small variations of the N-cap s-value have only minor effects on K_{eq}. As the simulation exhibits a considerable statistical error especially for s-values less than 1.1, we extrapolated the experimental equilibrium constants up to p=2000 MPa and computed $\ln(K_{eq})$ in 50 MPa steps from 0.1 to 500 MPa and in 100 MPa steps to 2000 MPa.

In the next step we scaled the reduced rate constants from the simulations to the experimentally determined rate constants with the scaling factor (SF). According to the model in equations 3.10 to 3.13, this factor denotes the elementary rate constant for helix growth, k_1. To find the SF for both k_u and k_f, we employed the *fminsearch* algorithm again assuming a linear pressure-dependence of ln(SF). The elementary rate constant for helix shrinking, k_{-1} was obtained from the s-value and k_1 using Eq. 3.10.

4 Results and Discussion

4.1 Testing the Diffusing Boundary Model for the Helix-Coil Transition in Peptides.

This chapter was published 2013 in Neumaier et al.[171].

Folding and unfolding dynamics of α-helices play a prominent role in folding and other physiologically important conformational transitions in proteins. In polyalanine-based model peptides the structure and dynamics of α-helices can be investigated in the absence of tertiary interactions which yields information on intrinsic helix properties[97]. Experimental and theoretical work showed that a linear Ising model is able to describe the equilibrium properties of the helix-coil transition both in long homopolymers and in short model peptides[98,124,125,129,130,136]. The kinetic mechanism of helix-coil dynamics has long been under debate. Temperature jump-induced unfolding experiments on short, Ala-based helices showed that global unfolding occurs on the hundreds of nanoseconds time scale[137,138]. In a previous study we applied triplet-triplet energy transfer (TTET) to investigate local folding and unfolding dynamics at different positions in a 21-amino acid Ala-based α-helix at equilibrium[90]. The results revealed a position-independent helix elongation time constant ($1/k_f$) of about 400 ns at 5° C and a position-dependent helix unfolding rate constant with faster unfolding at the termini ($1/k_u$ =250 ns) compared to the center ($1/k_u$ =1.4 μs). This behavior could be reproduced in simulations using a kinetic version of the linear Ising model[90,135], which suggested that helix elongation and unfolding mainly occur via a diffusing boundary mechanism, i.e. by the movement of the helix-coil boundary along the polypeptide chain. Helix nucleation in a completely unfolded chain and coil nucleation within a helical region are rare events in short model helices[90]. The helix-coil boundary is statistically more likely located near the peptide ends than near the center[90,98]. Thus it takes on average longer for the moving helix-coil boundary to reach

the helix center than the helix ends, which leads to the observed position-dependence of helix unfolding.

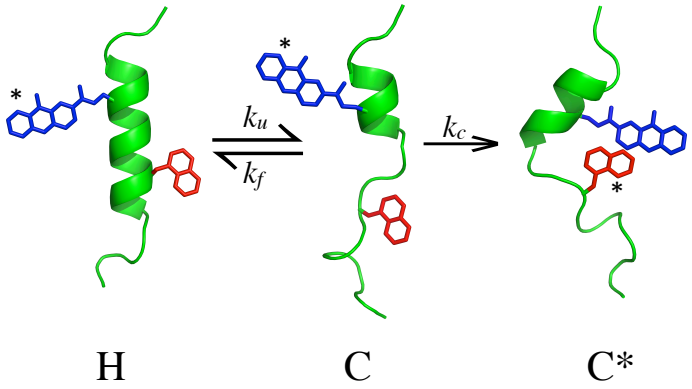

Figure 4.1: Schematic representation of TTET coupled to a helix-coil equilibrium. The triplet labels xanthonic acid (Xan, blue) and 1-naphthylalanine (Nal, red) are placed in the helix with i,i+6 spacing.

Here we use TTET to test the diffusing boundary mechanism and to investigate, whether diffusion of the helix-coil boundary along the polypeptide chain can be described by a classical, Einstein-type one-dimensional diffusion process. We further tested for local and non-local effects of changes in helix stability on folding and unfolding dynamics in different regions of α-helical peptides. The triplet donor xanthonic acid (Xan) and the acceptor naphthylalanine (Nal) were attached to helical peptides in i,i+6 spacing which places them on opposing sides of the helix and prevents TTET in the helical state (H, Fig. 4.1)[90]. When the helical structure between the labels is unfolded or partially unfolded (C conformations in Fig. 4.1) TTET can occur by van der Waals contact to the state C*. Since TTET between these groups is an irreversible process[29,76,77], the overall reaction can be described by the three-state model shown in figure 4.1. If helix-coil dynamics (k_f and k_u) and loop formation in the unfolded state (k_c) occur on a similar time scale, the observable rate constants for TTET and their corresponding amplitudes yield the rate constants for local helix formation and unfolding between the labels, k_f and k_u, as well as the rate constant for loop formation (k_c)[90] (see section 3.4). In addition, the local equilibrium constant (K_{eq}) for helix formation in the region of the labels can be calculated from $K_{eq} = k_f/k_u$. It should be noted that TTET experiments do not require perturbation of the helix-coil equilibrium and thus yield information on equilibrium fluctuations of the system.

Our results show that boundary diffusion in helical peptides can be described by a classical, one-dimensional diffusion process. Non-local effects of changes in helix stability exclusively affects the dynamics of helix unfolding, whereas helix formation is unchanged. Locally, in contrast, changes in helix stability alter both folding and unfolding dynamics with a Φ_f-value of about 0.35.

4.1.1 Effect of peptide length on helix folding and unfolding dynamics

As in our previous work[90] we studied alanine-based helical peptides with arginine residues introduced with i,i+5 spacing to increase solubility[97], which yields the canonical sequence Ac-AAAAA(AAARA)$_n$A-NH$_2$. Labels were inserted with i,i+6 spacing, which prevents TTET in the helical state (Fig. 4.1). The triplet donor 9-oxoxanthene-2 carboxylic acid (xanthonic acid, Xan) was attached to the side chain of the non-natural amino acid α,β-diaminopropionic acid via an amide bond and the non-natural amino acid 1-naphthylalanine (Nal) was introduced as triplet acceptor (Figs. 4.1 and 4.2).

Our previous results suggested that the experimentally observed position-dependence of helix formation and unfolding dynamics originates in a boundary diffusion mechanism that can be described by a kinetic linear Ising model[90,135] (see section 1.3.2 and 3.5 for a detailed description of the model). The boundary diffusion model predicts that the unfolding rate constant in the center of a helix is sensitive to helix length due to varying boundary diffusion distances. Unfolding at the termini and helix formation, in contrast, should be independent of helix length. To test this prediction we synthesized helical peptides of different length between 16 and 41 amino acids and placed the TTET labels either in the center of the peptide or at the N-terminus (Figs. 4.2 A,E). Shorter peptides did not form helices that are stable enough to yield reliable results on k_u and k_f. The far-UV CD spectra of all peptides display typical helical bands with a maximum of the ellipticity at 190 nm and minima at 208 nm and 222 nm (Figs. 4.2 B, F). A quantitative analysis of the helix content using the signal at 222 nm would be inaccurate as the TTET labels have CD bands in the far UV region. Our previous results showed that the average helical content of the centrally labeled 21-amino acid peptide is about 60 %[90,98], which suggests that the average helical content of the peptides is approximately between 35 % (16-mer) and 75 % (41-mer).

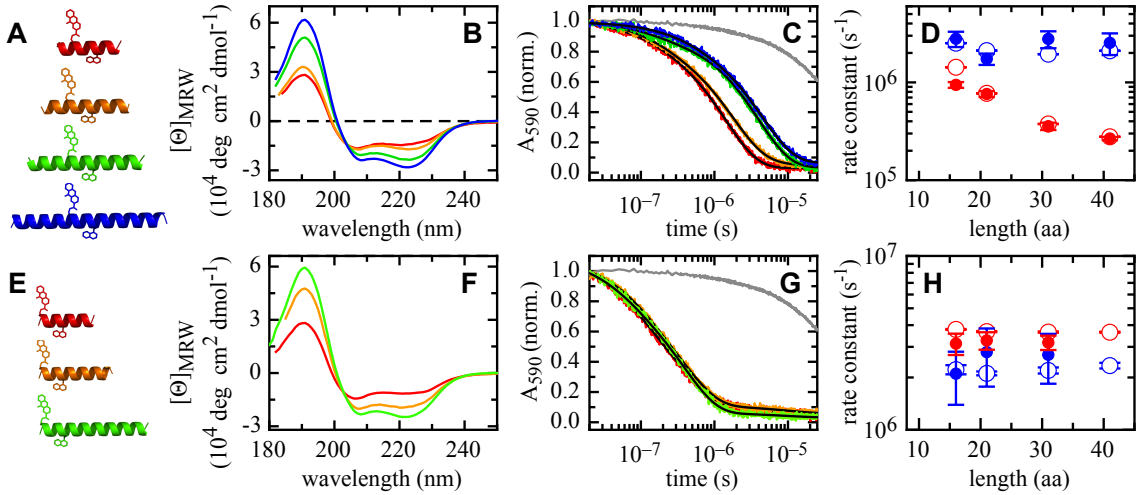

Figure 4.2: Effect of peptide length on local helix dynamics and stability. Peptides were labeled with the triplet donor/acceptor pair xanthone/naphthylalanine either in the center (A-D) or at the N-terminus (E-H). Far-UV CD spectra (B, F) and triplet decay curves of xanthone monitored by the change in absorbance at 590 nm (C, G) are displayed. The colors in the plot correspond to the colors of the helical peptides in panels A and E. The grey line represents the triplet decay for a donor-only peptide as a reference. The black lines represent double exponential fits to the kinetics. In some traces an additional phase with less than 5 % amplitude and a lifetime corresponding to the donor-only helix is observed. This phase is not considered in further analysis as it is probably due to small amounts of aggregated peptides. A global fit using the analytical solution of the three state model (Fig. 4.1) to the data yielded the rate constants for helix formation (k_f), unfolding (k_u) and loop formation (k_c). Panels D and H show the length dependence of k_f (blue) and k_u (red) in the helix center and at the N-terminus, respectively. The results are summarized in table 4.1. The experimental data (filled circles) agree well with results from Monte Carlo simulation (open circles) based on the linear Ising model (see section 3.5).

The increase in the strength of the CD band at 222 nm with increasing peptide length (Figs. 4.2 B, F; table 4.1) indicates a higher average helical content and thus on average longer helices in longer peptides in agreement with previous studies[132]. The labels destabilize the helix due to their lower helix propensity compared to Ala[90]. Centrally labeled peptides form less stable helices compared to the corresponding N-terminally labeled variants, in agreement with Lifson-Roig theory and with previous experimental results[98].

TTET kinetics were monitored by the decay of the xanthone triplet absorbance band at 590 nm. All peptides exhibit double exponential Xan triplet decay curves, indicating that both the helical state and the coil state are populated to detectable amounts at equilibrium (Fig. 4.2). An additional very fast kinetic phase is observed within the dead-time of the TTET experiments, which is due to fast loop formation

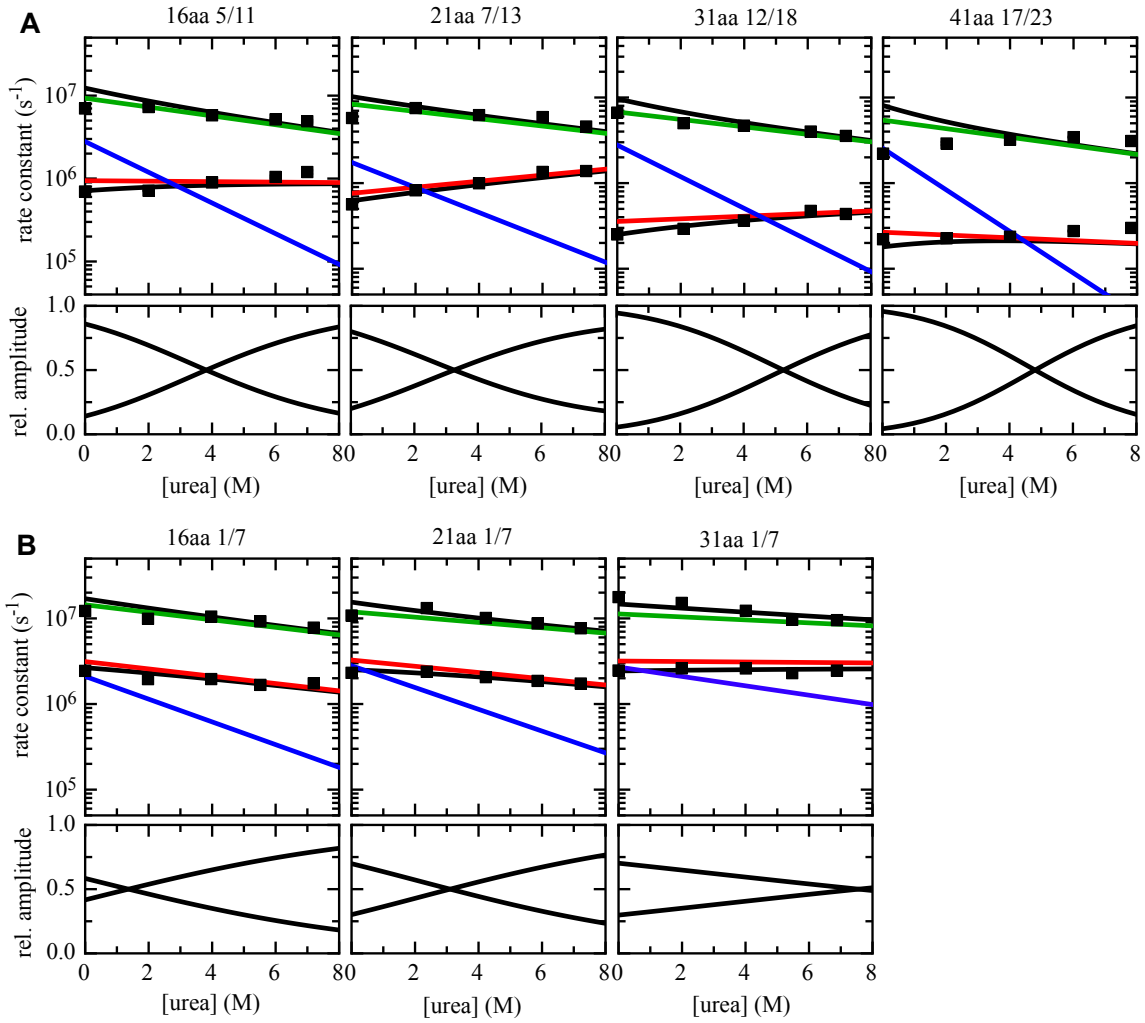

Figure 4.3: Urea dependence of the local dynamics in helical peptides of different length labeled in the center. The two observable rate constants $\lambda_{1,2}$ (squares) of single trace double exponential fits are shown. Global fitting of all traces yields the observable rate constants and relative amplitudes (black lines) as well as all microscopic rate constants, k_u (red), k_f (blue) and k_c (green). The measurements were performed in in 10 mM potassium phosphate buffer, pH 7 at 5°C with a peptide concentration of about 50 µM.

in the coil state in a subset of conformations[82]. Figure 4.2 C shows that TTET in the central region of the helical peptides becomes slower in longer peptides, whereas TTET in the N-terminal region is virtually independent of peptide length (Fig. 4.2 G). The data were fitted using the analytical solution of the three-state model shown in Figure 4.1 (see section 3.4) to obtain k_f, k_u and k_c[82]. All peptides, especially the strongly destabilized ones, show reduced amplitudes of the observable TTET kinetics compared to the traces of donor-only peptides, due to rapid loop formation in the unfolded state during the dead time of the instrument[82]. This effect is taken into account in the global fit by addition of the missing amplitude to the amplitude of the fast TTET process (A_2), which mainly represents TTET from the coil state[90]. The quality of the fits improves by performing a urea-dependence of the TTET kinetics and globally fitting all kinetic traces (Fig. 4.3) to the three-state model assuming a linear effect of urea on the logarithm of the rate constants for helix formation and unfolding[90] and on the rate constant for loop formation[83](Eq. 4.1).

$$\ln k_i = \ln k_i^0 - \frac{m[urea]}{RT} \tag{4.1}$$

Figures 4.2 D and 4.2 H show the effect of peptide length on k_f and k_u. Helix formation is independent of peptide length, both in the center (Fig. 4.2 D) and at the N-terminus (Fig. 4.2 H). Helix unfolding in the center, in contrast, becomes slower with increasing peptide length (Fig. 4.2 D) whereas unfolding at the N-terminus is unchanged (Fig. 4.2 H). As a result, increasing peptide length increases helix stability in the central region of the peptide, but does not affect helix stability at the N-terminus (Tab. 4.1). The rate constant for loop formation, k_c, slightly decreases with increasing peptide length (Tab. 4.1). This effect is stronger for the centrally labeled peptides compared to the N-terminally labeled peptides, in agreement with our previous results on the effect of tails on the dynamics of loop formation[30].

To quantitatively compare the experimental results with predictions from the kinetic linear Ising model, we performed Monte-Carlo simulations as described in section 3.5. The simulation procedure was slightly modified to obtain better statistics for the folding and unfolding transitions. The Monte Carlo simulations yield mean first passage times (MFPT) for helix unfolding and formation in the region between the labels. The rate constants k_f and k_u were determined from the distribution of MFPTs by fitting the data to a single exponential decay (Fig. 4.4). Both in the center

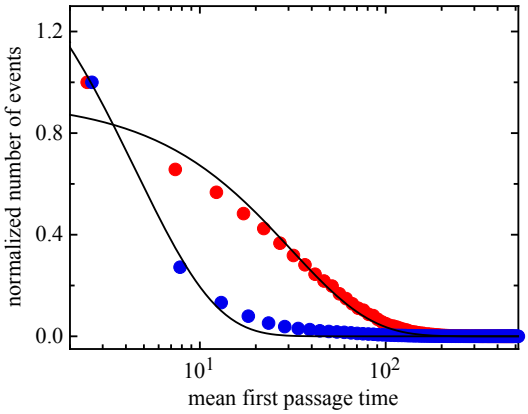

Figure 4.4: Histogram of first passage times for local unfolding (red) and folding (blue) in the center of a peptides of 21 amino acids length with s = 1.17. Only conformations with at least one helical residue were considered as starting conformations. The lines represent single exponential fits.

and at the N-terminus the simulations yield the same effect of peptide length on k_u, k_f and K_{eq} as the TTET measurements (Figs. 4.2 D, H). The data from experiments and simulations on all centrally labeled peptides can be quantitatively brought into agreement with rate constants for the elementary steps of helix elongation (k_1) and helix shrinking (k_{-1}) of $1.20{\cdot}10^7$ s^{-1} and $1.03{\cdot}10^7$ s^{-1}, respectively, which results in a s-value of 1.17 ($s{=}k_1/k_{-1}$, Eq. 3.10 and the description of the model in section 3.5). For the N-terminally labeled peptides agreement is achieved with $k_1{=}1.20{\cdot}10^7$ s_{-1} and $k_{-1}{=}$ $9.16 \cdot 10^6$ s_{-1}, resulting in a s-value of 1.31. The difference in s-values between N-terminally and centrally labeled peptides is probably due to the different location of the labels in the peptide. The TTET labels destabilize the helix more strongly in the center compared to the ends[98], which decreases the average s-value, used in our simulations. It should be noted that the elementary rate constants k_1 and k_{-1} represent the elementary steps for adding (k_1) and removing (k_{-1}) a single helical segment at the helix-coil boundary in the linear Ising model (Eq. 3.10 to 3.13). The rate constants k_f and k_u, in contrast, represent the rate constants for helix formation and unfolding in the region between the TTET labels and characterize the transition between conformations which have the helix formed between the labels (H) and conformations which allow TTET (C, Fig. 4.1).

A T-jump study on helix unfolding found that different s-values are required to describe the stability of helical peptides with varying length[133]. In our study, in contrast, the same s-value describes the behavior of the different length peptides,

which is in agreement with previous results by Rohl et al.[132] and with the Lifson Roig model. This discrepancy is likely due to the application of a two-state model to calculate rate constants for helix formation from T-jump unfolding experiments[133], which is not valid, since the helix-coil transition is a multi-state process[98,125,129,135,137].

The observed effect of helix length on unfolding dynamics in the peptide center is expected if helix unfolding occurs by one-dimensional diffusion of the helix-coil boundary. Increasing helix length increases the average diffusion distance from the helix-coil boundary to the helix center and thus the helix-coil boundary takes longer to reach the central region. This mechanism is equivalent to a one-dimensional diffusion process with two boundaries moving, each from one end. To test whether motion of the helix-coil boundary can be described by a Einstein-type, one-dimensional diffusion process, we analyzed the effect of the diffusion distance on the rate constant of helix unfolding. For a classical one-dimensional diffusion mechanism with diffusion from two sides the survival probability (S) for a helical segment in the center can be approximated by an exponential function[171]

$$S = e^{-\frac{4Dt}{< l^2 >}} = e^{k_u t} \tag{4.2}$$

where D represents an upper limit for the diffusion coefficient for one boundary and $< l^2 >$ is the average distance from the helix-coil boundary to the helix center. Equation 4.2 results in a modified Einstein equation for the relationship between diffusion distance of the boundary and the observed unfolding rate constant (Eq. 4.3).

$$< l^2 >= \frac{4D}{k_u} \tag{4.3}$$

For the calculation of $(< l^2 >)$ we considered that the N- and C-terminal residues are not in a helical conformation[124,125,129] and assumed the average helix-coil boundaries at residue 2 and n-1[90,98]. We further assumed that four helical segments between the labels in the center have to unfold for TTET to occur[90]. The plot of $< l^2 >$ vs. $1/k_u$ is linear (Fig. 4.5), which shows that helix-coil boundary diffusion in helical peptides follows a classical one-dimensional diffusion law. The slope of the plot yields D=$3.0 \cdot 10^7$ aa^2/s (Eq. 4.3) with $< l >$ given in units of amino acids (aa). The simulations reveal that unfolding in the central region of the helix contains increasing

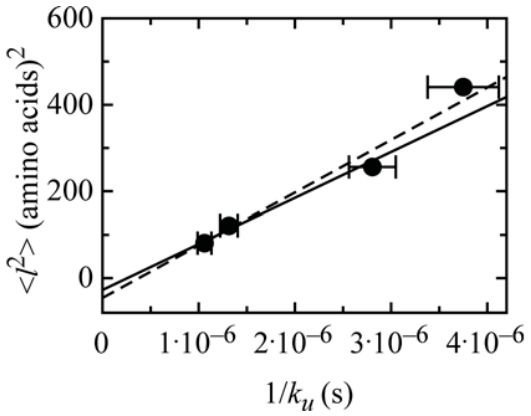

Figure 4.5: Correlation between the distance of boundary diffusion and the time constant for helix unfolding. The average diffusion distances, l, of the boundaries were calculated between position 2 and the C-terminal label (Nal) for diffusion from the N-terminus and between position n-1 and the N-terminal label (Xan) for diffusion from the C-terminus and are given in number of amino acids. Data for the centrally labeled peptides shown in Figure 4.2 are plotted. The plot of l^2 vs. $1/k_u$ is linear with a slope of $1.2 \cdot 10^8$ aa^2/s indicating that boundary diffusion can be described by equation 4.2 with D=$3.0 \cdot 10^7$ aa^2/s (dashed line). The solid line represents a fit of Eq. 4.3 to the data for the three shortest helices yields D=$2.7 \cdot 10^7$ aa^2/s.

contributions from coil nucleation with increasing helix length, which results in two separate helical segments (Fig. 4.6). This mechanism occurs in addition to boundary diffusion and increases the observed rate constant for helix unfolding in the central region. The simulations reveal that in the 41-mer only about 50% of helix unfolding events in the peptide center occur by boundary diffusion of a single helical segment compared to about 95% in the 21-mer (Fig. 4.6 C). This result shows that the single-sequence approximation, which assumes a single contiguous helix[129], does not hold for the unfolding kinetics in the center of the 41 amino acid peptide. Frequent helix unfolding by coil nucleation in the helix center of the longest helical peptide leads to faster unfolding in the center than expected from the diffusing boundary model. The good agreement between experimental unfolding rate constants and simulations for all peptides indicates that coil nucleation also contributes to the observed TTET kinetics. At equilibrium, however, about 90% of all helices formed in the 41-mer have a single helix, in accordance with the single sequence approximation (Fig. 4.6). The comparison between equilibrium and kinetic effects shows that coil nucleation occurs in the center of longer helices, but two isolated helices are not very stable, i.e. they rapidly re-form a single helix. The length-dependence of k_u for the three shortest pep-

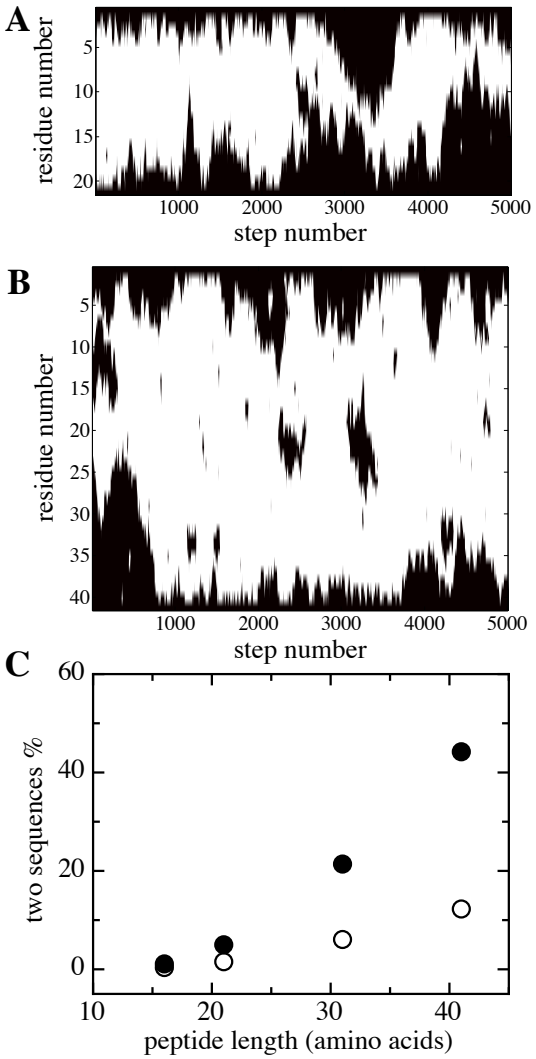

Figure 4.6: Typical time course of a simulation of helical peptides with 41 residues (A) and 21 residues (B). Black segments depict residues in the coil state, white segment depict helical conformation. Comparison of the simulations shows that coil nucleation in the helix center occurs more frequently for the 41-mer (C) Effect of peptide length on the percentage of coil nucleation events in the region of the TTET labels in the helix center (filled circles) which leads to TTET in addition to boundary diffusion. Further, the equilibrium fraction of helical peptides with two helical segments is shown (open circles).

tides, in which boundary diffusion is the dominant process, yields D =2.7·10^7 aa^2/s or 6.1·10^{-9} cm^2/s, with an axial translation of 1.5 Å/aa in an α-helix (Fig. 4.5). This value is low compared to free diffusion of small molecules and of globular proteins. At 5°C, sucrose has a diffusion coefficient of about 2.5·10^{-6} cm^2/s and small globular proteins like ribonuclease and lysozyme have diffusion coefficients around 7·10^{-7} cm^2/s[172]. This indicates that boundary diffusion in an α-helix encounters barriers, which are probably due to steric effects and to opening/closing of hydrogen bonds during helix growth and shrinking. Helix boundary diffusion is, however, as fast as the fastest reported one-dimensional diffusion processes of DNA-binding proteins along double-stranded DNA, for which diffusion coefficients in the range of 10^{-12} cm^2/s and 10^{-8} cm^2/s were determined at room temperature, corresponding to a range from 10^3 bp^2/s to 10^7 bp^2/s[173–175].

length (aa)	Label position	k_u (10^6 s^{-1})	k_f (10^6 s^{-1})	k_c (10^6 s^{-1})	K_{eq}
16	5/11	0.94±0.06	2.8±0.5	9.3±0.3	3.0±0.6
21	7/13	0.76±0.05	1.7±0.2	8.3±0.1	2.3±0.3
31	12/18	0.36±0.03	2.8±0.5	6.8±0.2	7.8±1.7
41	17/23	0.27±0.01	2.5±0.6	5.4±0.3	9.5±2.4
16	1/7	3.1±0.4	2.1±0.7	14.4±3.0	0.7±0.2
21	1/7	3.2±0.4	2.8±1.0	11.9±3.5	0.9±0.3
31	1/7	3.2±0.3	2.7±0.9	11.3±3.2	0.9±0.3

length (aa)	Label position	m_u (J/(molM))	m_f (J/(molM))	m_c (J/(molM))	Amiss	Θ^a_{222} (%)
16	5/11	15±70	986±131	284±82	32	-14300
21	7/13	-187±77	776±111	227±52	24	-17100
31	12/18	-81±57	985±101	262±89	15	-23300
41	17/23	86±105	1292±181	266±165	13	-28100
16	1/7	228±88	708±151	234±65	43	-11500
21	1/7	194±89	677±167	166±89	37	-19200
31	1/7	15±70	166±89	93±94	35	-24800

Table 4.1: Effect of helix length on stability and dynamics in different regions of an α-helical peptide. The canonical sequence for the helices is Ac-AAAAA(AAARA)$_n$A-NH$_2$ with n=2-7. The triplet labels xanthone (Xan) and naphthylalanine (Nal) were introduced at the indicated positions and span either the N-terminal region or the central region of the helix (see figure 4.1). Xan was always placed N-terminal of Nal. [a] θ_{222} represents the CD signal at 222 nm and is indicative of the overall helical content. It is given in units of deg cm^2 dmol^{-1}.

4.1.2 Effect of capping motifs on helix stability and dynamics in the peptide center.

Specific N- and C-capping motifs are frequently found in protein α-helices[119,176,177] and were shown to increase helix stability by favorably interacting with the helix dipole[178–180] or by forming side-chain to backbone hydrogen bonds[94,116,119]. To investigate the effect of stabilizing the helix termini on helix dynamics in the central region we made several stabilizing or destabilizing sequence variations at the termini of the 21 amino acid Ala-based peptide (Tab. 4.2). Fig. 4.7 A compares the effect of the different N- and C-terminal sequences on global helix stability as judged by the CD signal at 222 nm and reveals large effects on the global helix content (Tab. 4.2). Especially, free N- or C-termini lead to a major destabilization of the helix, whereas stabilization of the helix dipole by succinylation of the N-terminus has a strongly stabilizing effect, as previously observed for the C-peptide derived from the N-terminal helix of RNase A[123].

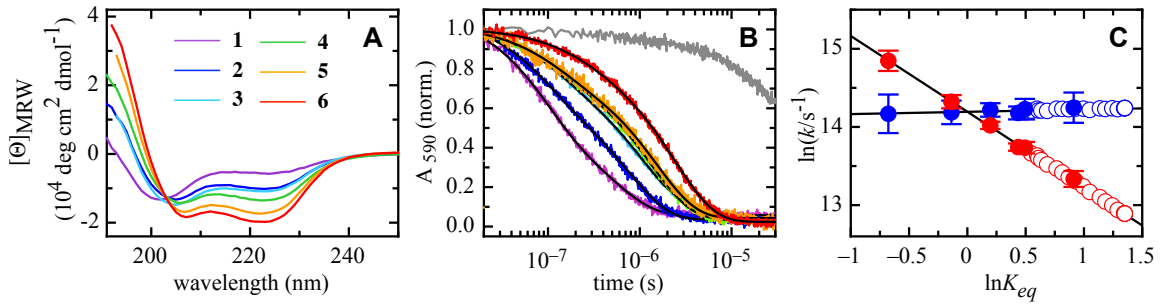

Figure 4.7: Effect of end capping motifs on local dynamics and stability in the peptide center. Local helix-coil dynamics in the center of a 21 amino acid helical peptide measured by TTET between residues 7 (Xan) and 13 (Nal). (A) Far-UV CD spectra and (B) xanthone triplet decay monitored by the absorbance change at 590 nm for peptides with different N- or C-capping motifs. The numbers of the peptides correspond to the numbers in table 4.2. The gray line in panel B represents the donor only reference. The black lines represent double exponential fits to the data. In some traces an additional phase with less than 5 % amplitude and a lifetime corresponding to the donor-only helix is observed. This phase is not considered in further analysis as it is probably due to small amounts of aggregated peptides. The results of the fits are given in table 4.2. (C) Leffler plots of helix growth (k_f; blue) and unfolding (k_u; red) (Eq. 4.4). Experimental data (closed circles) and results from simulation (open circles) are shown.

TTET kinetics in the peptide center become slower with increasing helix stability induced by favorable capping motifs (Fig. 4.7 B). The global fit of the urea-dependence of the TTET kinetics (Fig. 4.8) gave the values of k_f, k_u, k_c and K_{eq}

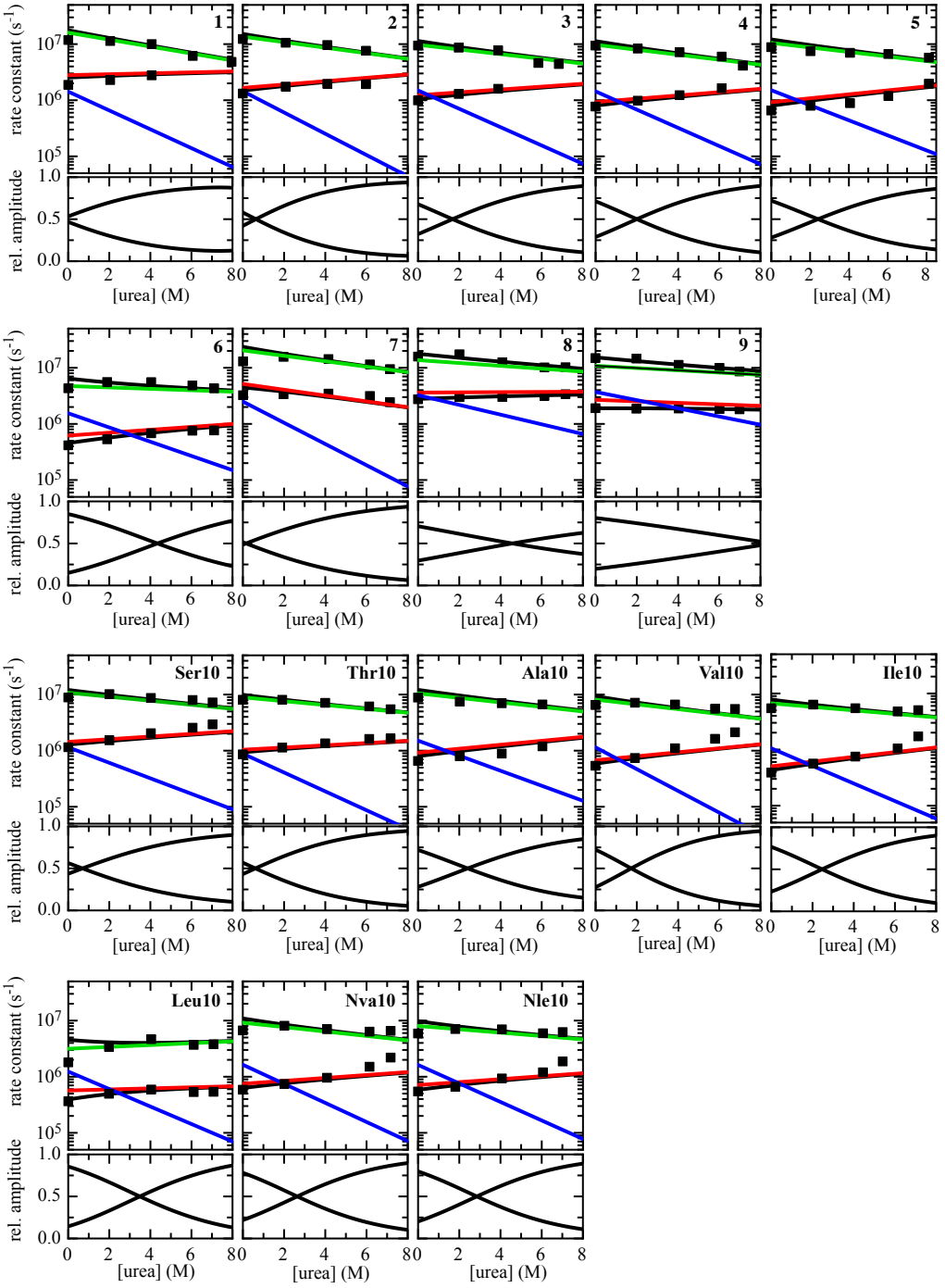

Figure 4.8: Urea dependence of the local dynamics in the different helices investigated in this study. The names of the peptides are indicated in each panel and correspond to the peptides in tables 4.2 and 4.3. The two observable rate constants $\lambda_{1,2}$ (points) of single trace double exponential fits are shown. Global fitting of all traces yields the observable rate constants and relative amplitudes (black line) as well as all microscopic rate constants, k_u (red), k_f (blue) and k_c (green). The measurements were performed in in 5 mM cacodylic acid buffer, pH 7 at 5°C with a peptide concentration of about 50 µM.

shown in table 4.2. Stabilizing the termini slows down helix unfolding (k_u) in the central region of the peptide but has virtually no effect on helix growth (k_f) leading to helix stabilization in the center. To quantify the effect of changes in helix stability on the folding and unfolding dynamics we used the Leffler relationship (Φ-value analysis) which correlates the effect of changes in equilibrium free energy of a reaction (ΔG^0) with the corresponding effect on the free energies of activation ($\Delta G^{0\ddagger}$)[9,36,181].

$$\Phi_f = \frac{\delta\Delta G_f^{0\ddagger}}{\delta\Delta G^0} = \frac{\delta\ \ln k_f}{\delta\ \ln K_{eq}}, \qquad \Phi_u = \frac{\delta\Delta G_u^{0\ddagger}}{\delta\Delta G^0} = \frac{\delta\ \ln k_u}{\delta\ \ln K_{eq}} = 1 - \Phi_f \tag{4.4}$$

The Leffler plot for the effect of helix capping groups on the rate constants for helix folding/unfolding in the peptide center is shown in Figure 4.7 C. The Leffler plot yields a Φ_f-value of 0.03±0.16. The error is large due to the errors in the k_f-values, which depend on k_u and on the amplitudes of the fast and slow phase in TTET (Fig. 4.8). The k_u-values are more accurate, since they are nearly exclusively reflected by the rate constant of the slower observable kinetic phase in TTET (Fig. 4.8). The corresponding Leffler plot for unfolding yields Φ_u-value of 0.97±0.08, confirming the result that only the helix unfolding rate constant in the peptide center is affected by changes in the stability at the termini but not the folding rate constant. All helix capping variants fall on the same line in the Leffler plot indicating that changes in stability at the N- or the C-terminus have the same effect on helix dynamics, which suggests that boundary diffusion is identical from both directions. The overall stability difference in the central region between the most and the least stable helices is only about 2 kJ/mol, which would not yield reliable results in a classical, two-point Φ_f-value analysis. However, the use of data from many variants in this stability range increases the accuracy of the analysis[182,183].

These results from TTET experiments were compared to results from the kinetic linear Ising model, with varying local helix stability at the N-terminus (see section 1.3.2 and 3.5). In the simulations the capping motifs were assumed to change the stability of residues 1 to 4, which were given the same s-value ($s = k_1/k_{-1}$, see section 1.3.2 and 3.5) between 0.1 and 2. The k_u-, k_f- and K_{eq}-values in the helix center from the simulations agree well with the experimental results and also give a Φ_f-value of 0.03 (Φ_u=0.97) (Fig. 4.7 C).

In summary, both experiment and simulations show that increasing helix length and stabilizing the terminal regions of an α-helix do not affect k_f but slow down helix

unfolding in the center of a helical peptide. These results demonstrate that non-local effects play an important role in modulating stability and dynamics of α-helices.

#	Label position	N-cap	C-Cap	k_u (10^6 s^{-1})	k_f (10^6 s^{-1})	k_c (10^6 s^{-1})
1	7/13	$^{+}NH_3$-AAA	A-NH2	2.8±0.4	1.4±0.4	16.0±2.2
2	7/13	$^{+}NH_3$-TAA	A-NH2	1.7±0.1	1.4±0.2	13.6±1.6
3	7/13	Ac-AAA	A-H	1.2±0.6	1.5±0.1	9.7±0.8
4	7/13	Ac-AAS	A-NH2	0.93±0.04	1.4±0.1	9.7±0.9
5	7/13	Ac-AAA	A-NH2	0.92±0.07	1.5±0.2	10.5±1.6
6	7/13	Suc-AAA	A-NH2	0.62±0.06	1.5±0.3	4.7±1.8
7	1/7	$^{+}NH_3$-XanAA	A-NH2	5.2±0.7	2.5±0.8	20.5±3.4
8	1/7	Ac-XanAA	A-NH2	3.6±0.2	3.3±0.5	13.7±2.0
9	1/7	Suc-XanAA	A-NH2	2.6±0.1	3.7±0.6	10.9±1.8

#	m_u (J/(molM))	m_f (J/(molM))	m_c (J/(molM))	K_{eq}	Amiss (%)	Θ^a_{222}
1	-43±171	894±286	330±36	0.5±0.1	59	-5600
2	-159±159	1010±238	263±34	0.9±0.1	46	-10100
3	-136±66	871±98	223±27	1.2±0.1	29	-10900
4	-156±67	865±94	237±29	1.5±0,1	32	-13500
5	-187±96	714±137	215±42	1.6±0.2	11	-17400
6	-139±85	672±129	66±113	2.5±0.5	8	-19700
7	277±127	1008±200	258±50	0.5±0.2	70	-18800
8	-10±52	461±104	136±45	0.9±0.2	34	-18800
9	72±29	389±75	107±57	1.4±0.2	15	-20500

Table 4.2: Effect of end capping motifs on stability and dynamics in the center and at the N-terminus of a 21 amino acid α-helical peptide. The canonical sequence for helices 1 to 6 is N-cap-AAAXanARAAANalRAAAARA-C-cap. The canonical sequence for helices 7 to 9 is N-cap-AAANalARAAAARAAAARA-C-cap. The numbers give the position of the TTET labels. Xan was always placed N-terminally of Nal. ^{a} θ_{222} represents the CD signal at 222 nm and is indicative of the overall helical content. It is given in units of deg cm^2 dmol^{-1}.

4.1.3 Local effects of capping motifs and amino acids sequence on helix dynamics and stability.

Local stability of α-helices can be varied by introducing helix stabilizing or destabilizing amino acids[94,99,184]. We synthesized two series of Ala-based 21 amino acid peptides to investigate the effect of local changes in helix stability on the local fold-

ing and unfolding dynamics. In the first series of peptides we introduced different N-capping motifs and placed the TTET labels at positions 1 and 7 to probe local effects on dynamics and stability in the N-terminal region (Tab. 4.2). In the second series position 10 was varied and the labels were placed at positions 7 and 13, which yields information on local changes in helix stability and dynamics in the center of the peptide.

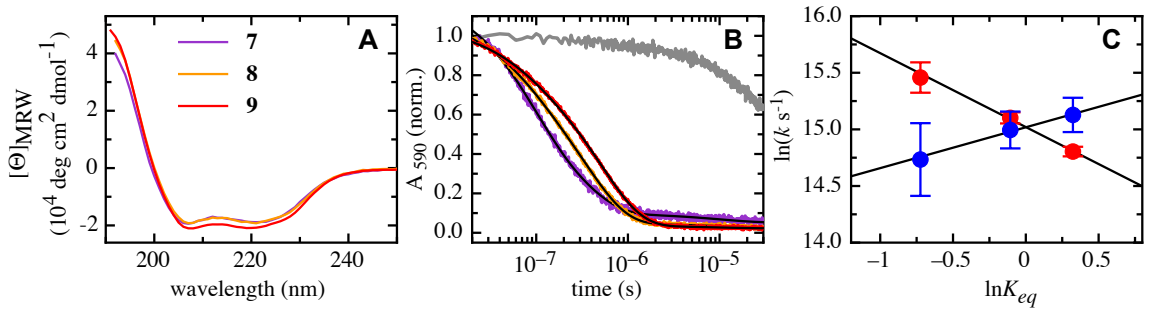

Figure 4.9: Effect of N-capping motifs on local helix dynamics and stability at the N-terminus. Local helix-coil dynamics at the N-terminus of a 21 amino acid helical peptide measured by TTET between residues 1 (Xan) and 7 (Nal) (see table 4.2). (A) Far-UV CD spectra and (B) xanthone triplet decay monitored by the absorbance change at 590 nm. The numbers of the peptides correspond to the numbers in table 4.2. The gray line in panel B represents the donor only reference. The black lines represent double exponential fits to the kinetics. In some traces an additional phase with less than 5 % amplitude and a lifetime corresponding to the donor-only helix is observed. This phase is not considered in further analysis as it is probably due to small amounts of aggregated peptides. The results are summarized in table 4.2. (C) Leffler plots for helix growth (k_f; blue) and unfolding (k_u ; red) (Eq. 4.4).

Varying the N-capping region has only minor effects on the CD spectra of the N-terminally labeled peptides indicating similar overall helix content (Fig. 4.9 A). Despite this small effect on overall helicity, the stabilizing capping groups slow down the TTET kinetics in the N-terminal region (Fig. 4.9 B). Global analysis of the urea-dependence of the TTET kinetics 4.8 in the different helices shows that k_f, k_u and K_{eq} are affected by changes in stability at the N-terminus (Tab. 4.2). The effect on K_{eq} is as expected from the stabilizing effects of the different capping groups (Tab. 4.2). The Leffler plot (Fig. 4.9 C) gives a Φ_f-value of 0.36±0.32 and a corresponding more accurate Φ_u-value of 0.65±0.11, which yields a Φ_f-value of 0.35±0.11.

Local dynamics in the N-terminal region of helical peptides were previously measured in T-jump induced helix unfolding experiments on fluorescence-labeled peptides[137,185]. Both a 4-(methylamino)benzoic acid (MABA) group at the N-terminus,

which changes its fluorescence upon formation of a hydrogen bond to the helix backbone[137] and an i,i+4 Trp-His interaction at the N-terminus[185] gave faster time constants for helix unfolding of about 10 ns at 5°C and 1 ns at 30°C, respectively. The faster dynamics compared to TTET-detected helix unfolding may be due to different processes monitored by the different methods. TTET requires at least partial unfolding of a five amino acid region between the labels, whereas the fluorescence probes monitor local changes involving the fluorophores, namely formation of a single hydrogen bond in the case of the MABA label and local opening of a single helical segment at the Trp residue in the Trp-His pair.

Prominent sequence effects on the local dynamics are also observed in the central region of the helical peptides when position 10 is varied (Fig. 4.10). Host-guest studies on different helical model systems showed that Ala, which is the canonical amino acid at position 10 in the host-guest peptides, is the most helix stabilizing amino acid with an s-value around 1.5[94,99,184]. Thus, any amino acid replacement at position 10 should lead to a destabilization of the helix. The short, polar side chains Ser and Thr at position 10 lead to the expected decrease in overall helical content as judged by the decrease in CD signal at 222 nm (Fig. 4.10 A and table 4.3). The larger hydrophobic side chains Leu and Ile, in contrast, have only little effect on the CD signal (Fig. 4.10 A and table 4.3).

TTET becomes slower in the center of the peptide when local helix stability is increased (Fig. 4.10 B). The values for k_f, k_u and K_{eq} obtained from a global fit of the kinetics at different urea concentrations are shown in table 4.3. Interestingly, Leu and Ile at position 10 locally stabilize the center of the helix but leave the overall helical content unchanged (Fig. 4.8). The Leffler plot for amino acid substitutions at position 10 is complex (Fig. 4.10 C). Linear slopes of Φ_f=0.33±0.13 and Φ_u=0.67±0.07 are obtained if only linear side chains are considered. These values are similar to the Φ_f-value observed for local effects in the N-terminal region (Fig. 4.9 C). However, k_f and k_u for Val, Ile, Leu and Thr fall below the lines of the Leffler plots for the linear side chains, indicating that both helix unfolding and folding are slowed down by branched side chains. This observation suggests that branched side chains interfere both with helix folding and unfolding. To test this idea we introduced the non-natural amino acids norvaline and norleucine at position 10, which have linear side chains but the same number of methylene groups as valine and leucine/isoleucine, respectively. Also norvaline and norleucine at position 10 lead to a local stabilization of the helix

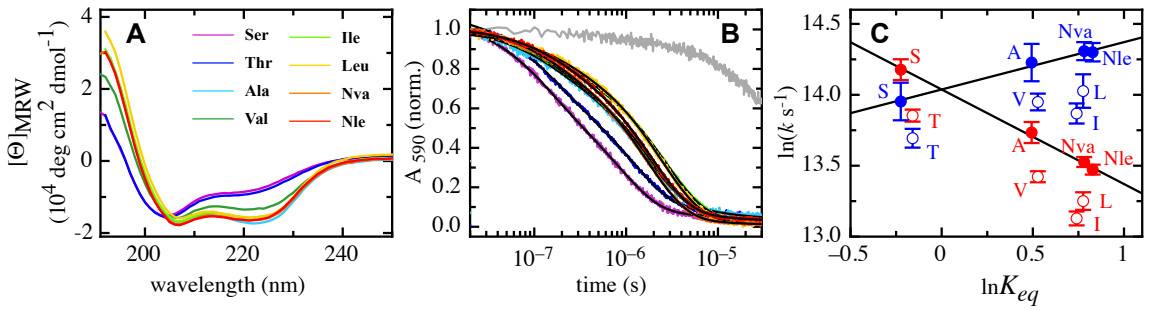

Figure 4.10: Effect of amino acid replacements in the peptide center on local helix dynamics and stability in central region of the peptide. Local helix-coil dynamics in the center of a 21 amino acid helix measured by TTET between residues 7 (Xan) and 13 (Nal). Guest amino acids were introduced at position 10. (A) Far-UV CD spectra and (B) xanthone triplet decay monitored by the absorbance change at 590 nm. The gray line in panel B represents the donor only reference peptide. The black lines represent double exponential fits to the kinetics. In some traces an additional phase with less than 5 % amplitude and a lifetime corresponding to the donor-only helix is observed. This phase is not considered in further analysis as it is probably due to small amounts of aggregated peptides. The results are summarized in table 4.3. (C) Leffler plots for helix growth (k_f; blue) and unfolding (k_u ; red) (Eq. 4.4). Data for peptides with linear side chains are shown as filled circles, for branched side chains as open circles.

compared to Ala (Tab. S 3) and to slower TTET kinetics (Fig. 4.10 B). In contrast to the branched side chains, k_f and k_u for the non-natural linear side chains fall onto the same line in the Leffler plot as all other linear amino acids (Fig. 4.10 C), indicating that branching is the origin for slower local folding and unfolding dynamics of the helix.

The unexpected helix stabilizing effect of large hydrophobic side chains at positions 10 may be due to stabilizing van der Waals interactions between the side chain at position 10 and the TTET labels. The spacing between each label and position 10 is i,i+3, which brings them into close vicinity in the helical conformation and may lead to the formation of a hydrophobic helical stair around the helix.

Xaa	k_u (10^6 s^{-1})	k_f (10^6 s^{-1})	k_c (10^6 s^{-1})
Ser	1.4±0.1	1.2±0.2	10.8±1.1
Thr	1.04±0.04	0.89±0.06	8.9±0.5
Ala	0.92±0.07	1.5±0.2	10.5±1.6
Val	0.67±0.03	1.14±0.07	8.1±0.5
Ile	0.50±0.02	1.05±0.07	6.7±0.5
Leu	0.57±0.04	1.2±0.1	3.2±0.6
Nva	0.75±0.03	1.6±0.1	9.2±0.8
Nle	0.71±0.02	1.6±0.1	8.0±0.7

Xaa	m_u (J/(molM))	m_f (J/(molM))	m_c (J/(molM))	K_{eq}	Amiss (%)	Θ^a_{222}
Ser	-126±94	736±139	191±32	0.8±0.1	56	-8100
Thr	-106±58	896±79	183±17	0.9±0.1	53	-8900
Ala	-187±96	714±137	215±42	1.6±0.2	30	-17400
Val	-189±60	1032±76	227±22	1.7±0.1	26	-13400
Ile	-224±59	835±72	167±27	2.1±0.2	19	-15700
Leu	-50±55	830±78	-87±62	2.2±0.3	12	-15800
Nva	-139±50	906±66	210±27	2.2±0.2	21	-16400
Nle	-141±47	879±61	160±29	2.3±0.2	26	-16400

Table 4.3: Effect of single amino acid replacements in the helix center on local dynamics and stability of a 21-amino acid α-helical peptide. The canonical sequence for the helices is Ac-AAAAAAXanARXaaAANalRA AAARAA-NH2. In the center of the helix at position 10 (Xaa) different guest amino acids were introduced and the local changes in stability and dynamics were probed by TTET between the triplet labels at position 7 and 13. [a] θ_{222} represents the CD signal at 222 nm and is indicative of the overall helical content. It is given in units of deg cm^2 dmol^{-1}.

4.1.4 Local and non-local effects on helix dynamics and stability.

Our results demonstrate that local and non-local effects of amino acid replacements on α-helix dynamics and stability have different origin. Stabilizing the ends of a helix slows down helix unfolding and thus increases helix stability remote from the region of stabilization. This non-local effect can be attributed to longer boundary diffusion distances (Fig. 4.5). The dynamics of helix formation, in contrast, are not affected by non-local changes in helix stability, since helix formation monitors a local process and is thus independent of the position in the helix[90]. Changes in helix stability locally affect both helix formation and unfolding with a Φ_f-value of about 0.35, both at the

N-terminus and in the helix center. This observation suggests that helix stabilizing and destabilizing interactions that lead to different helix propensities for different amino acids, influence both elementary steps of helix elongation and shrinking (k_1 and k_{-1} in Eq. 3.10). Φ_f-values of about 0.3 are also found for the effect of most mutations on folding of small, single-domain proteins, when only reliable Φ_f-values are considered[183,186].

For many peptides the local changes in helix stability measured by TTET do not correlate with the global helix content measured by the CD signal at 222 nm. When the TTET labels are located in the N-terminal region, N-capping motifs have little effect on overall helicity as judged by CD, but they locally increase helix stability at the N-terminus (Fig. 4.9 A). The helical CD signal at 222 nm was proposed to contain only minor contributions from the N-terminal region, since their amide protons are not involved in hydrogen bonds[187]. The center of the 21 amino acid peptide has a high helical content, independent of the capping sequence. Thus N-caps will mainly affect the helical content in the N-terminal region, which changes the local stability in the N-terminal region but has only little influence on the CD signal at 222 nm. Similarly, helix-stabilizing amino acids in the center of the helices locally increase helix stability but have only little effect on the overall helix content. The central region of a helical peptide has a very high helical content[90,98]. Local stabilization of this region thus only leads to minor increase in the intensity of the CD band at 222 nm, whereas TTET measurements directly measure local K_{eq}-values and thus directly give information on local stabilities.

Comparing the effect of N-capping motifs on local helix stability in the helix center (Fig. 4.7) and in the N-terminal region (Fig. 4.9) reveals a 1.5-fold stronger effect on the central region (Fig. 4.11). Stabilizing the helix ends leads to slower unfolding both at the helix ends (Fig. 4.9) and in the helix center (Fig. 4.7). However, the effect on k_u in the helix center is larger than at the termini. Stabilizing the helix termini obviously has a strong effect on the efficiency of boundary diffusion. These results show that long-range effects of capping motifs have a strong influence on local stability and unfolding dynamics in distant regions of the helix.

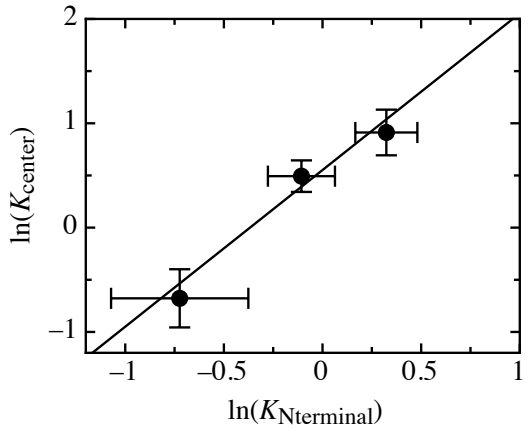

Figure 4.11: Comparison of the effect of the N-capping capping motifs on local helix stability in the peptide center and at the N-terminus. The fit gives a 1.5-fold stronger effect on stability (lnK_{eq}) in the peptide center compared to the N-terminus. The effect of an N-cap on the K_{eq} at the N-terminus was compared to the effect of the same N-cap on K_{eq} in the center of the peptide (Tab. 4.2).

Acknowledgement

For synthesis of the peptides for the length dependence and some of the measurements of the length dependence I thank Andreas Reiner and Beat Fierz. For the collaboration on the simulations with the linear Ising model I thank Maren Büttner. I also like to thank Buzz Baldwin and George Rose for comments and discussion and I thank Attila Szabo for help in deriving Eq. 4.2 and 4.3.

4.2 Transition State and Ground State Properties of the Helix-Coil Transition in Peptides Deduced from High Pressure Studies

This chapter was published 2013 in Neumaier et al.[188].

Understanding the effect of pressure on protein stability and dynamics provides insight into fundamental principles and mechanisms of protein folding[54]. For most proteins increasing pressure shifts the folding equilibrium towards the unfolded state, which, according to Le Chatelier's principle, shows that the native state has a larger volume than the unfolded state[56–58]. The origin of the volume increase upon folding has been discussed controversially for a long time. The major obstacle in the interpretation of volume changes are opposing contributions from different effects. Analysis of high resolution X-ray structures suggested that formation of intramolecular hydrogen bonds and van-der-Waals interactions in the native state lead to a decrease in atomic volumes and thus to a decrease in protein volume upon folding[66]. Further, water around hydrophobic groups has a larger volume than bulk water, which also leads to a decrease in volume upon burial of hydrophobic groups in the native protein[68]. On the other hand, formation of ordered water structures around charged groups[69] and solvation of the peptide backbone decrease the water volume[68], which leads to a volume increase upon folding. Recent experimental results suggested that volume changes associated with transfer of groups from solvent to the protein interior upon folding are small and that compared to the formation of void volumes in native proteins is the major origin of the volume increase upon folding[65].

Volume changes associated with the formation of protein folding transition states are only poorly characterized. High pressure stopped-flow experiments on tendamistat[70] and cold shock protein[72] as well as pressure-jump experiments on cold-shock protein[72] and an ankyrin repeat domain[74] revealed that volumes of protein folding transition states are close to the volume of the native state and may even exceed the native state volume under some conditions[70,72,74]. Similar results were found for the folding and unfolding reactions of ribonuclease A[189], which are both complex and dominated by kinetic coupling between slow prolyl isomerization and protein folding reactions[190–193]. All folding and unfolding reactions of RNase A show positive acti-

vation volumes, indicating that the transition state volumes are larger than those of the native and unfolded state[74].

To understand the origin of volume changes associated with protein folding it is important to dissect contributions of intramolecular interactions, like secondary structure formation, from contributions of packing deficiencies in the native state. Volume changes associated with the formation of protein α-helices can be obtained by studying the effect of pressure on stability and folding/unfolding dynamics of α-helical peptides. Alanine-based peptides form helical structures with intramolecular hydrogen bonds and solvent-accessible side-chains and are thus well-suited to study the effect of pressure on secondary structure formation in the absence of void volumes formed in the protein core of native proteins. The effect of pressure on the stability of Ala-based helical peptides has been addressed both experimentally and in simulations albeit with different conclusions. FTIR experiments revealed an increases in helix stability with increasing pressure, indicating a smaller volume of the helical state compared to the unfolded state[142]. Molecular dynamics simulations on alanine-based peptides, in contrast, suggested that the unfolded state has a slightly smaller volume than the helical state[143]. The simulations further revealed a change in geometry and length of hydrogen bonds with increasing pressure, which should have an effect on FTIR bands and NMR chemical shifts. Changes in hydrogen bond length in protein secondary structures with increasing pressure were experimentally confirmed in high pressure NMR studies on ubiquitin[194].

To determine the effect of pressure on stability and dynamics of α-helices in the absence of tertiary structure and without contributions from changes in spectroscopic properties, we measured triplet-triplet energy transfer (TTET) at various pressures in an alanine-based 21-amino acid helical peptide. TTET coupled to a folding/unfolding equilibrium yields information on local conformational stability and dynamics on the nanoseconds to microseconds time scale[53,90,171]. Intrachain TTET in polypeptide chains occurs through loop formation and is based on van-der-Waals contact between a triplet donor and a triplet acceptor group[28,29]. If the triplet labels are introduced in proteins and peptides at sites that are not in contact in the folded structure, unfolding in the region between the labels has to occur prior to TTET. The resulting TTET kinetics yield information on the local folding/unfolding dynamics and on the local stability in the region between the TTET labels[53,171,195]. In our previous work we introduced the triplet donor xanthone (Xan) and the triplet acceptor naphthylalanine

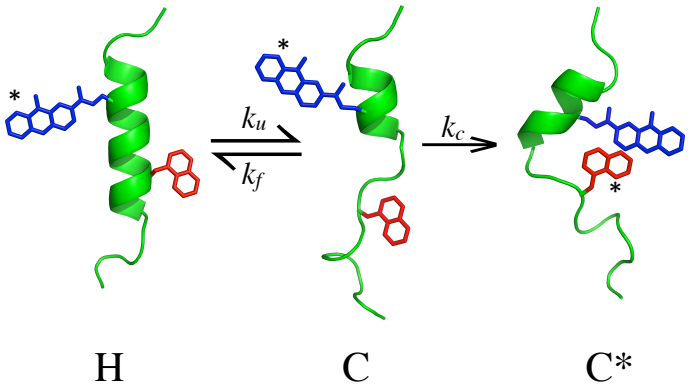

Figure 4.12: Schematic representation of TTET coupled to a helix-coil equilibrium. The equilibrium between a helical (H) and an unfolded or partially unfolded (C) conformation between the labels is monitored by fast and irreversible TTET through loop formation in the ensemble of unfolded conformations (C*). The triplet labels xanthonic acid (Xan, blue) and 1-naphthylalanine (Nal, red) are placed on opposite sides in the central region of the helix with i,i+6 spacing.

(Nal) into α-helical peptides with i,i+6 spacing, which places them at opposite sides of the helix and prevents TTET in the helical state (Fig. 4.12). Thus, at least partial unfolding of the helix in the region between the labels is required before TTET can occur[90,171]. The overall reaction can be described by the three-state model shown in figure 4.12. Since the folding/unfolding dynamics and loop formation occur on a similar time scale[90,171], the two observable rate constants, $\lambda_1$and λ_2, for TTET and their corresponding amplitudes, $A_1$and A_2, yield the rate constants for local helix formation and unfolding between the labels, k_f and k_u, as well as the rate constant for loop formation (k_c) (see section 3.4). In addition, the local equilibrium constant (K_{eq}) for helix stability in the region between the labels can be obtained from K_{eq}=k_f /k_u. TTET experiments do not require perturbation of the helix-coil equilibrium and thus yield information on equilibrium fluctuations of the helix. We have previously investigated local stability and dynamics in various regions of the 21 amino-acid Ala-based helical peptide, which showed a position-independent helix formation rate constant (k_f) and a position-dependent helix unfolding rate constant (k_u) with faster unfolding at the termini compared to the center[90]. This results in higher local helix stability in the center compared to the ends, which is expected from helix-coil theory based on a linear Ising model and in agreement with previous results from hydrogen/deuterium exchange experiments[196].

Since TTET coupled to the helix-coil transition gives information on local equilibrium constants, independent of changes in spectroscopic properties of the helix, this method is perfectly suited to study the effect of pressure on local helix stability. In addition, pressure-dependent TTET experiments yield the activation volumes for helix folding and unfolding, which have not been reported up to date. Here, we investigate the effect of pressures on stability and dynamics of the α-helix-coil transition in the center of the 21-amino acid Ala-based peptide using a high pressure laserflash setup. The results show that the helical structure becomes stabilized with increasing pressure indicating a volume decrease upon helix formation. The dynamics of helix formation and unfolding both slow down with increasing pressure, which shows that the transition state for growth and shrinking of the helical structure has a larger volume than both helical and unfolded state and points at a non-hydrogen bonded transition state structure.

4.2.1 Effect of pressure on local helix stability and dynamics.

To investigate the effect of pressure on local helix dynamics and stability we used a 21 amino acid Ala-based model peptide with arginine residues placed with i,i+5 spacing. The triplet pair Xan and Nal was introduced in the central region of the peptide at positions 7 and 13, respectively, which yields the peptide sequence:

$$^{*}NH_3\text{-AAAAA A}\mathbf{Xan}\text{ARA AA}\mathbf{Nal}\text{RA AAARA A-}NH_2$$

Xan was introduced by coupling 9-oxoxanthen-2-carboxylic acid to the side chain of the non-natural amino acid α,β-diaminopropionic acid. The non-natural amino acid 1-naphthylalanine was directly incorporated into the peptide during solid phase peptide synthesis. The C-terminus was amidated but, in contrast to our previous work, the helical peptide studied here has a free N-terminus, which decreases helix stability and leads to about 50% helical conformations in the center of the peptide at ambient pressure[171]. The similar populations of unfolded and helical conformations provide a high sensitivity of the measurements for both an increase and a decrease in helix stability, since it was not clear whether pressure stabilizes or destabilizes the helical structure.

We investigated the effect of pressure on helix stability in the center of the peptide by TTET measurements in the range between 0.1 to 390 MPa (1 and 3900 bar).

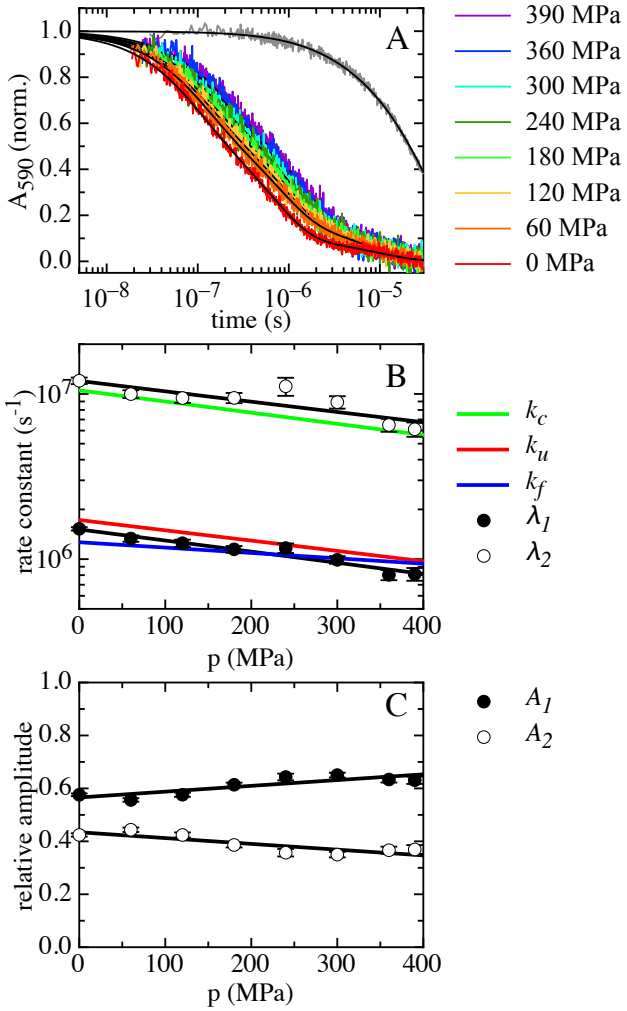

Figure 4.13: Pressure-dependence of helix-coil dynamics in the center of a 21-amino acid helical peptide measured by TTET. (A) Xanthone triplet decay at the indicated pressures monitored by the absorbance change at 590 nm. The grey curve shows the xanthone triplet decay in a donor-only control peptide for comparison. All curves were fitted by the sum of two exponentials. Additionally, a minor slow kinetic phase is observed in the triplet decay curves, which corresponds to the intrinsic triplet lifetime of xanthone and probably reflects a small fraction of oligomeric molecules. (B) Pressure dependence of the two observable rate constants λ_1 and λ_2 and of their respective amplitudes, A_1 and A_2 (C). The black lines in panels (B) and (C) show the results forλ_1 and λ_2 and their amplitudes from global fits of all kinetic traces according to the analytical solution of the three-state model shown in Fig. 4.12 (see section 3.4). Global fitting of all kinetic traces additionally yields the pressure-dependence of the microscopic rate constants, k_u (red), k_f (blue) and k_c (green) and indicated in panel (B), which results in activation volumes of $\Delta V_u^{0\ddagger}$ =3.3±0.3 cm^3/mol, $\Delta V_f^{0\ddagger}$=1.7±0.5 cm^3/mol and $\Delta V_c^{0\ddagger}$ =3.6±0.4 cm^3/mol. The measurements were performed in 10 mM potassium phosphate buffer, pH 7 at 5°C with a peptide concentration of about 50 µM.

The experiments were initiated by a 4 ns laserflash at 355 nm, which produces the xanthone triplet state that can be detected by its strong absorbance band at 590 nm[5,29]. TTET to naphthylalanine leads to a decay in xanthone triplet absorbance band (Fig. 4.13 A). The triplet decay curves can be described by the sum of two exponentials under all conditions with the rate constants λ_1 and λ_2 (Fig. 4.13 B) and their respective amplitudes A_1 and A_2 (Fig. 4.13 C). This result indicates that both the unfolded and the helical conformation are populated to significant amounts in equilibrium at all pressures[90]. Figure 4.13A shows that TTET kinetics become slower with increasing pressure. The results from the double exponential fits reveal that increasing pressure decreases both λ_1 and λ_2 and leads to a gain in amplitude of the slower kinetic phase at the expense of the amplitude of the faster phase (Fig. 4.13).

The effect of pressure on the rate constant of a reaction depends on the activation volume ($\Delta V^{0\ddagger}$) according to

$$\frac{\delta \ln k}{\delta p} = -\frac{\Delta V^{0\ddagger}}{RT} \tag{4.5}$$

However, the two rate constants observed for TTET (λ_1 and λ_2) do not directly correspond to folding or unfolding rate constants in Fig. 4.12 but are functions of k_f, k_u and k_c (see section 3.4), which can be determined by fitting the solution of the three state mechanism (see section 3.4) to the observable rate constants (Fig. 4.13 B) and their amplitudes (Fig. 4.13 C). The quality of the fit improves significantly when the kinetic traces measured at the different pressures are fitted globally assuming a linear pressure dependence of $\ln(k_f)$, $\ln(k_u)$and $\ln(k_c)$ according to Eq. 4.5. The results from the global fit reveal that all rate constants decrease with increasing pressure with activation volumes of 1.7±0.5 cm^3/mol, 3.3±0.3 cm^3/mol and 3.6±0.5 cm^3/mol for $\Delta V_f^{0\ddagger}$, $\Delta V_u^{0\ddagger}$ and $\Delta V_c^{0\ddagger}$, respectively (Figs. 4.13 B, 4.14 B). This result indicates that the transition state for helix formation and unfolding has a larger volume than both the helical state and the unfolded state. In addition, loop formation in the coil state (k_c) slows down with increasing pressure.

The equilibrium constants at the various pressures can be obtained from K_{eq}=k_f/k_u. Applying the Planck equation (Eq. 4.6)

$$\frac{\delta \ln K_{eq}}{\delta p} = -\frac{dV^0}{RT} \tag{4.6}$$

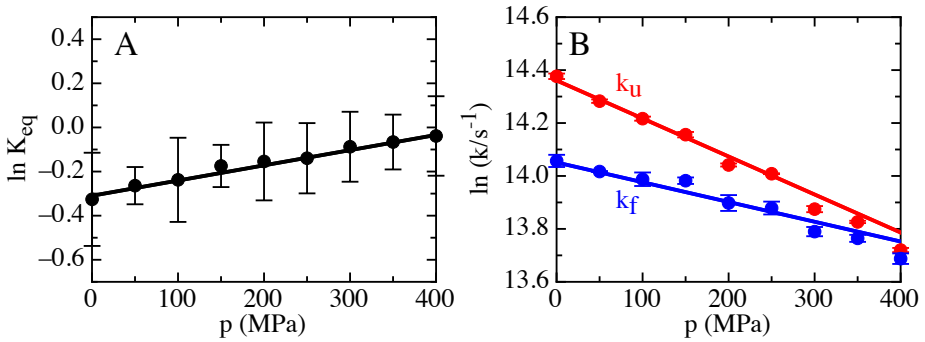

Figure 4.14: Pressure-dependence of (A) the equilibrium constant for helix formation (K_{eq}=k_f/k_u) in the peptide center and (B) the rate constants for helix formation (k_f) and unfolding (k_u). The lines represent the results from global fits to the experimental data (Fig. 4.13 B) resulting in a reaction volume, ΔV^0, of -1.6 cm^3/mol. The filled circles are the results from the simulations based on the linear Ising model with the parameters given in Eqs. 4.13-4.15. The quality of the results was improved by performing simulations up to s-values corresponding to p=2000 MPa (Fig 4.18).

yields the reaction volume for helix formation in the region between the TTET labels, which equals the difference between the activation volumes for helix formation and unfolding (Eq. 4.7).

$$dV^0 = dV_f^{0\ddagger} - dV_u^{0\ddagger} \tag{4.7}$$

The equilibrium constant for helix formation increases with increasing pressure and the fit according to Eq. [2] gives a negative reaction volume (ΔV^0) of -1.6±0.6 cm^3/mol (Fig. 4.14 A). This result shows that the helical state has a smaller volume than the unfolded state and thus becomes stabilized with increasing pressure.

Dissociation of phosphate has a reaction volume of about -25 cm^3/mol, which leads to a decreases in its pKa-value of about 0.3 units per 100 MPa and results in a decrease in pH of about 1.2 units in the pressure range applied in our TTET experiments[197]. The Ala-based helical peptide used in this study contains three arginine residues and a free N-terminus, which have pKa values of 12.2 and 9.6, respectively. These values should be independent of pressure since the deprotonation reaction of neither Arg nor the N-terminus leads to a change in the number of charged species[197]. The pressure-induced decrease in pH from 7.0 to 5.8 between 0.1 and 390 MPa applied in our experiments does therefore not lead to a change in the protonation state of the helical peptide and should not influence the helix-coil transition. This was confirmed by measuring TTET kinetics in the pH-range between 5.8 and 7.0, which are insensitive

to pH (Fig. 4.15). In addition, pressure in the applied range does not influence the donor triplet lifetime (Fig. 4.16).

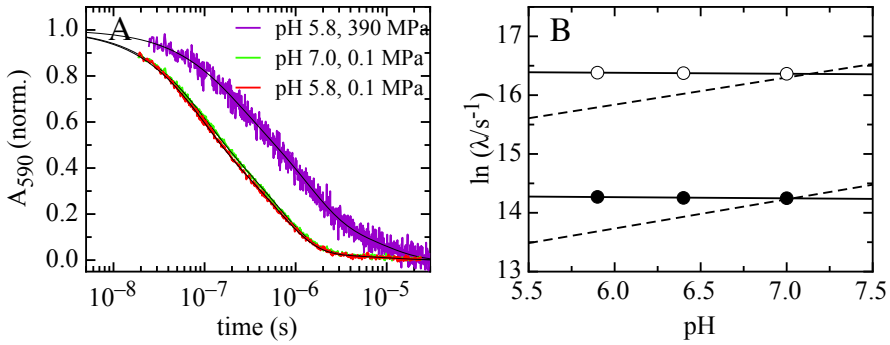

Figure 4.15: Effect of pH on TTET kinetics in the 21-amino acid alanine-based helical peptide. (A) Xanthone triplett decay curves at pH 7.0 and pH 5.8 at 0.1 MPa, as indicated. The results from double exponential fits are shown as black lines. For comparison, the TTET kinetics at 390 MPa (Fig. 4.13 A) are shown. Due to the effect of pressure on the *pKa*-value of the phosphate buffer, the pH of the solution is 5.8 at 390 MPa. (B) pH-dependence of the two apparent rate constants, λ_1(open circles) and λ_2 (closed circles) in the range from pH 5.8 to pH 7.0. A linear fit yields a minor linear decrease in ln(λ) with pH with values of (-1.7$\pm$0.1)$\cdot 10^{-2}$/pH-unit for λ_1 and of (-2.0$\pm$0.7)$\cdot 10^{-2}$/pH-unit for λ_2 (solid lines). For comparison the slopes of the pressure-dependencies on λ_1 and λ_2 derived from the values at 0.1 MPa (pH 7.0) and 390 MPa (pH 5.8) are shown as dashed lines (Fig. 4.13 B). These results show that the change in pH induced by pressure does not contribute to the observed effects of pressure on helix dynamics and stability. The measurements were performed in 10 mM potassium phosphate buffer at 5°C with a peptide concentration of about 50 µM.

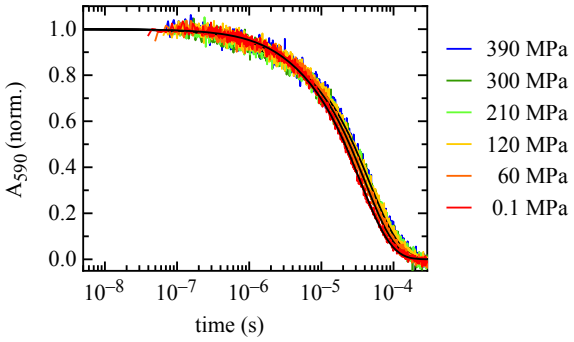

Figure 4.16: Effect of pressure on the donor lifetime in the 21-amino acid alanine-based peptide labeled only with the xanthone donor. The Nal acceptor group was replaced by alanine. The results show that pressure does not significantly change the donor lifetime. Since observed TTET kinetics occur on a much faster time scale (Fig. 4.13 A) they do no contain significant contributions from spontaneous triplet decay. The measurements were performed in 10 mM potassium phosphate buffer, pH 7 at 5°C with a peptide concentration of about 50 µM.

4.2.2 Effect of pressure on the elementary rate constants for helix elongation and shrinking.

The activation and reaction volumes obtained from the TTET experiments are apparent volume changes for helix formation and closure between the labels that can not be directly converted to the volume changes for addition or removal of a single helical residue, since the helix-coil transition is not a two-state process[90,125,129,135,137,198,199] The dynamics and stability in the helix center are rather influenced by the coupling of many microscopic opening and closing events at the different positions in the peptide. Our previous studies showed that a kinetic linear Ising model with 1-D boundary diffusion mechanism is quantitatively able to describe the experimentally determined position-dependence[90] and length-dependence[171] of dynamics and stability of the helix-coil transition. Applied to the helical peptide used in our study, the helix is represented by a finite sequence of 21 identical residues, which can be either in the helical state h or the coil state c leading the following type of conformations:

$$\mathbf{ccccchhhhhhhhhhhcccc} \tag{4.8}$$

The following equations describe the dynamic and equilibrium properties of the system[124,135]:

- Helix elongation:

$$hcc \underset{k_{-1}}{\overset{k_1}{\rightleftharpoons}} hhc \quad cch \underset{k_{-1}}{\overset{k_1}{\rightleftharpoons}} chh \qquad \frac{k_1}{k_{-1}} = s \tag{4.9}$$

- Helix nucleation:

$$ccc \underset{k_{-2}}{\overset{k_2}{\rightleftharpoons}} chc \qquad \frac{k_2}{k_{-2}} = \sigma s \tag{4.10}$$

- Coil nucleation:

$$hhh \underset{k_{-3}}{\overset{k_3}{\rightleftharpoons}} hch \qquad \frac{k_3}{k_{-3}} = \frac{\sigma}{s} \tag{4.11}$$

Although this model only accounts for nearest neighbor interactions[124] it is able to quantitatively describe experimental data on the helix-coil transition in a variety of different peptides[98,129,184]. We further used the kinetic extension of the model introduced by Schwarz[135], which introduces additional factors for helix nucleation, γ_h, and coil nucleation, γ_c to account for kinetic effects on the nucleation reactions relative to elongation:

$$\begin{aligned} k_2 &= \gamma_h \cdot \sigma \cdot k_1 \qquad & k_{-2} &= \gamma_h \cdot k_{-1} \\ k_3 &= \gamma_c \cdot \sigma \cdot k_{-1} \qquad & k_{-3} &= \gamma_c \cdot k_1 \end{aligned} \tag{4.12}$$

We performed Monte-Carlo simulations based on Eqs. 4.8 to 4.12 and compared the results with the experimental data to obtain information on the activation volumes of the elementary rate constants for helix growth ($\Delta V_1^{0\ddagger}$) and shrinking ($\Delta V_{-1}^{0\ddagger}$) and on the reaction volume for adding a single helical residue at the helix-coil border (ΔV_s^0 , see Eq. 4.9). In all simulations k_1 was set to 1, the nucleation parameter σ was 0.003 and the kinetic parameters were $\gamma_c = \gamma_h = 2$[90,171]. As the model peptide has a destabilized N-capping region, we distinguish between the average s-value of the positions 5 to 21 and the s-value for the N-terminal cap assigned to positions two to four[171]. The folding and unfolding dynamics were simulated for different s-values (Fig. 4.17 A) and analyzed by computing first-passage-times (FPTs)[90,171]. Since the experiments probe a region of five residues between the labels we analyzed the results from the simulations by monitoring the dynamics of the whole segment between the labels instead of single-site fluctuations. The segment of five residues between the

labels was counted as helical if at least four of its residues were helical at a certain time[90,171]. In addition, the starting conformations had to contain at least one helical residue. The distribution of the FPTs was fitted by single-exponential functions yielding the reduced rate constants of local helix folding and unfolding k_f/k_1 and k_u/k_1 for each s-value (Fig. 4.17 B).

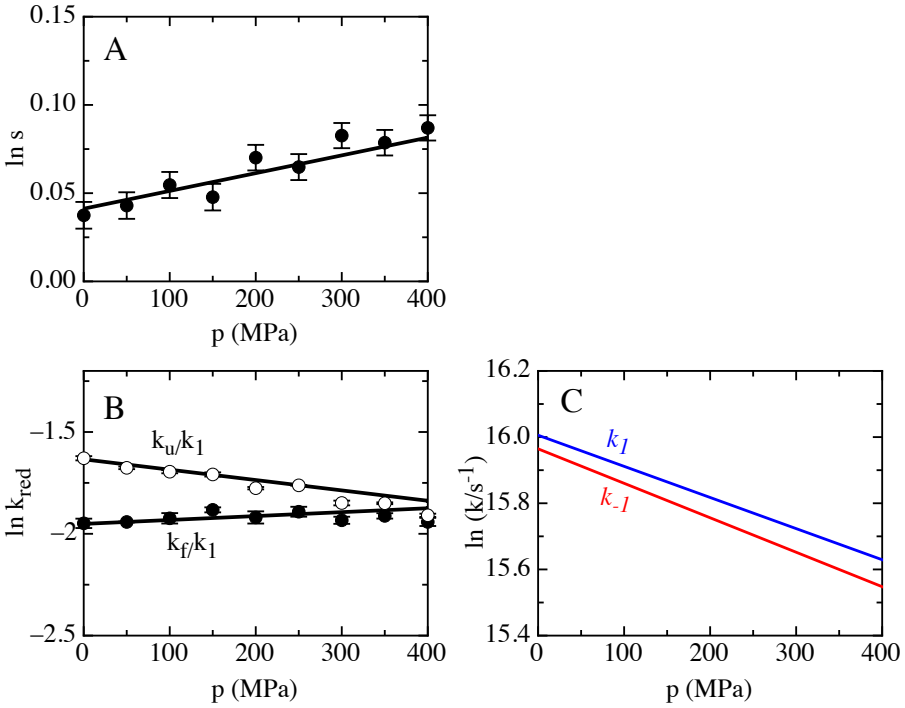

Figure 4.17: Pressure-dependence of (A) the s-value (Eq. 4.9) and (B) the reduced rate constants for local helix folding and unfolding, k_f/k_1 and k_u/k_1, respectively, obtained from the Monte Carlo simulations. The solid circles in panel (A) represent the results from the simulations that describe the experimental data (Fig. 4.14 A) and the solid line represents the fit with the results given in equation 4.13 resulting in ΔV_s^0 =-0.23 cm^3/mol. (C) Pressure-dependence of s the rate constants for adding (k_1) and removing (k_{-1}) a single helical residue to/from an existing helix (Eq. 4.9), corresponding to activation volumes of $\Delta V_1^{0\ddagger}$ = 2.2 cm^3/mol and $\Delta V_{-1}^{0\ddagger}$ = 2.4 cm^3/mol. The quality of the results was improved by performing simulations up to s-values corresponding to p=2000 MPa (Fig 4.18).

Since the simulations exhibit a considerable statistical error, especially for small s-values, they were performed up to s-values corresponding to p=2000 MPa (Fig 4.18), which gave more reliable results for the pressure-dependence of the kinetic and equilibrium parameters in the experimentally accessible region between 0.1 and 390 MPa (see SI). The best agreement between simulated and experimental data (Fig. 4.14 A) is obtained with a pressure- independent s-value for the N-capping region of

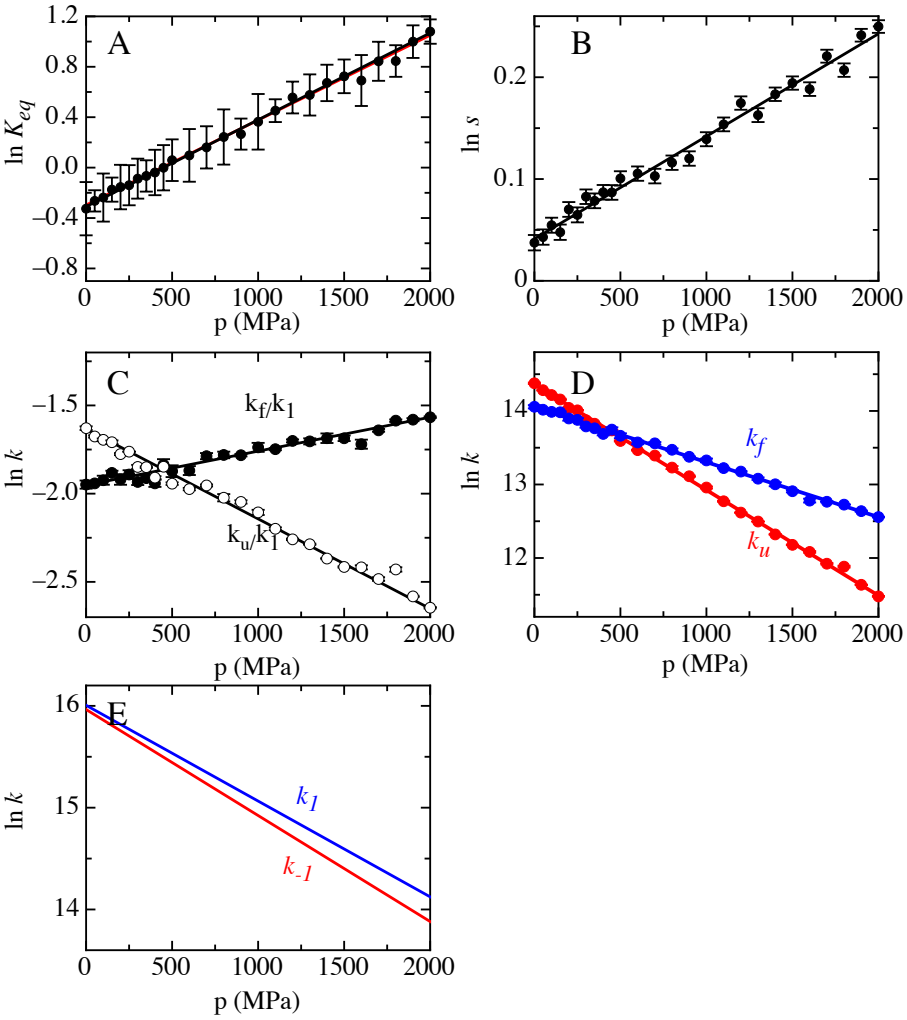

Figure 4.18: Results of Monte Carlo simulations on helix-coil stability and dynamics between 1 and 2000 MPa. (A) Pressure-dependence of the equilibrium constant for helix formation (K_{eq}=k_f/k_u) in the helix center from the global fit of the experimental data (-) with results from Monte Carlo simulations (cirlces). In addition, the result from a linear fit (red line) to the simulated data is shown. (B) Effect of pressure on the simulated s-value used to describe the data in panel (A). The line is the result of a linear fit with the parameters given in Eq. 4.13 of the main text. (C) Pressure-dependence of the reduced rate constants for helix formation and unfolding, k_f/k_1 and k_u/k_1, respectively, resulting from the Monte Carlo simulations. (D) The results from the simulations (filled circles) describe the experimentally determined rate constants for helix formation (k_f) and unfolding (k_u) with the scaling factor (SF) given in Eq. 4.14 of the main text. (E) Scaling yields the pressure-dependence of the elementary steps for helix growth (k_1) and shrinking (k_{-1}), by a single segment.

0.099±0.004 and a pressure-dependent general s-value that can be described by (Fig. 4.17 A)

$$\ln s = 0.041 + 1.01 \cdot 10^{-4} \cdot p \tag{4.13}$$

According to Eq. 4.6 this corresponds to s(0.1MPa)=1.04 and ΔV_s^0=-0.23 cm^3 /mol (0.38 Å^3/molecule) for addition of a single helical residue.

The simulations further yield reduced rate constants, k_f/k_1 and k_u/k_1 for helix formation and unfolding in the helix center (Fig. 4.17 B). Comparison of the reduced rate constants, with the experimentally determined rate constants for helix folding and unfolding in the region between the labels, k_f and k_u (Fig. 4.14 B) yields a scaling factor for k_1, which gives the actual rate constant for addition of a single helical residue (see Eq. 4.9). The experimentally determined rate constants for folding and unfolding are described by the simulations (Fig. 4.14 B) with a pressure-dependent scaling factor (Fig. 4.17 C) that is described by

$$\ln k_1 = 16.01 + 9.4 \cdot 10^{-4} \cdot p \tag{4.14}$$

which corresponds to an elementary rate constant for adding a helical residue at 0.1 MPa of k_1(0.1 MPa)= 8.7·10^6 s^{-1} and $\Delta V_1^{0\ddagger}$ =2.2 cm^3/mol (3.7 Å^3/molecule). The pressure-dependence of k_{-1} is obtained from k_1 in combination with the s-value (see Eq. 4.9) which yields (Fig. 4.17 C)

$$\ln k_{-1} = 15.96 + 1.04 \cdot 10^{-3} \cdot p \tag{4.15}$$

corresponding to k_{-1}(0.1 MPa)= 8.4·10^6 s^{-1} and $\Delta V_{-1}^{0\ddagger}$ =2.4 cm^3/mol (4.0 Å^3/molecule).

These results show that the reaction volume for adding a single helical residue is small and negative, whereas the activation volumes for adding or removing a helical residue are both large and positive. When a residue is added to a helix backbone/water hydrogen bonds and non-specific intramolecular hydrogen bonds are lost (Fig. 4.19). Concomitantly, an intramolecular i,i+4 backbone hydrogen bond is formed and additionally, the peptide backbone becomes partially shielded from solvent. However, this solvent-shielding contribution is expected to be relatively minor for alanine-based peptides, which permit water to solvate the intrahelical hydrogen

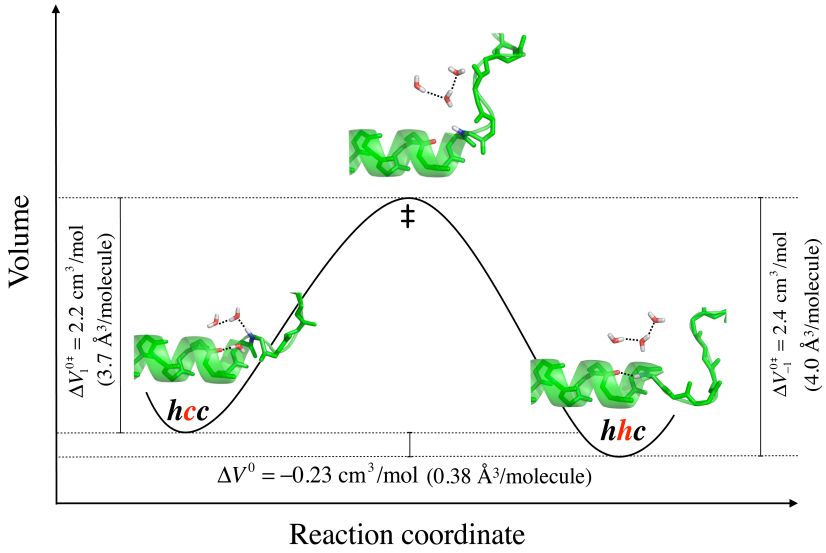

Figure 4.19: Schematic representation of the structural and volume changes during addition of a single helical residue to an existing α-helix. The coil state (hcc) has the carbonly oxygen and amide proton hydrogen bonded to water molecule. Upon adding a helical residue (hhc) an intramolecular hydrogen bond is formed and water is released. The large volume of the transition state (‡) indicates that neither an intramolecular hydrogen bond nor peptide/water hydrogen bonds are formed.

bonds due to the small size of the Ala side chains[108]. The negative reaction volume for adding a helical residue suggests that intrahelical i,i+4 hydrogen bonds have a slightly smaller volume than backbone/water and long-range backbone/backbone hydrogen bonds in the unfolded state. Contributions from void volumes to the reaction volume are probably small, since the α-helix is a close-packed structure. However, we cannot exclude the possibility that small void volumes accompany helix formation but are compensated by the volume decrease upon formation of intramolecular hydrogen bonds.

The larger volume of the transition state compared to the volumes of either the helical or the coil state shows that formation or removal of a single helical residue proceeds through a high energy state with a large volume. A plausible explanation for this large transition state volume is the presence of amide groups that are neither satisfied by hydrogen-bonds to water nor by intramolecular hydrogen bonds (Fig. 4.19). In this case the loss of a hydrogen bond between a carbonyl oxygen and an amide hydrogen in the peptide backbone would correspond to a volume increase of about 2.4 cm^3/mol ($\Delta V_{-1}^{0\ddagger}$) compared to a non hydrogen bonded structure. Then,

2.2 cm^3/mol ($\Delta V_1^{0\ddagger}$) are regained upon formation of backbone-water or non-specific intramolecular hydrogen bonds in the unfolded state (Fig. 4.19). We cannot exclude the possibility that steric effects and unfavorable packing contribute to the large transition state volume, but this seems unlikely to have be a major factor, since only a single amino acid at the helix-coil border changes its Φ,Ψ angles andthere is an energetically favorable and sterically allowed route through Φ,Ψ space from the unfolded/extended region to the helical region[4].

The volume decrease upon helix formation observed in TTET experiments is in agreement with FTIR studies on Ala-based peptides, which also observed a stabilization of the helical state[142]. Using an equilibrium linear Ising model to analyze the FTIR data yielded a reaction volume of 0.98±0.04 cm^3/mol per residue, which is larger than the reaction volume of 0.23 cm^3/mol per residue determined by TTET (Fig. 4.14). This discrepancy may be due to the difference in temperature between the FTIR studies (25.4°C) and the TTET experiments (5°C), since it is commonly observed that reaction volumes for protein folding are strongly temperature-dependent[56,57]. The volume decrease upon formation of intramolecular helical hydrogen bonds is further in agreement with results on collagen folding, which showed a volume decrease upon triple helix formation[200]. As in α-helical structures formation of the collagen triple helix mainly leads to formation of solvent accessible hydrogen bonds between carbonyl oxygens and amide protons in the peptide backbone.

Comparison of the reaction and activation volumes for adding/removing a single helical residueΔV_s^0 , $\Delta V_1^{0\ddagger}$ and $\Delta V_{-1}^{0\ddagger}$, with the respective volume changes for folding and unfolding of the helix in the center between the labels, ΔV^0, $\Delta V_f^{0\ddagger}$ and $\Delta V_u^{0\ddagger}$, shows that the experimentally determined values are apparent reaction and activation volumes, that do not represent properties of individual kinetic steps during growth and shrinking of a helix. Due to the non-two-state nature of the helix-coil transition the measured folding and unfolding rate constants are influenced by many microscopic steps of adding or removing individual helical residues[90,135,137,171]. The Monte Carlo simulations show that this mechanism leads to an increase in the reduced folding rate constant (k_f/k_1) and a decrease in the reduced unfolding rate constant (k_u/k_1) in the helix center with increasing pressure, i.e. with increasing s-value (Fig. 4.17). As a result, scaling of the pressure-dependence of the reduced rate constants to the experimentally observed values gives $\Delta V_1^{0\ddagger}$ =2.2 cm^3/mol compared to $\Delta V_f^{0\ddagger}$=1.7 cm^3/mol. At the same time, scaling leads to a decrease from $\Delta V_u^{0\ddagger}$ =3.3 cm^3/mol to

$\Delta V_{-1}^{0\ddagger}$ =2.4 cm^3/mol (Fig. 4.17). These opposing effects of the scaling factors give rise to the observed large difference in reactions volumes for helix stability in the center (ΔV^0 =-1.6 cm^3/mol) and for adding a single helical residue (ΔV_s^0 =-0.23 cm^3/mol). These comparisons show that kinetic coupling between the microscopic shrinking and growth steps at the individual positions in the peptide leads to macroscopically observable rate constants for helix folding and unfolding that can not be analyzed by a simple two-state model.

4.2.3 Effect of pressure on loop formation in the unfolded state.

The analysis of the TTET experiments shows that loop formation in the unfolded or partially unfolded state of the helical peptides (k_c) is pressure-dependent with an activation volume of 3.6 cm^3/mol (Fig. 4.13). To test whether this large activation volume is characteristic for loop formation in an unfolded Ala-based polypeptide chain we investigated the pressure-dependence of the dynamics of loop formation in an 11-amino acid peptide that corresponds to the central 11 amino acids in the 21-amino acid helical peptide including the TTET labels

$$^*NH_3\text{-AA}\mathbf{Xan}\text{ARAAA}\mathbf{Nal}\text{AA-COO}^-.$$

Leaving both the N- and the C-terminus unprotected prevents formation of detectable amounts of helical structure as judged by its CD spectrum (Fig. 4.20 A). Further, the temperature- dependence of the CD signal at 222 nm reveals a monotonous decrease in ellipticity with increasing temperature (Fig. 4.20 B), which is characteristic for an ensemble of unfolded conformations[201–203]. The positive CD band around 227 nm and the negative band around 198 nm indicate the presence of significant amounts of polyproline II (PPII) structure in the ensemble of unfolded states of the 11-amino acid peptide[204] in agreement with the observation of PPII structure in a seven alanine residue peptide[205].

Loop formation in the 11-amino acid unfolded polypeptide exhibits only a weak pressure dependence (Fig. 4.20 C) with an activation volume of 0.51±0.09 cm^3/mol, determined in a global fit of the kinetic traces (Fig. 4.20 D). This result shows that the underlying fast conformational transitions in the unfolded state of an Ala-based peptide do not involve major volume changes. Comparison of these results

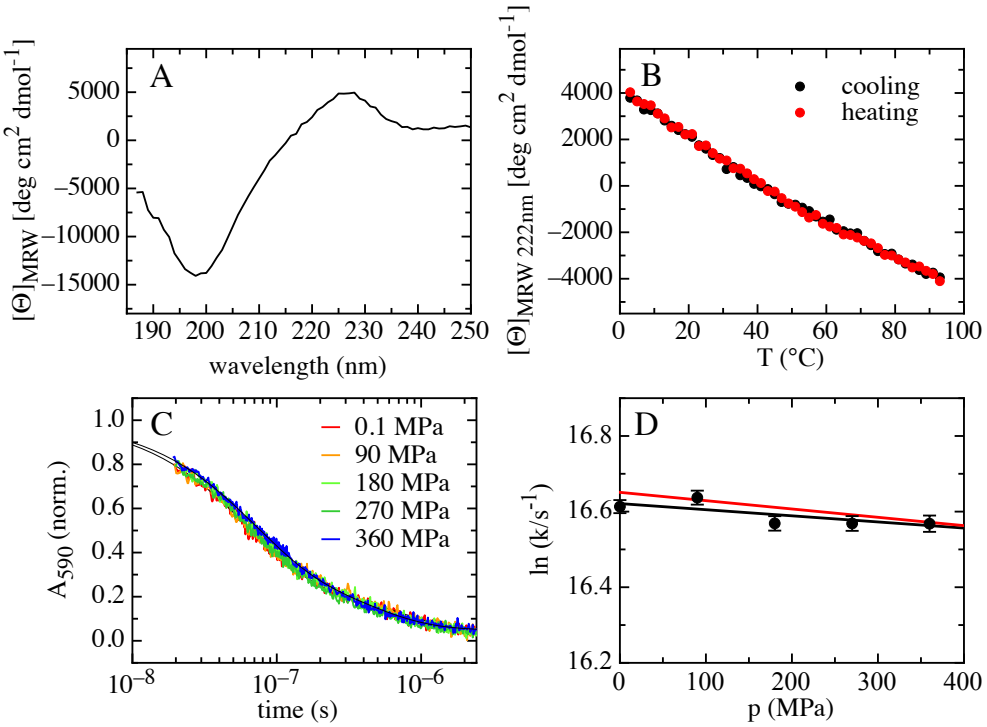

Figure 4.20: (A) CD spectrum and (B) temperature dependence of the ellipticity at 222 nm of the 11-amino acid unfolded model peptide. The pressure-dependence of the TTET kinetics (C, D) yields an activation volume for loop formation ($\Delta V^{0\ddagger}$) of 0.41±0.15 cm^3/mol for the pressure-dependence of the rate constants from the individual fits (D, black line) and of 0.51±0.09 for a global fit (D, red line) of the kinetic traces shown in panel (C). Additionally a minor slow kinetic phase is observed in the triplet decay curves (C), which corresponds to the intrinsic triplet lifetime of xanthone and probably reflects a small fraction of oligomeric molecules. The measurements were performed in 10 mM potassium phosphate buffer, pH 7 at 5°C with a peptide concentration of about 50 µM.

to the pressure-dependence of loop formation reaction (k_c) in the helical peptide shows that the large activation volume for loop formation of the unfolded state is not characteristic for an unfolded polypeptide chain. The results rather suggest that only partial local unfolding of the helical structure between the labels is required to enable donor and acceptor to come into van-der-Waals contact, as assumed in our previous work[90,171]. Loop formation in the partially unfolded coil-state of the peptide requires structural re-arrangements that are associated with volume changes.

4.2.4 Conclusions

The TTET experiments on the helix-coil dynamics in helical peptides reveal that the volume decreases by 0.23 cm^3/mol (0.38 $Å^3$/molecule) per helical residue upon helix formation. This volume change for formation of a single helical residue is small, but the coupling of many of these steps leads to a significant stabilization of the central part of a 21-amino acid helix by pressure with a reaction volume for unfolding of -1.6 cm3/mol (Fig. 4.14 A). Thus, the commonly observed increase in volume upon formation of the native state is not due to the formation of helical secondary structure, consistent with the idea that the volume increase upon protein folding is mainly due to void volumes formed in the native state[65]. Notably, the actual void volumes in folded proteins are larger than the observed volume increase upon folding, since helix formation decreases the protein volume. Our results further show that the decrease in helix stability in folded proteins with increasing pressure, as observed in hydrogen-deuterium exchange studies[206], is not due to an effect of pressure on intrinsic helix stability. Rather, increasing pressure destabilizes the tertiary structure of proteins, in turn, destabilizes helical structures due to a cooperative destabilization of the folded state. Equilibrium intermediates with residual helical structure have frequently been observed in pressure-induced unfolding experiments monitored by NMR[194,207–209]. The population of these persisting helical structure can be explained by the opposing effects of pressure on the stability of tertiary and helical structure. Whereas the native structure becomes destabilized with increasing pressure, helices become increasingly stable. Thus, sequences with high intrinsic helix propensity may remain helical even in the absence of long-range tertiary interactions and even become stabilized with increasing pressure. In addition, pressure may induce helix formation in sequences with marginal intrinsic helix stability. This effect is in contrast to thermal- and denaturant-induced equilibrium unfolding transitions of small proteins, which typically exhibit two-state behavior since both tertiary interactions and helical structures are destabilized under such conditions[102,103,199]. Residual helical structure is also frequently observed in cold-denaturation and alcohol-induced unfolding of proteins. Similar to high pressure, these conditions lead to a destabilization of tertiary structure but to a stabilization of helices.

The results further show that the transition state for adding or removing a single helical residue has a 2.2 cm^3/mol and 2.4 cm^3/mol larger volume compared to either

the helical or coil state, respectively. Thus, even small structural re-arrangements in the polypeptide chain may proceed through high energy states with large volumes, because large activation volumes are already observed for changing only a single pair of Φ,Ψ angles in a secondary structural element. These effects will contribute to the volume of protein folding transition states, which are typically large and often exceed the volume of the native state[70,72,74,189].

Acknowledgement

I like to thank Annett Bachmann for synthesis and purification of the 11-amino acid unfolded model peptide and Maren Büttner for the collaboration on the simulations with the linear Ising model. I also like to thank Cathy Royer, George Rose and Buzz Baldwin for discussion and comments on the manuscript.

4.3 Compact locked and unlocked states and a dry molten globule transition state in native-state dynamics of the villin headpiece subdomain revealed by high pressure measurements.

Proteins can adopt different conformations besides the native state and the ensemble of unfolded states. Native proteins typically exist in different conformational sub-states that are important for protein function, like ligand binding and enzyme activity[210–212]. Partially folded intermediate states of proteins are frequently observed during folding of larger proteins[39] but were also shown to be important in folding of apparent two-state folders[37,38]. The large majority of transiently populated intermediates, that have been observed experimentally, are located on the unfolded side of the major folding barrier between U and N and typically contain large amounts of secondary structure with the polypeptide chain being still highly solvent accessible. Intermediates on the native state of the major free energy barrier have only been detected during unfolding of a few proteins. Time-resolved 1-D NMR unfolding experiments on ribonuclease A revealed a state with increased side-chain flexibility that transiently accumulates prior to the rate-limiting step for unfolding[49]. The intermediate has a solvent shielded protein interior, native secondary structure and a native hydrogen bonding network[49,50]. Similar unfolding intermediates were detected during unfolding of DHFR by time-resolved ^{19}F NMR experiments[51] and in monellin by FRET[52]. It was suggested that these unfolding intermediates represent dry molten globule states (DMGs), which have been predicted based on theoretical considerations and were proposed to be expanded native states with increased side-chain flexibility and a solvent inaccessible core[45].

We recently investigated native-state dynamics in the villin headpiece subdomain HP35 by triplet-triplet energy transfer (TTET) and detected an equilibrium between two folded states with identical secondary structure and a solvent-shielded core[53]. The major native state (N) is rigid and locked into conformations with low amplitude motions. In the minor state (N′) rapid, large-scale structural fluctuations occur including local unfolding of helix 3 (Fig. 4.21). The reaction from N to N′ is associated with an increase in both entropy and enthalpy, which suggested that formation of N′

is associated with a loss in interaction energy and an increase in conformational flexibility. Due to these properties N′ was termed the unlocked state. The unlocked state was also observed in molecular dynamics simulations, which were able to reproduce the results from native state TTET experiments[164]. The similarities between N′ and the transiently populated unfolding intermediates observed in RNase A, DHFR and monellin suggested that they represent the same type of intermediate[53].

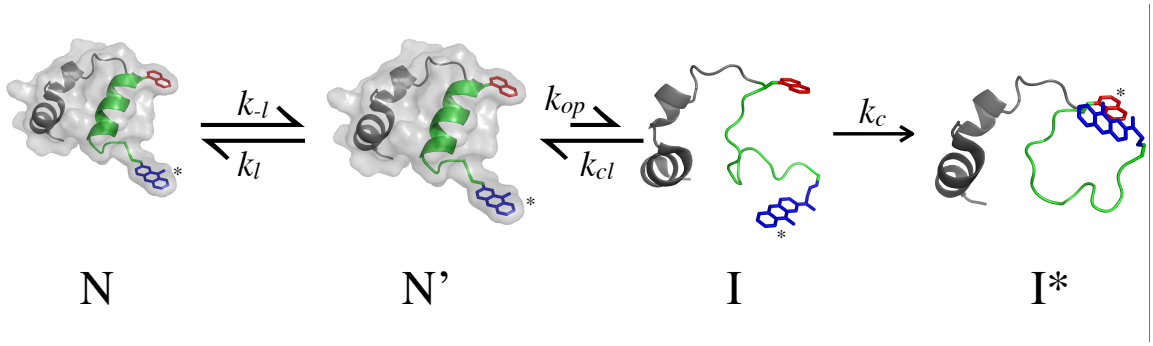

Figure 4.21: Schematic representation of TTET experiments to investigate native-state dynamics of HP35. The locked (N) and unlocked (N′) native state are in equilibrium. Local unfolding of helix 3 to a partially unfolded intermediate (I) only occurs from N′. The TTET labels xanthone (blue) and naphthylalanine (red) were placed at the N- and C-terminal ends of helix 3, respectively. After unfolding of helix 3 loop formation can occur, which brings xanthone and naphthylalanine into van-der-Waals contact and leads to TTET from xanthone to naphthylalanine. These experiments yield the rate constants for unlocking and unfolding of helix 3 as well as information on the populations of N and N′ in equilibrium.

To test whether the properties of the unlocked state are in agreement with a DMG, we determined the volume difference between N and N′ in high pressure TTET measurements. Since DMGs were suggested to represent expanded native states with a dry core, they should have a larger volume than N. According to Le Chateliers principle increasing pressure would thus shift the equilibrium from N′ towards N. However, the results from TTET experiments show that increasing pressure shifts the equilibrium from N to N′ with a reaction volume of -1.8±1.3 cm^3/mol. The transition state for the unlocking/locking reaction has a larger volume than both N and N′ with respective activation volumes of 6.8 cm^3/mol and 8.6 cm^3/mol. These results show that the unlocked state represents a more compact, alternatively folded state whereas the properties of the transition state for unlocking show characteristics of a DMG.

4.3.1 Effect of pressure on the equilibrium between the locked and the unlocked native state in HP35.

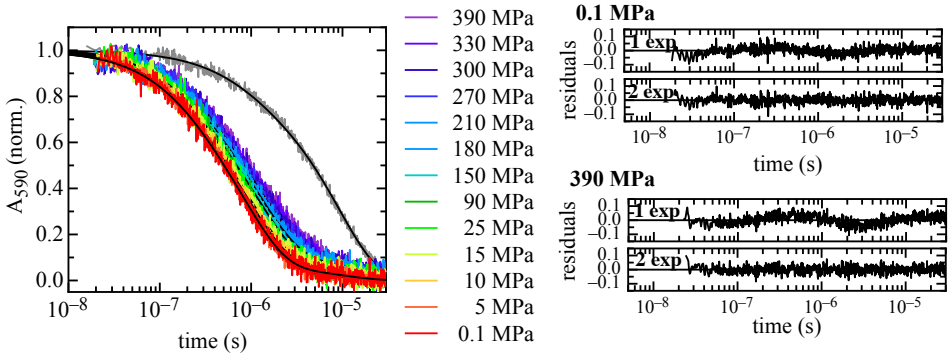

Figure 4.22: Pressure dependence of the unlocking/relocking dynamics in HP35 Nal23/Xan35. The triplet decay curves of xanthone were monitored by the transient absorbance at 590 nm at the indicated pressures. The signal was normalized between 1 and 0. The grey trace shows the xanthone triplet decay in the donor-only HP35 Xan35 protein as a reference. All curves were fitted with double exponential functions. The residuals of the fits are shown for 0.1 MPa and 390 MPa. The sum of two exponentials is sufficient to describe the data over the whole pressure range. Additionally a minor slow kinetic phase with less than 10% amplitude with the intrinsic triplet lifetime of xanthone is observed, due to small amount of aggregated protein. This phase is not used for further analysis.The measurements were performed in 10 mM potassium phosphate buffer, pH 7 at 5°C at peptide concentrations of 50 µM.

To test whether the unlocked state of HP35 represents a DMG we determine the volume difference between N and N′ in high-pressure TTET experiments. The experiments were performed on the HP35 variant labeled with the triplet donor xanthone at position 35 and the triplet acceptor naphthylalanine at position 23 (Nal23/Xan35 variant), which places the TTET labels at the opposite ends of helix 3 (Fig. 4.21). In this variant the populations of N and N′ and the rate constants for their interconversion can be determined, since the two states exhibit different behavior in the TTET kinetics[53]. TTET between xanthone and naphthylalanine is a diffusion-controlled process that requires van der Waals contact between donor and acceptor[29,76]. The xanthone triplet state is produced by a 4 ns laserflash at 355 nm and detected by its absorbance band at 590 nm. TTET from Xan to Nal leads to a decay in Xan triplet absorbance (Fig. 4.22). In the Nal23/Xan35 variant local unfolding of helix 3 is required for donor and acceptor to come into van-der-Waals contact. In the unlocked state, helix 3 unfolds fast, which leads to TTET from Xan to Nal by intrachain loop formation. From the locked state, in contrast, helix 3 can not unfold (Fig. 4.21).

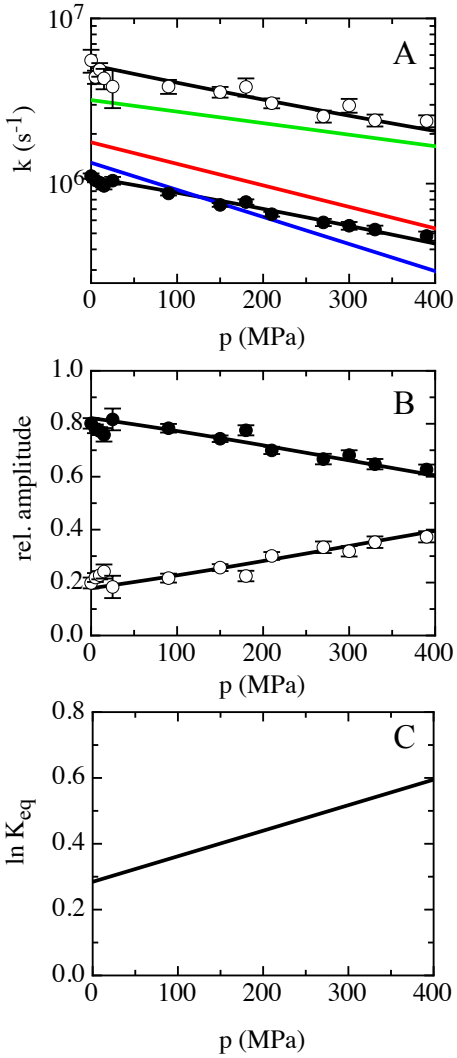

Figure 4.23: Pressure dependence of (A) the two observable rate constants λ_1 (closed circles) and λ_2 (open circles) and (B) their corresponding amplitudes A_1 (closed circles) and A_2 (open circles) obtained from double exponential fits to the kinetics traces at each pressure (circles). Global fitting of the pressure dependence of all kinetic traces according to Eqs. 3.6 to 3.8 yields the observable rate constants λ_1 and λ_2 respective amplitudes A_1 and A_2 relative amplitudes (black lines in panels A and B) as well as the microscopic rate constants for unlocking k_{-l} (red), relocking k_l (blue), and helix 3 unfolding/TTET k_T (green). The slopes of the pressure-dependence of the microscopic rate constants yields the activation volumes of $\Delta V_{-l}^{0\ddagger}$=6.8 cm^3/mol, $\Delta V_l^{0\ddagger}$=8.6 cm^3/mol and $\Delta V_t^{0\ddagger}$=3.6$\pm$0.4 cm^3/mol (Eq. 4.17). (C) Pressure dependence of the equilibrium constant for formation of N′ (K_{eq}=[N′]/[N]=k_f/k_u) calculated from the results of the global fit resulting in ΔV^0=-1.8 cm^3/mol (Eq. 4.18).

This mechanism leads to double exponential kinetics for native-state TTET in the Nal23/Xan35 variant at ambient pressure (Fig. 4.22) with apparent rate constants of λ_1=1.0·10^{-6} s^{-1} (τ_1=1/λ_1=1 µs) and λ_2=5.9x10^{-6} s^{-1} (τ_2=1/λ_2=170 ns) (Fig. 4.23 A). From the apparent rate constants and their amplitudes (A_1=0.25, A_2=0.75, Fig. 4.23 B) the microscopic rate constants for locking (k_l), unlocking (k_{-l}) can be determined using the analytical solution of the kinetic model shown in Fig. 4.21 (Eq. 3.6 to 3.8), which yields k_{-1}=1.78·10^6 s^{-1} and k_1=1.34·106 s^{-1}. From these values the equilibrium constant for unlocking can be calculated using K_{eq}=N′/N=k_{-l}/k_l=1.33. Thus, in equilibrium at 1 bar N′ is populated to 57 %. In addition, the rate constant for TTET from N′ through unfolding of helix 3 is obtained. This reaction proceeds through a high energy intermediate (I) with helix 3 unfolded from which TTET by loop formation can occur (Fig. 4.21). Since I is populated to only small amounts, a single rate constant, k_T, describes the TTET process from N′, which is a function of k_{op}, k_{cl} and k_c (Fig. 4.21) according to:

$$k_T = \frac{k_{op} \cdot k_c}{k_{cl} + k_c} \tag{4.16}$$

Equation 4.16 is identical to the formalism that describes hydrogen exchange kinetics in folded proteins, which proceeds by the same kinetic mechanism as TTET but on a much slower time scale[213]. The fit according to equations 3.6 to 3.8 gives k_T=3.20·10^6 s^{-1}.

Figure 4.22 shows the effect of pressure between 0.1-390 MPa (1 - 3900 bar) on the TTET kinetics in the HP35 Nal23/Xan35 variant. All Xan triplet decay curves can be described by the sum of two exponentials indicating that both N and N′ are populated in equilibrium at all pressures[53,90]. Both kinetic phases and their amplitudes are sensitive to pressure (Fig. 4.23 A,B). The apparent rate constants, λ_1 and λ_2 , both decrease with increasing pressure (Fig. 4.23 A) whereas the amplitude of the faster kinetic phase (A_2) increases at the expense of the slower phase (A_1; Fig. 4.23 B). The analytical solution of the kinetic model for native state TTET in the Nal23/Xan35 variant (Eq. 3.6 to 3.8) was fitted globally to the pressure-dependence of the TTET kinetics (Fig. 4.22) assuming a linear effect of pressure on the microscopic rate constants, k_l, k_{-l} and k_c according to

$$\frac{\delta \ln k_i}{\delta p} = -\frac{\Delta V^{0\ddagger}}{RT} \tag{4.17}$$

where $\Delta V^{0\ddagger}$ represents the activation volume of the reaction, i.e. the volume change between the ground state and the transition state of the respective reaction (Fig. 4.24). The result of the global fit reveals that all reactions become slower with increasing pressure (Fig. 4.23 B) with activation volumes of 6.8 cm^3/mol (11.3 $Å^3$/molecule), 8.6 cm^3/mol (14.3 $Å^3$/molecule) and 3.8 cm^3/mol (3.3 $Å^3$/molecule) for unlocking (k_{-l}), locking (k_l) and triplet transfer through unfolding of helix 3 (k_T), respectively (Fig. 4.23 A). This result shows that the transition states both for unlocking and for local unfolding of helix 3/TTET have larger volumes than all ground state (Fig. 4.24). The observed $\Delta V^{0\ddagger}$ for the partial unfolding reaction of helix 3 is nearly identical to the activation volume observed for unfolding of the central part of an Ala-based α-helical peptide ($\Delta V^{0\ddagger}$=3.3 cm^3/mol) (section 4.2[188]).

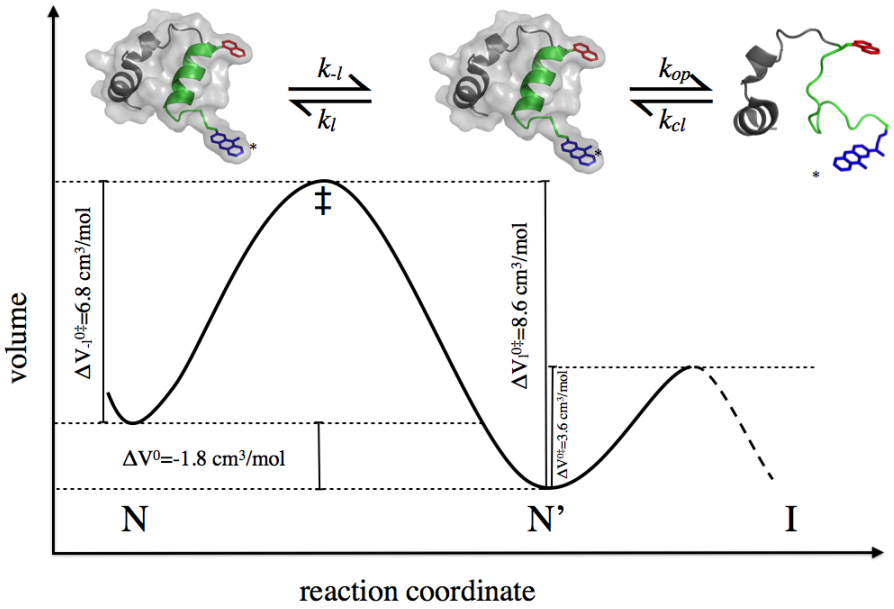

Figure 4.24: Schematic representation of the volume changes for the equilibrium between the locked (N) and the unlocked native state (N′) of HP35. In addition, the volume change for unfolding of helix 3 is shown. Data were taken from the results of the pressure-dependence of native state TTET shown in Fig. 4.22.

From the activation volumes for the unlocking and locking reactions the reaction volume for unlocking (ΔV^0) can be obtained using eq. 4.17

$$\frac{\delta \ln K_{eq}}{\delta p} = \frac{\delta \ln \frac{k_l}{k_{-l}}}{\delta p} = -\frac{\Delta V^0}{RT} \tag{4.18}$$

Figure 4.23 C shows that the equilibrium constant for forming N′ increases with increasing pressure, due to a negative reaction volume of ΔV^0=-1.8±1.3 cm^3/mol (Fig. 4.23C). This result shows that the unlocked state has a slightly smaller volume than N. This negative activation volume leads to an increase in the population of N′ from from 57 % at 0.1 MPa to 64 % at 390 MPa (3.0 Å^3/molecule). Consequently, N′ does not represent an expanded dry molten globule state. Rather, the unlocked state is a compact folded state with a similar volume as the native state. The similar volumes of N′ and N show that the structural rearrangements that occur upon unlocking do not lead to an expansion of the molecule, which indicates that different ways to tightly pack the HP35 structure exits. Our previous results have shown that unlocking leads to an increase in conformational flexibility and entropy with a concomitant decrease in enthalpy[53]. Thus, the unlocked state may have non-optimized geometry and orientation of intramolecular interactions, which leads to weaker intramolecular interactions and increased conformational flexibility and explains the unfavorable enthalpy change and the increase in conformational entropy upon unlocking. The effects on entropy and enthalpy almost compensate, which leads to similar free energies of N and N′. It is unlikely that changes in interactions with water significantly contribute to the observed differences in volume, entropy and enthalpy between N and N′ and the transition state for unlocking. It was shown that these states have similar C_p indicating similar solvent interactions. In addition, the equilibrium between N and N′ and the unlocking kinetics are virtually insensitive to denaturant concentration, indicating similar SASA of all states. It is further unlikely that the observed decrease in volume is due to partial unfolding or fraying of helical structures upon formation of N′, since helices were shown to become more stable with increasing pressure and the volume of an unfolded chain is slightly larger than the volume of an α-helix (section 4.2[188]), which would result in an increase in volume upon formation of N′.

4.3.2 Conclusions

Comparison of the kinetic and equilibrium properties of the N/N′ transition (Fig. 4.22 B, D) shows that the volume of the transition state for locking/unlocking is

increased compared to both N and N′ (Fig. 4.23), which suggests that the structural rearrangements during the locking/unlocking process require a significant expansion of the molecule. Recent results on volume changes associated with the helix-coil transition in peptides showed that the transition state for adding/removing a single helical residue to an existing helix has a 2 cm^3/mol increased volume compared to the helical and coil state (section 4.2[188]). This increased volume was ascribed to be mainly due to the presence of an unsatisfied H-bond in the transition state. The volume of the transition state for unlocking/locking has about a 4-fold larger volume than the volume of the helix-coil transition state. It is plausible that this increased volume is due to a combination of expansion of the molecule and structural re-arrangements of that require formation and breaking of hydrogen bonds. Since the overall secondary structures of N and N′ are very similar, is likely that structural re-arrangements involving hydrogen-bonding mainly occur in the C-terminal region of HP35, which was shown to have different orientations in N and N′[53]. This model would further be compatible with results from NMR studies[214] and MD simulations[164], which both revealed conformational heterogeneity in the C-terminal region of HP35.

The dry molten globule was initially proposed to represent a high energy state that can not be observed directly in experiments[45]. This idea is in agreement with the results from our experiments. As predicted for a DMG, the unlocked native state of HP35 has increased flexibility compared to the locked state and both states have similar SASA, but also similar free energy and volume, which is not compatible with an expanded DMG. The properties of the DMG are rather compatible with the transition state properties for both unlocking and unfolding of helix3/TTET, i.e. these states with increased volume represent states of highest free energy on the reaction coordinate for locking/unlocking and for partial unfolding of helix 3 (Fig. 4.23). Transition states with increased volume compared to the native state were also observed for folding/unfolding of tendamistat[70], ribonuclease A[189], cold shock protein[72] and of an ankyrin repeat domain[74]. These results in combination with the large volumes for the transitions states for unlocking and partial unfolding of HP35 suggest that dry molten globules represent transition states for folding/unfolding and structural rearrangements in native states rather than local free energy minima that may be significantly populated under in equilibrium of transiently during unfolding.

The transient unfolding intermediates observed during unfolding of several proteins[49,51,52]

[50] have properties similar to the unlocked state of HP35. In the light of our results these intermediates may also represent unlocked states rather than dry molten globules, which suggests that unlocked states are commonly present on the native side of the major folding/unfolding barrier. Unlocking of the optimized intramolecular interactions seems to be required prior to local and global protein unfolding. Similarly, during the folding process an unlocked state seems to be more easily accessible and precedes optimization of the geometry and the energetics of the intramolecular interactions. The presence of a compact folded state on the native side of the major folding/unfolding barrier was also observed in high pressure NMR studies on several proteins[215]. Comparison with our results suggests that these states may also represent compact and flexible unlocked states. The increase in conformational flexibility and the ability to undergo large scale conformational fluctuations from the unlocked state may be important for modulating protein function like binding and catalysis.

4.4 Dynamics of the Unlocking/Relocking Reaction in Villin Headpiece Subdomain Variants studied by TTET.

The protein folding reaction is an equilibrium reaction between an unfolded conformation U and the native state N, separated by a energy barrier. In this reaction also intermediates can be populated on either side of the barrier. To study conformational dynamics on the native side of the major unfolding barrier I characterized HP35 variants with TTET.

The villin headpiece subdomain HP35 is a model system to study fast folding processes in proteins. With only 35 amino acids it is one of the smallest cooperatively folding domains[145]. It consists of a three-helix bundle and is stabilized by a hydrophobic core[146,147]. Equilibrium measurements showed a two-state behaviour in GdmCl and temperature induced unfolding experiments[145] and in kinetic studies the timescale for the folding reaction was found to be within µs[153,154] (see section 1.4).

To monitor dynamics in this time regime we used triplet-triplet energy transfer (TTET). Therefore, the triplet donor xanthone and the acceptor naphthalene were incorporated in the sequence in positions that are well separated in the folded state the labels. TTET from xanthone to naphthalene only occurs via van der Waals contact after partial or complete unfolding of the region between the labels (see section 1.2).

In a previous study[53] our group characterized different variants of HP35 (see section 1.4, Fig. 1.10) and found two alternative native states, the locked state N and the unlocked state N′, on the native side of the major unfolding barrier. The unlocking reaction to N′ involves a positive change in ΔH as well as ΔS which reveals that the unlocking weakens the interactions but facilitates more structural flexibility. From the unlocked state helix 3 can partially unfold to a high energy intermediate intermediate (I) (Eq. 4.19) (see section 1.4).

Including this information the kinetic model for TTET coupled to the unlocking/relocking equilibrium in HP35 is:

$$N \underset{k_{\mathrm{l}}}{\overset{k_{\text{-l}}}{\rightleftharpoons}} \mathrm{N}' \underset{k_{\mathrm{cl}}}{\overset{k_{\mathrm{op}}}{\rightleftharpoons}} \mathrm{I} \xrightarrow{k_{\mathrm{c}}} \mathrm{I}^{*} \tag{4.19}$$

The intermediate I is not visible in equilibrium experiments like temperature or GdmCl induced unfolding transitions measured by CD spectroscopy[145]. Therefore, I is a high energy intermediate that is not populated in the equilibrium. In the TTET experiment only one rate constant for the unfolding of helix3/TTET k_T is measured that is composed of the local opening and closing rate constants and the contact formation rate constant (Eq. 4.20).

$$k_T = \frac{k_{op} \cdot k_c}{k_{cl} + k_c} \tag{4.20}$$

In this case the rate constants for the unlocking k_{-l} and relocking k_l as well as for the unfolding of helix3/TTET k_T can be calculated from the two apparent rate constants λ_1 and λ_2 and their amplitudes A_1 and A_2 (Eq. 3.8) if HP35 is completely folded and no additional contributions from the unfolded ensemble arise.

4.4.1 Design of the HP35 variants

For TTET experiments the labels were incorporated in HP35 in solvent exposed positions. The triplet donor 9-oxoxanthene-2 carboxylic acid (Xan) was either attached to the side chain of the nonnatural amino acid α, β-diaminopropionic acid (Dpr) or to the N-terminus via an amide bond and the triplet acceptor was introduced as the nonnatural amino acid 1-naphthyalanine (Nal) in solid phase peptide synthesis. Additionally, if the sites Met12 and Trp23 were not used to incorporate the TTET labels, they were replaced by norleucine or phenylalanine, respectively, due to the TTET quenching properties of the side chains of methionine and tryptophane[75].

Previously four variants of HP235 with different TTET label positions were characterized (see section 1.4 Fig. 1.10)[53]. In the variants HP35 Xan0Nal23 and HP35 X7Nal23 the labels span the core region of HP35. TTET experiments in these variants revealed that no TTET occurs in the native state and therefore global unfolding does not takes place within the experimental time window of several µs, which is the intrinsic lifetime of the xanthone triplet state[53]. First indications on conformational heterogeneity in the native state was found in the variant HP35 Xan0Z35. In these positions the labels are in contact in the native state. In addition, to the kinetics from the unfolded state two kinetic processes were found, one with about 70% of the amplitude in the dead-time of the instrument and one with about 30% of the

amplitude and 30 ns time constant[53]. The variant HP35 Nal23Xan35 gives information on dynamics in the C-terminal helix 3 as the TTET labels can only come into contact if helix 3 is at least partially unfolded (Tab. 4.4 and Fig. 4.25 A). In this variant the heterogeneity in the native state of HP35 was further analyzed revealing the presence of two alternative native states, the locked and the unlocked state[53] (see section 4.4.2).

Here I further characterize the equilibrium between the locked and the unlocked native state, N and N′, to gain information on the properties of N′. Therefore, I ask the following questions concerning the effects on the N′/N equilibrium and its dynamics:

a) What are the effects of the solvent on the unlocking/relocking reaction?
The variant HP35 Nal23Xan35 (Tab. 4.4 and Fig. 4.25 A) yielded valuable information on the N′/N equilibrium and the properties of the two states. The effect of solvent additives, especially the effect of urea, salt and sodium sulfate, will therefore be determined in this variant.

b) How do mutations influence the unlocking/relocking reaction and the unfolding of helix 3?
Especially mutation that influence the packing might have impact on the N′/N equilibrium and its dynamics. The Leu28 contributes to the hydrophobic core and substitution of the L28 should lead to destabilization of interactions and hence destabilize the packing of HP35. It is replaced by an alanine in order reduce the hydrophobic interactions and at the same time stabilize helix 3 (HP35 L28A Nal23Xan35, Tab. 4.4).

c) Can helix 1 unfold from the unlocked state N′ and form a high energy intermediate?
From the unlocked state N′ helix 3 can unfold and form a intermediate. Previous studies showed that both helices 1 and 2 together only unfold during the global unfolding reaction[53]. But it is conceivable that also helix 1 is able to unfold after the unlocking reaction and form a high energy intermediate. To test this hypothesis I introduced the TTET labels at the N-terminus and in the linker between helix 1 and 2 (Tab. 4.4 and Fig. 4.25 B).

d) Is it possible to obtain an even smaller cooperative folding unit than HP35? The fragment that only consists of helix 1 and 2 was proposed to be stable and folded in isolation[158,160]. To determine the folding and unfolding rate constants the TTET labels were introduced at the termini of the fragment (Tab. 4.4 and Fig. 4.25 C).

HP35 variant	mutations and sequence
HP35 Nal23Xan35	M12Nle W23Nal F35Dpr(Xan) LSDEDFKAVFGNleTRSAFANLPLNalKQQNLKKEKGLXanG
HP35 L28A Nal23Xan35	M12Nle L28A W23Nal F35Dpr(Xan) G LSDEDFKAVFGNleTRSAFANLPLNalKQQNAKKEKGLXanG
HP35 Xan0Nal12	Xan0 M12Nal W23F Xan-LSDEDFKAVFGNalTRSAFANLPLFKQQNLKKEKGLF
HP23 Xan0Nal23	Xan0 M12Nle W23Nal GS Xan-LSDEDFKAVFGNleTRSAFANLPLNalGS-NH_2
HP35 Xan35	Donor only M12Nle W23F F35Dpr(Xan) LSDEDFKAVFGNleTRSAFANLPLFKQQNLKKEKGLXanG
HP35 Xan0	Donor only Xan0 M12Nle W23F Xan-LSDEDFKAVFGNalTRSAFANLPLFKQQNLKKEKGLF

Table 4.4: List of HP35 variants. Xan: xanthone attached to the side chain of α,β-diaminopropionic acid (Dpr) or the N-terminus; Nal: 1-Naphthylalanine.

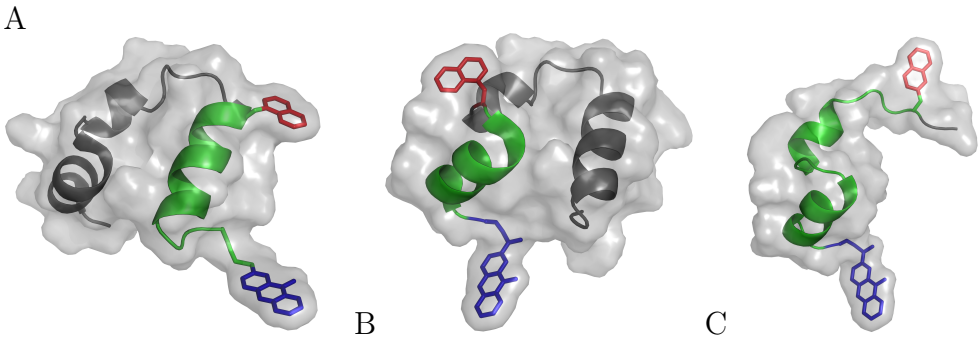

Figure 4.25: Label positions in the HP35 variants. The donor xanthone is shown in blue, the acceptor naphthalene in red and the probed region is highlighted in green. A) HP35 Nal23Xan35 B) HP35 Xan0Nal12 C) HP23 Xan0Nal23. Images were created using the MacPyMOL software.

4.4.2 Effect of solvents on native-state TTET in the HP35 Nal23Xan35 variant

Our group studied the GdmCl dependence of the dynamics in HP35 Nal23Xan35 in CD and TTET experiments[53]. The far-UV CD transition showed that in the absence of denaturant >99% of the protein is folded (Fig. 4.27 B). Two apparent kinetic phases occurred in native-state TTET with rate constants of $6 \cdot 10^6$ s^{-1} and $1 \cdot 10^6$ s^{-1}. These two phases indicate the presence of two native states N and N′. The slower process has only a very low m-value showing no significant ΔSASA during the unlocking reaction. The fast process originates mainly from unfolding of helix3/TTET from the unlocked state N′. The m-value of -1.8 kJ/(mol M) points to a exposure of about 50 % of the SASA of the complete unfolding reaction.

Nevertheless a direct correlation between the amplitude of the kinetic phase and the concentration of N or N′ is not valid as the unlocking and relocking as well as the unfolding of helix3/TTET occur on similar time scales (Fig. 4.26)(Eq. 3.6 - 3.8). With the two apparent rate constants λ_1 and λ_2 and their amplitudes A_1 and A_2 the microscopic rate constants were determined to $k_{-l} = 1.7 \cdot 10^6$ s^{-1}, $k_l =$ of $1.6 \cdot 10^6$ s^{-1} an $k_T = 3.7 \cdot 10^6$ s^{-1} for HP35 Nal23Xan35 in the absence of denaturant. This yields equilibrium constant of $K_{eq} = k_{-l}/k_l = \text{N}'/\text{N} = 1.1$ showing that the two states are almost equally populated.

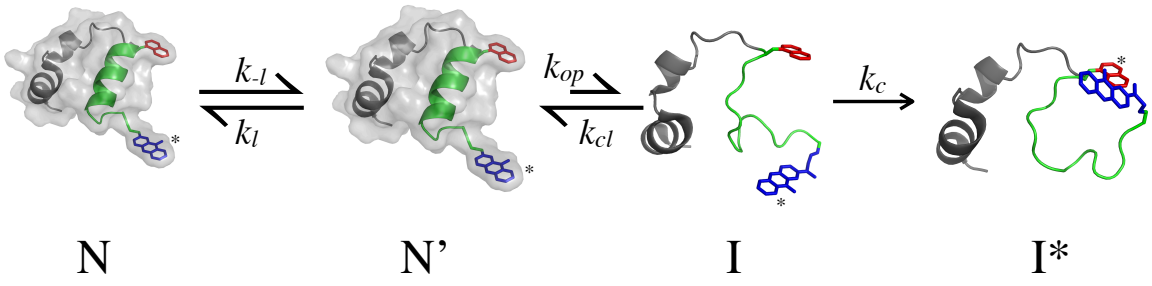

Figure 4.26: Kinetic model for TTET coupled to the dynamics in HP35 Nal23Xan35. Images were created using the MacPyMOL software.

To eliminate salt effects the denaturant dependence was also recorded in urea. The denaturant induced unfolding transitions were recored by fav-UV CD (Fig. 4.27) and show that the midpoint of the transition is shifted from 2.2 M of GdmCl to 3.4 M of urea in accordance with the stronger denaturing properties of GdmCl. Both transitions were fit globally with the same ΔG^0. The stability was determined to

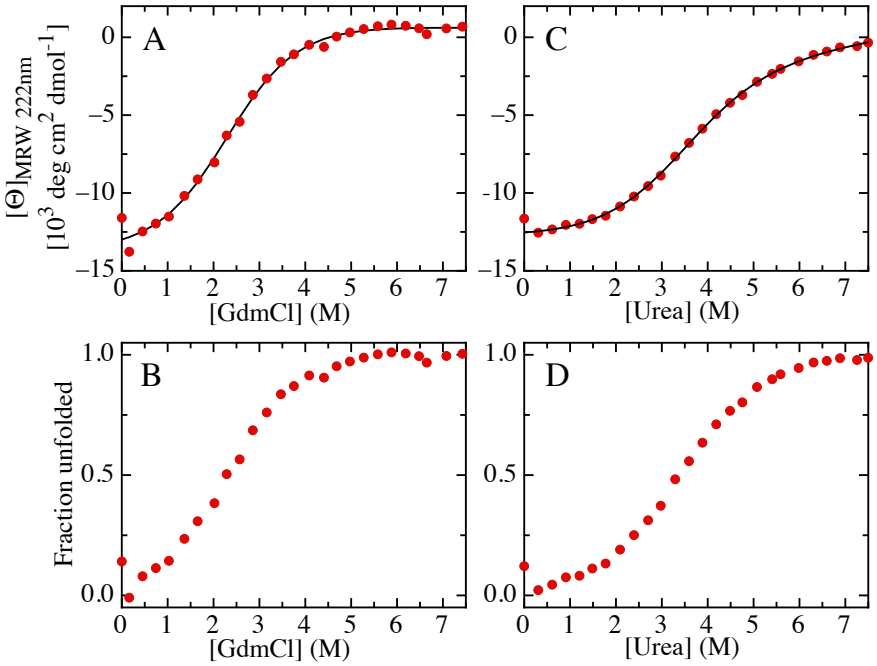

Figure 4.27: Denaturant induced CD transitions of HP35 Nal23Xan35 in the presence of GdmCl (A,B) and urea (C,D). Ellipticity (A,C) and calculated fraction of unfolded protein (B,D) in dependence of denaturant concentration. The data of the GdmCl transition was taken from [53].

ΔG^0 = -7.8 kJ/mol with a m-values of 3.2 kJ/(mol M) for GdmCl and 2.3 kJ/(mol M) for urea. Compared to the wild type (WT) HP35 in the absence of the TTET labels and with methionine in position 12 the stability of HP35 Nal23Xan35 is reduced by 4 kJ/mol (ΔG^0_{WT} = -12 kJ/mol) [152].

TTET kinetics between 0 M and 6.5 M urea of HP35 Nal23Xan35 show that urea has only little effect on the TTET kinetics (Fig. 4.28 A), although it is known that urea does unfold HP35 Nal23Xan35. The data was fit double or triple exponential (Fig. 4.28 B,C). The two rate constants in the absence of urea correspond to the two apparent rate constants that are expected from the TTET coupled to the N′/N equilibrium. The slow phase $lambda_1$ (blue, Fig. 4.28) shows only little denaturant dependence (m-value= -0.09 kJ/(mol M)). The amplitude of this phase drops with increasing concentrations of urea following the CD transition. It comes very close with only a factor 2-3 difference to the kinetics from the unfolded ensemble (black, Fig. 4.28). So these two phases are difficult to separate in the fitting procedure and the amplitudes might mix at higher concentrations of denaturant. At low concentrations of denaturant the fast rate constant $lambda_2$ (red, Fig. 4.28) is too close to the

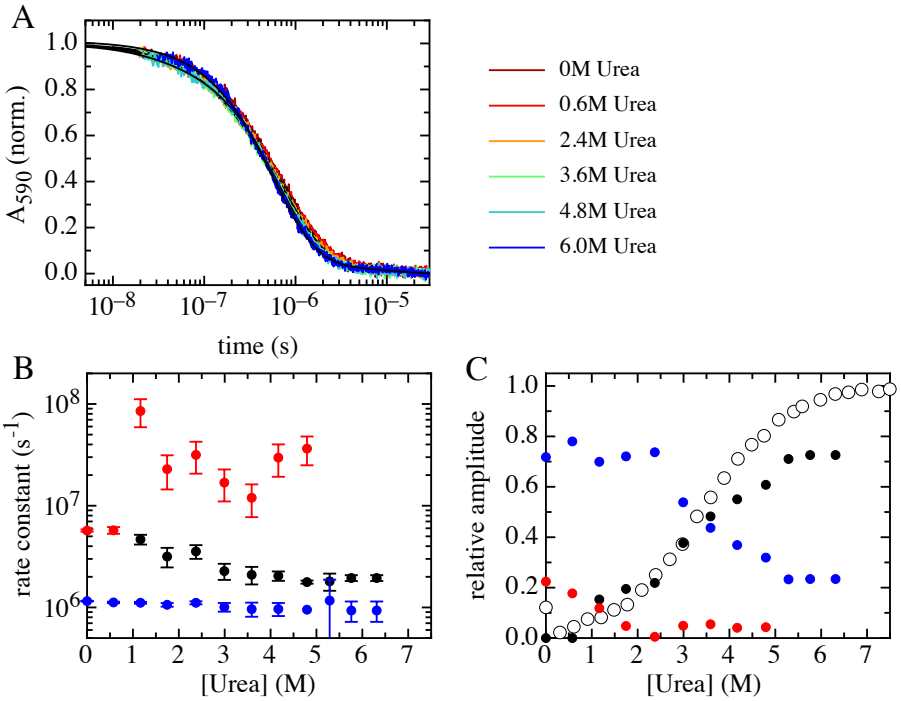

Figure 4.28: TTET kinetics of HP35 Nal23Xan35 in the presence of urea. (A) Triplet absorbance decay recorded at 590 nm between 0 M and 6.5 M urea. Data from the donor only HP35 Xan35 was taken from[53]. Urea dependence of the rate constant (B) and their relative amplitudes (C). The colors of the rate constant and their corresponding amplitudes are equivalent. The open circles represent the fraction of unfolded molecules calculated from the CD unfolding transition.

rate constant from the unfolded ensemble. The difference in the urea dependence of the fast phase compared to the GdmCl dependence might hint to a effect of salt on the undocking reaction of helix 3. This will be examined in a separated salt dependence of the dynamics in HP35 Nal23Xan35 (Fig. 4.29). Just above one molar urea the third kinetic phase (black, Fig. 4.28), that arises from the unfolded state, becomes visible. It has also a very low but positive m-value of 0.5 kJ/(mol M). The amplitude of this kinetic phase shows the shape of a typical unfolding transition and also follows the fraction of unfolded molecules calculated from the far-UV CD data. However, the transitions seems not to be complete, as even at the highest concentrations of denaturant the phase of the unfolded HP35 only reaches 72 % of the complete amplitude. As discussed above this may be due to the small separation from kinetics in the native state. The original kinetic traces do not shift visibly during the urea induced unfolding transition as the kinetics arising from the unfolded state have similar rate constants as the one from one of the native states. The data

recorded in the presence of urea and GdmCl seem to agree with the model although the data in the presence of urea is hard to evaluate.

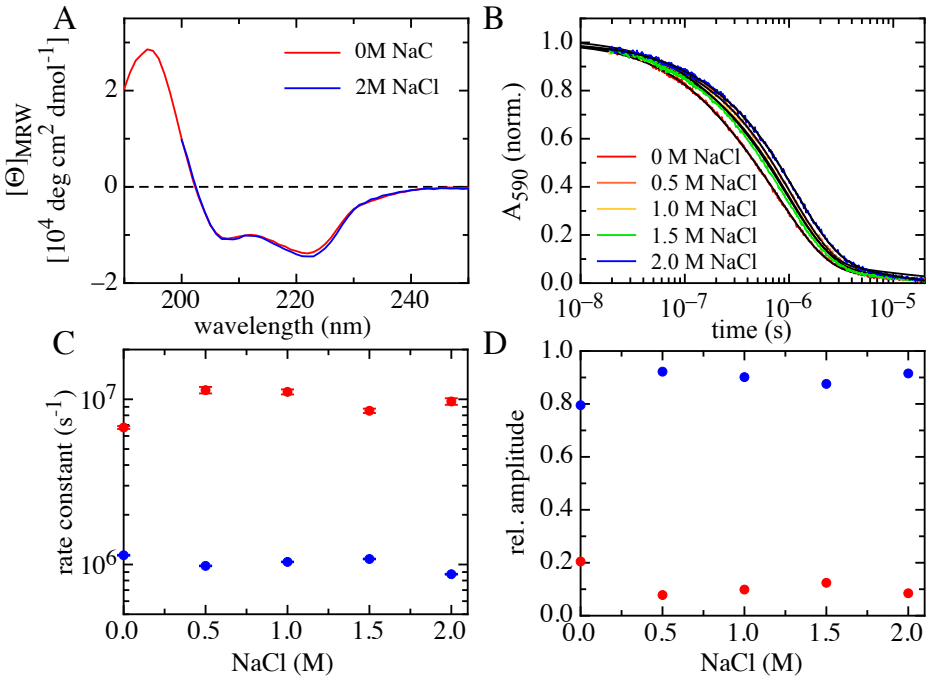

Figure 4.29: CD spectra and TTET kinetics of HP35 Nal23Xan35 in the presence of $NaCl$. (A) Comparison of the CD spectrum of HP35 Nal23Xan35 in the presence and absence of 2 M $NaCl$. (B) TTET kinetics recorded at 590 nm at various concentrations of salt. Rate constants (C) and the corresponding amplitudes (D) of the exponential fit of the TTET traces.

The $NaCl$ dependence was recorded to test for salt effects. The results (Fig. 4.29) show that between 0 and 2 M $NaCl$ there is no effect neither in the far-UV CD spectra nor in TTET kinetics.

The GdmCl transition of HP35 Nal23Xan35 already starts at low concentration of denaturant. In the presence of 0.5 M Na_2SO_4 the folded state is stabilized and the transition is shifted to higher GdmCl concentrations (Fig. 4.30). The ΔG^0-value increases from 7.5 kJ/mol in the absence of Na_2SO_4 to 12.8 kJ/mol in the presence of Na_2SO_4. Thus the protein is stabilized by more than 5 kJ/mol by 0.5 M Na_2SO_4. The m-values of 3.8 kJ/(mol M) in the presence of Na_2SO_4 is only slightly higher than the m-value of 3.3 kJ/(mol M) in the absence of Na_2SO_4, which suggest that the change in the SASA is not altered by the additive.

The TTET kinetics of HP35 Nal23Xan35 in the presence Na_2SO_4 show the two apparent rate constants $\lambda_{1/2}$ that are expected for TTET in the native state (Fig.

4.31). At 0 M GdmCl they are with $9 \cdot 10^5$ s^{-1} and $4.7 \cdot 10^6$ s^{-1} within the error of the values in the absence of Na_2SO_4. The slower phase $lambda_1$ has no significant denaturant dependence whereas the faster $lambda_2$ one has an m-value of -2.2 kJ/(mol M) which is slightly larger compared to the published value of -1.8 kJ/(mol M) in the absence of Na_2SO_4[53]. At 2 M GdmCl the kinetic phase of the unfolded ensemble (black, Fig. 4.31) arises and the amplitudes follow the fraction of unfolded protein calculated from the CD unfolding transition.

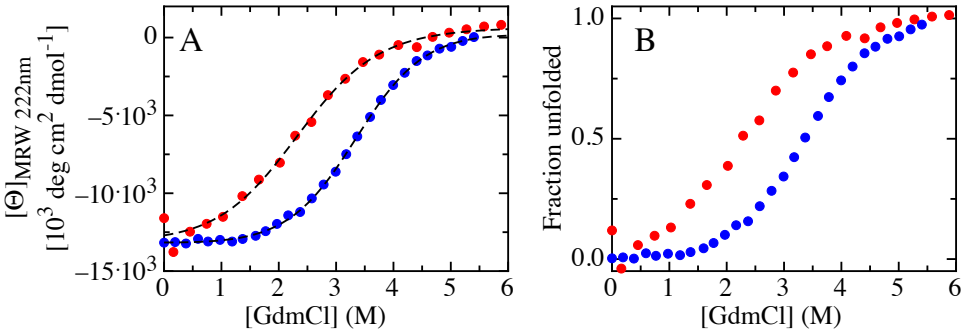

Figure 4.30: CD transitions of HP35 Nal23Xan35 in the presence (blue) and in the absence of (red) 0.5 M of Na_2SO_4 in 10 mM potassium phosphate, pH7

The three-state model (Eq. 3.6 to 3.8) is applied to the TTET trace at 0 M GdmCl, 0.5 M Na_2SO_4 and yields a unlocking rate constant k_{-l} of $1.6 \cdot 10^6$ s^{-1} and a relocking rate constant k_l of $1.7 \cdot 10^6$ s^{-1}. This gives a equilibrium constant $K_{eq} = k_{-l}/k_l = N'/N$ of 0.9. The values are in good agreement to the ones in the absence of Na_2SO_4 (Tab. 4.5). The unlocking reaction is slightly reduced whereas the relocking is slightly accelerated which results in a smaller equilibrium constant. The rate constant for unfolding of helix3/TTET k_T is slowed down from $3.7 \cdot 10^6$ s^{-1} to $3.2 \cdot 10^6$ s^{-1} which might be due to a stabilization of the docking of helix 3 to the core in Na_2SO_4.

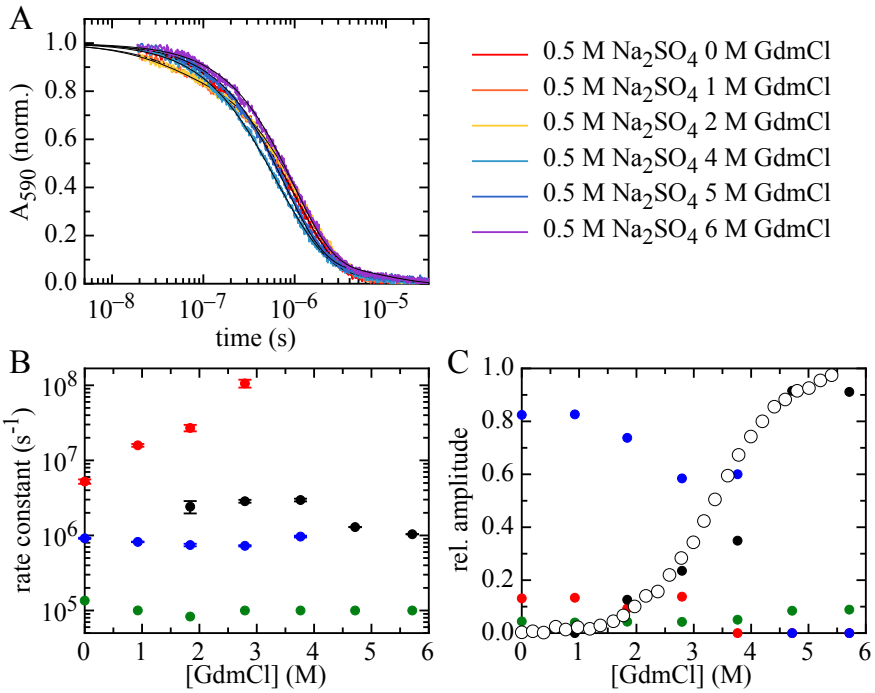

Figure 4.31: GdmCl dependence of TTET kinetics of HP35 Nal23Xan35 in the presence of 0.5 M Na_2SO_4(A) Triplet absorbance decay recorded at 590 nm at various concentrations of GdmCl . GdmCl dependence of the rate constant (B) and their relative amplitudes (C). The colors of the rate constant and their corresponding amplitudes are equivalent. The open circles represent the fraction of unfolded molecules calculated from the CD transition.

4.4.3 Stability and dynamics of the HP35 L28A Nal23Xan35 variant

In the variant HP35 L28A Nal23Xan35 a leucine 28 has been replaced by an alanine. The mutation is located in helix 3 that has been shown to unfold to an high energy intermediate after global unlocking of the native structure. The structure shows that leucine 28 takes part in the hydrophobic core and thereby it could contribute to the energy barrier of the unlocking reaction. I chose to replace leucine 28 with alanine as it lacks the bulky and hydrophobic side chain and at the same time stabilizes helix 3. By altering the interactions that govern the unlocking reaction the dynamics or the ratio of N′ to N could change and yield information on the mechanism.

Already in the far-UV CD spectrum of HP35 L28A Nal23Xan35 a lower helicity compared to the non-mutated variant is found (Fig. 4.32 A). Due to contributions of the TTET labels to the CD signal the helix content cannot be evaluated quanti-

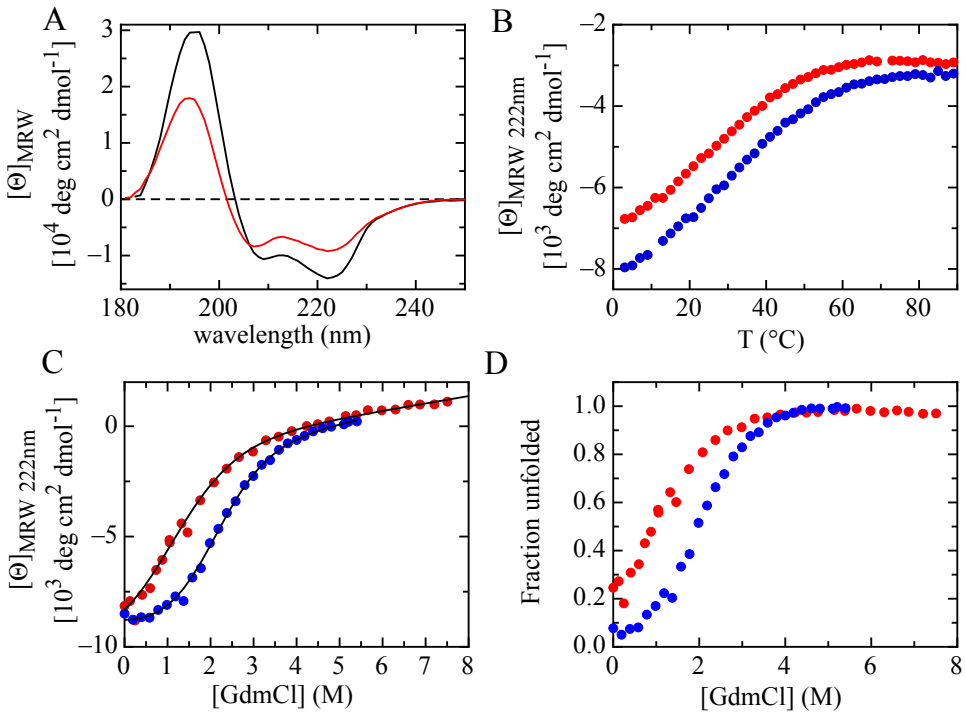

Figure 4.32: Far-UV CD spectra and unfolding transitions of HP23 L28A Nal23Xan35. A) CD spectra of HP23 L28A Nal23Xan35 (red) in comparison to HP23 Nal23Xan35 (black). B) Temperature transition of the CD signal at 222 nm in the absence (red) and in the presence of 0.5 M Na_2SO_4 (blue) in 10 mM potassium phosphate, pH7. C) GdmCl unfolding transition of the ellipticity at 222 nm and D) the calculated fraction of unfolded protein under the same conditions.

tatively. The temperature transition shows the stabilization of the native state by Na_2SO_4 (Fig. 4.32 B). Also the GdmCl transition has been recorded in the presence and in the absence of Na_2SO_4. in the absence of Na_2SO_4 the unfolded state is populated to a significant amount and only 75% of HP35 L28A Nal23Xan35 is folded at 5 °C. In the presence of Na_2SO_4 more than 95% of the protein is in the native state. The global fit of the two GdmCl induced unfolding transitions yields a stability of HP35 L28A Nal23Xan35 of only 2.8 kJ/mol with an m-value of 3.1 kJ/(mol M). Thus, the stability is reduced by 5 kJ/mol compared to HP35 Nal23Xan35 and by 9 kJ/mol compared to the WT.

In TTET experiments between 0 and 7 M GdmCl (Fig. 4.33 A) the kinetic phase that originates from the unfolded ensemble is visible and the amplitude follows the ratio of unfolded protein calculated from the far-UV CD transition (Fig. 4.33 B,C). It has a small m-value of 0.4 kJ/(mol M). At low denaturant concentrations two addi-

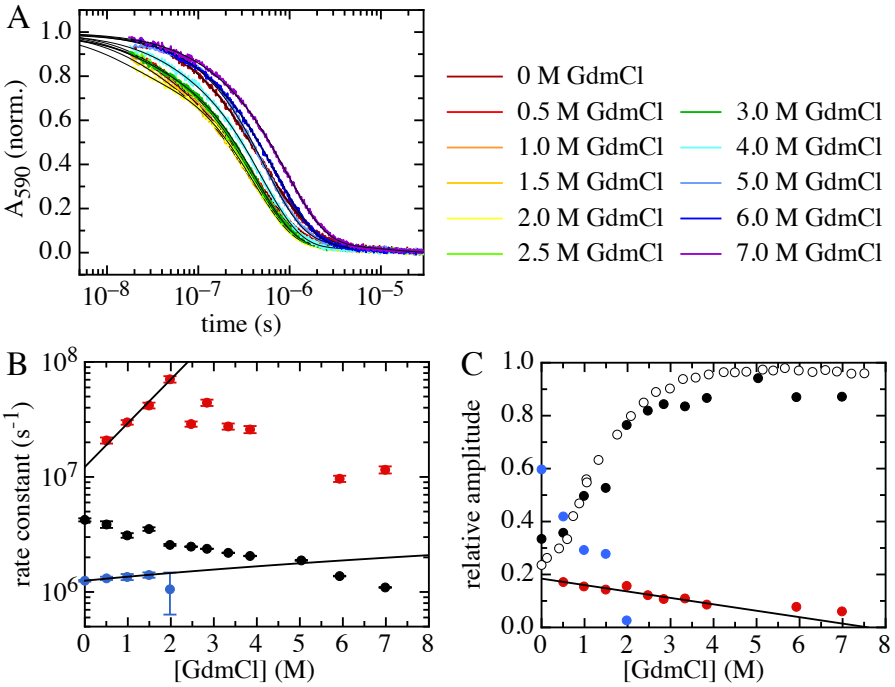

Figure 4.33: GdmCl dependence of TTET kinetics of HP35 L28A Nal23Xan35. (A) Triplet absorbance decay recorded at 590 nm at various concentrations of GdmCl . GdmCl dependence of the rate constant (B) and their relative amplitudes (C). The colors of the rate constant and their corresponding amplitudes are equivalent. The open circles represent the fraction of unfolded molecules calculated from the CD transition.

tional kinetic phases are present. As the unlocking/relocking reaction is a equilibrium reaction these two kinetics are apparent rate constant λ_1 and λ_2 of TTET coupled to the equilibrium reaction (Eq. 4.19). In this variant not only the two native states are present at low concentrations of denaturant but also the unfolded state is populated to a significant amount. At 0M GdmCl the kinetics from the unfolded ensemble and λ_2 get very close and cannot be separated in the fit. To gain information on the microscopic rate constants the apparent rate constants $\lambda_{1/2}$ are extrapolated to 0M GdmCl. Additionally the sum of the amplitudes of $\lambda_{1/2}$ is normalized to 1 neglecting the amount of unfolded protein. With these assumptions the microscopic rate constants can be calculated to $k_{-l} = 1.6 \cdot 10^6$ s^{-1}, $k_l = 2.4 \cdot 10^6$ s^{-1} and $k_T = 9.5 \cdot 10^6$ s^{-1}. In comparison with the leucine containing reference HP35 Nal23Xan35 the slower kinetic phase λ_1 remains unchanged with also a very small m-value whereas the faster kinetic phase λ_2 is accelerated (Tab 4.5). In HP35 Nal23Xan35 the faster phase λ_2 extrapolates to $5.9 \cdot 10^6$ s^{-1} at 0 M GdmCl and in HP35 L28A Nal23Xan35 to $1.2 \cdot 10^7$

s^{-1}. The m-value remains mainly unchanged with m = -1.8 kJ/(mol M) for HP35 Nal23Xan35 and m = -2.0 kJ/(mol M) for HP35 L28A Nal23Xan35. The unlocking rate constant k_{-l} in the L28A variant is unchanged in contrast to the relocking k_l which is accelerated. This results in a reduced equilibrium constant K_{eq}. k_T is significantly faster in the L28A variant than the in the leucine containing variant. Nevertheless these values might be not very reliable as many assumptions have been made and the values are only calculated form the apparent rate constants and their amplitudes and not fitted to a experimental trace.

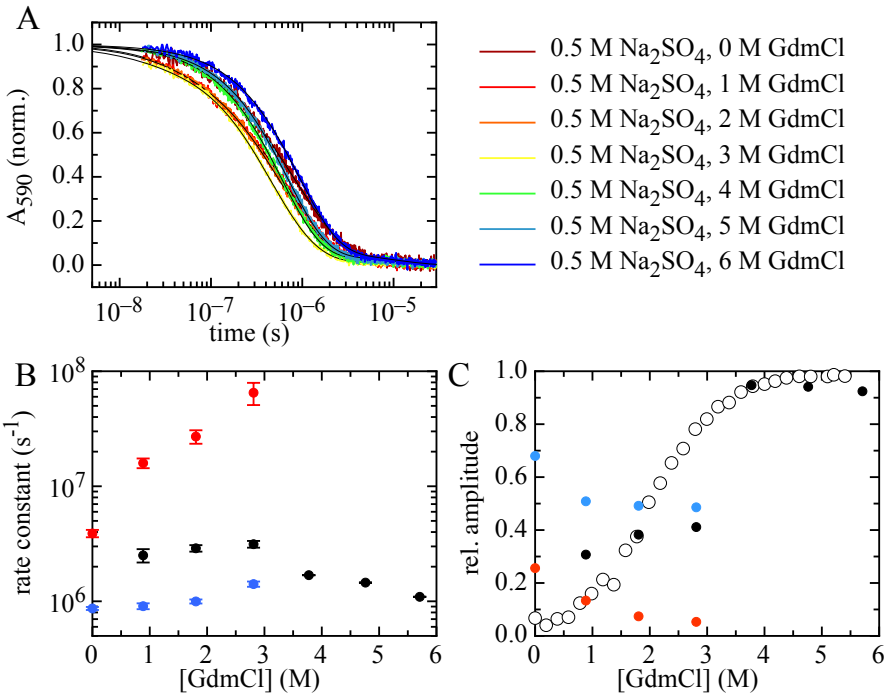

Figure 4.34: GdmCl dependence of the TTET kinetics of HP23 L28A Nal23Xan35 in the presence of 0.5 M Na_2SO_4. (A) Triplet absorbance decay recorded at 590 nm. GdmCl dependence of the rate constant (B) and their relative amplitudes (C). The colors of the rate constant and their corresponding amplitudes are equivalent. The open circles represent the fraction of unfolded molecules calculated from the CD unfolding transition.

TTET kinetics were also recorded in the presence of 0.5 M Na_2SO_4. The additive Na_2SO_4 stabilizes the compact structures of the protein and more than 95% of the HP35 L28A Nal23Xan35 is folded in the absence of GdmCl (Fig. 4.32 D). The kinetics of the unfolded ensemble appear at 1 M GdmCl and show the same m-value of -0.4 kJ/(mol M) as in the absence of denaturant. Additionally the two apparent rate constants $\lambda_{1/2}$ of the folded states are present. Between 1 and 3 M GdmCl the

slow phase λ_1 is close within a factor of 2 to 3 to the kinetics from the unfolded proteins and the fit cannot separate them which results in amplitudes that are not well defined. in the absence of denaturant but in the presence of Na_2SO_4 the slow phase λ_1 of $9 \cdot 10^5$ s^{-1} corresponds well to the one in the absence of Na_2SO_4 and due of the stabilization of the native states the fast phase λ_2 can be determined to $4 \cdot 10^6$ s^{-1} with an m-value of -1.8 kJ/(mol M). This is in very good agreement with λ_1 and λ_2 from HP35 Nal23Xan35.

In the presence of the stabilizing agent Na_2SO_4 HP23 L28A Nal23Xan35 is folded to more than 95 % und the unfolded population can be neglected. Thus the three-state system (Eq. 4.19) can be used to determine the microscopic rate constants k_l and k_{-l} to $7.7 \cdot 10^5$ s^{-1} and $1.2 \cdot 10^6$ s^{-1}, respectively. With $K_{eq} = k_{-l}/k_l$ the equilibrium constant can be calculated to 1.6. Comparison to the value that were gained in the absence of Na_2SO_4 shows that all apparent and microscopic rate constants are slowed down. This might be due to the addition of Na_2SO_4 but as Na_2SO_4 does not show this effect in the HP35 Nal23Xan35 variant it could also be due to the inaccuracy of the values that were determined in the absence of Na_2SO_4.

Hence the values in the presence of Na_2SO_4 give more reliable information on the difference of the L28A variant to the leucine containing HP35 Nal23Xan35 and the effect of the amino acid replacement. The unlocking rate constant is slightly decreased in the L28A variant but the rate constant for the relocking reaction is decreased by a factor of 2. This yields a higher equilibrium constant of 1.6 than the equilibrium constant of 0.9 of the leucine containing HP23 Nal23Xan35 and thus the equilibrium is shifted to the N′ state in the L28A variant. Alanine has a higher helix propensity than leucine (see section 1.3, Tab. 1.2) and therefore favors α-helix formation. This might be the explanation for the reduced rate constant for the unfolding of helix3/TTET k_T in the L28A variant.

4.4.4 Stability and dynamics of the HP35 Xan0Nal12 variant

The variant HP35 Xan0Nal12 was chosen to examine if also helix 1 can unfold to a partial unfolding intermediate after unlocking of N to N′. Therefore, the donor was introduced at the N-terminus and the acceptor between helix 1 and 2 in position 12 (Fig. 4.25).

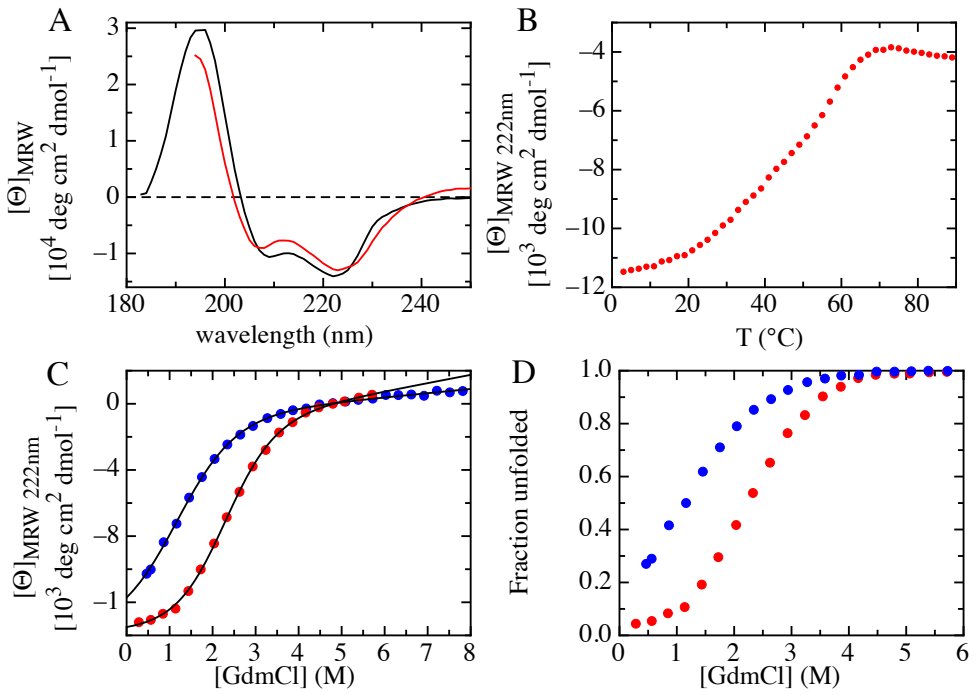

Figure 4.35: CD spectra and transition of HP35 Xan0Nal12. (A) Far-UV CD spectra of HP35 Xan0Nal12 (red) and HP35 Nal23Xan35 (black) for comparison. (B) CD Temperature transition of HP35 Xan0Nal12 measured at 222 nm. Ellipticity (C) and calculated fraction of unfolded protein (D) in dependence of GdmCl in the presence (red) and absence of (blue) 0.5 M Na_2SO_4.

The CD spectrum shows that HP35 Xan0Nal12 is helical to a similar amount as the reference variant HP35 Nal23Xan35 (Fig. 4.35 A) and the temperature unfolding is cooperative (Fig. 4.35 B). However, the denaturant dependence of the ellipticity reveals the low stability of the HP35 Xan0Nal12 variant (Fig. 4.35 C,D) and at low denaturant concentrations only 70% of HP35 Xan0Nal12 is folded. Only upon addition of 0.5 M Na_2SO_4 >95% of HP35 Xan0Nal12 is folded. The stability in the absence and presence of Na_2SO_4 is 3.8 kJ/mol and 8.9 kJ/mol, respectively, which shows that HP35 Xan0Nal12 is folded but strongly destabilized.

A one-dimensional ^{1}H NMR spectrum of the HP35 Xan0Nal12 variant was compared to the NMR spectrum of HP35 N23Xan35 and the WT (Fig. 4.36). The signal/noise ratio of the ^{1}H NMR spectrum of HP35 Xan0Nal12 is not very good due to its low solubility. The ^{1}H NMR spectra of HP35 variants usually exhibit some typical peaks, especially the signal of the valine 9 methyl group at -0.5 ppm is characteristic. This peak is completely missing in the spectrum of HP35 Xan0Nal12 which points to some disturbance in the structure in the first helix. In the aromatic region

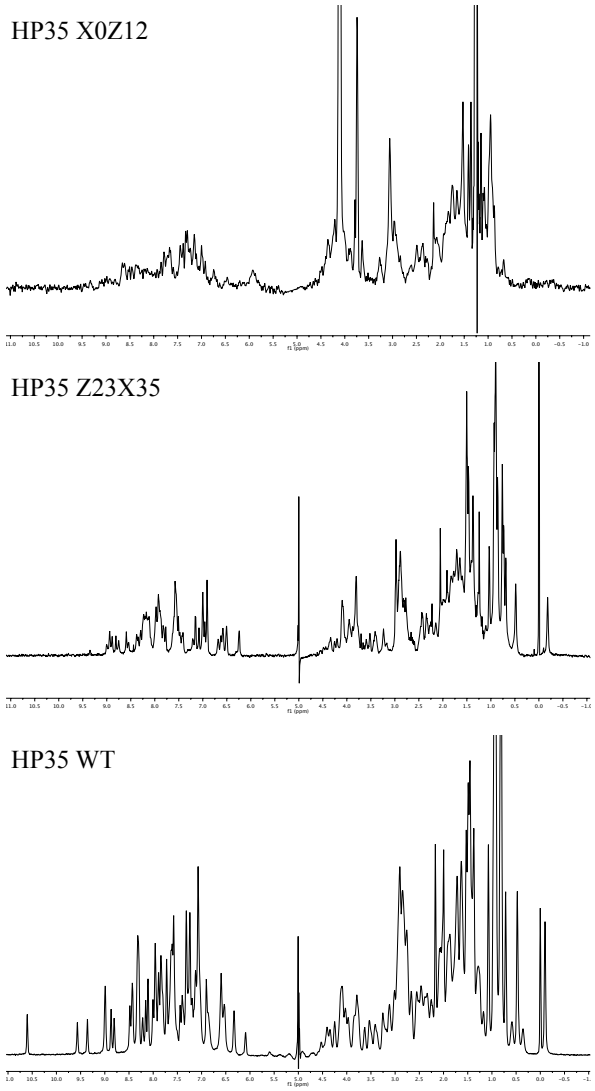

Figure 4.36: Comparison of the one-dimensional ^{1}H NMR spectrum of HP35 Xan0Nal12, HP23 Nal23Xan35 and HP23 WT in 10 mM potassium phosphate, pH 7, 10 (v/v) % D_2O, 5°C. The spectrum from HP35 WT was recorded by Jeremy Sloan.

the peaks are not well separated and the overall spectrum resembles mainly the spectrum of a unfolded protein. Nevertheless the temperature and the GdmCl induced unfolding transition measured by CD spectroscopy show a cooperative unfolding.

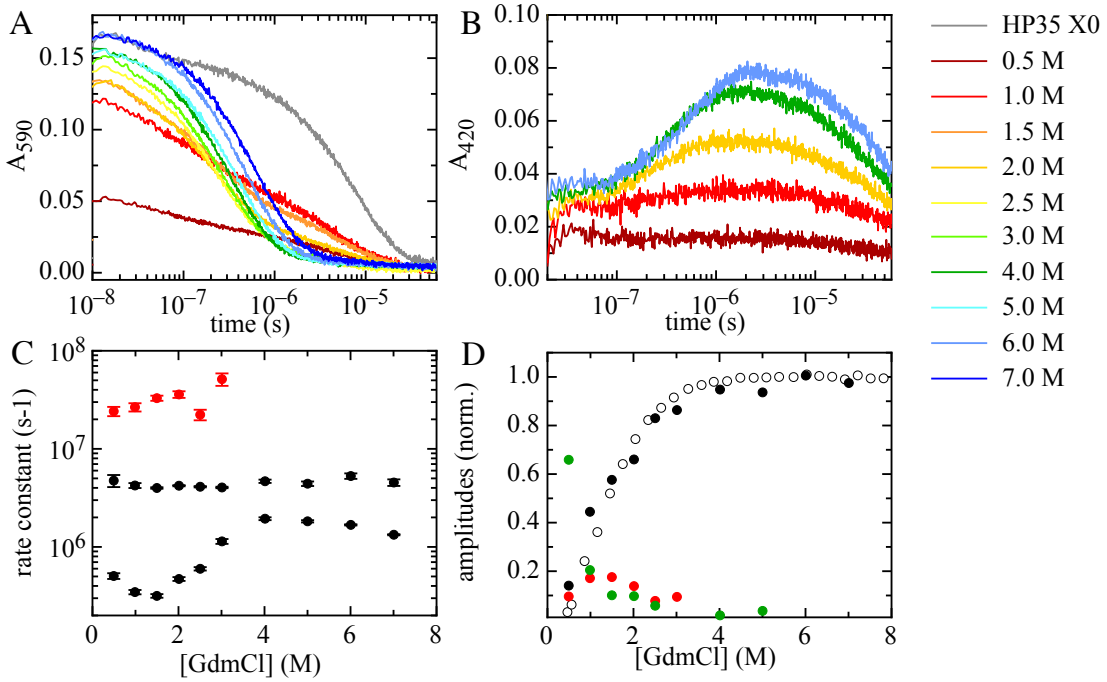

Figure 4.37: GdmCl dependence of the TTET kinetics of HP35 Xan0Nal12. Data of HP35 Xan0 were taken from[53]. Triplet absorbance decay of Xan recorded at 590 nm (A) and 420 nm (B) between 0 M and 7 M GdmCl as indicated. The GdmCl dependence of the rate constant (B) and their relative amplitudes (C) are shown. The colors of the rate constant and their corresponding amplitudes are equivalent. The missing amplitude is shown in green. and the open circles represent the fraction of unfolded molecules calculated from the CD transition.

In the TTET kinetics in the absence of denaturant more than 70% of the amplitude is missing (Fig. 4.37 A). The triplet state of this population does not occur at the acceptor absorbance of 420 nm (Fig. 4.37 B), which suggests that the labels are in close contact at the time of excitation and undergo triplet quenching in the dead-time of the instrument. The positions of the two labels were chosen such as they are not in contact in the folded state based on the X-ray structure[147]. Nevertheless these measurements reveal that xanthone and naphthalene interact closely in the native state and therefore the structure of helix 1 must be disturbed by the labels.

All kinetic traces were fitted double or triple exponentially (Fig. 4.37 C,D). A comparison of the amplitudes of the kinetic phases with the calculated fraction of

unfolded protein from CD measurement reveal that the two slower kinetic phases arise from the unfolded ensemble as the sum of the two amplitudes add up well to the amount of unfolded protein. Additionally a faster phase that extrapolates to $2.0 \cdot 10^7$ s^{-1} at 0 M GdmCl is present. Further evaluation of the data of HP35 Xan0Nal12 does not allow any conclusions on the unlocking/relocking reaction of HP35 folding in general as the overall structure of this variant is strongly perturbed by the labels.

4.4.5 Fragment comprised of helix 1 and 2 of HP35

It was proposed by Tang *et al.*[158,160] that the fragment of the villin headpiece subdomain consisting of helix 1 and 2 is folded in isolation. Here this fragment containing amino acid 1 to 23 of HP35 was chosen to investigate its dynamics (HP23 Xan0Nal23). The TTET labels were inserted at the two termini, Xan at the N-terminus and Nal in position 23 replacing the Trp in the WT sequence. Methionine 12 was replaced by norleucine, as it quenches the triplet state and for synthesis reasons an additional Gly-Ser motif was added at the C-terminus. Hence the sequence is Xan-LSDEDFKAVFGNleTRSAFANLPLNalGS-NH_2 (Fig. 4.25).

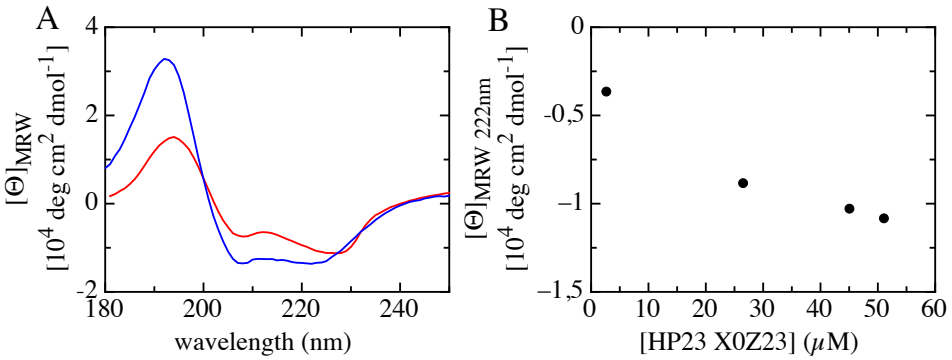

Figure 4.38: A) Far-UV CD spectra of HP23 Xan0Nal23 in the absence (red) and presence of 40% TFE (blue) in 10 mM potassium phosphate. B) Dependence of the Far-UV CD signal of the protein concentration in 10 mM potassium phosphate.

The far-UV CD spectrum shows a positive band at 194 nm and negative bands at 208 and 227 nm (Fig. 4.38 A). These bands are slightly shifted from what is expected for normal α-helical structures. The minimum at 227 nm is deeper than the one at 208 nm indicating additional contributions from the labels to this band. Nonetheless the HP23 Xan0Nal23 is helical. In the presence of 40% trifluoroethanol (TFE) the shape

of the CD spectrum changes and the maxima and minima are as expected for α-helices at 192 nm, 208 nm and 222 nm. However, in the absence of TFE the helix content is strongly dependent on the protein concentration and at low concentration HP23 Xan0Nal23 has very little helical structure (Fig. 4.38 B). This points to association of HP23 Xan0Nal23 into oligomers in which the helical structure is stabilized. If it is assumed that the HP23 Xan0Nal23 variant can oligomerize and the TTET labels get into close proximity, this also explains the distortion of the spectrum. In the presence of TFE the helical structure is stabilized and HP23 Xan0Nal23 remains monomeric.

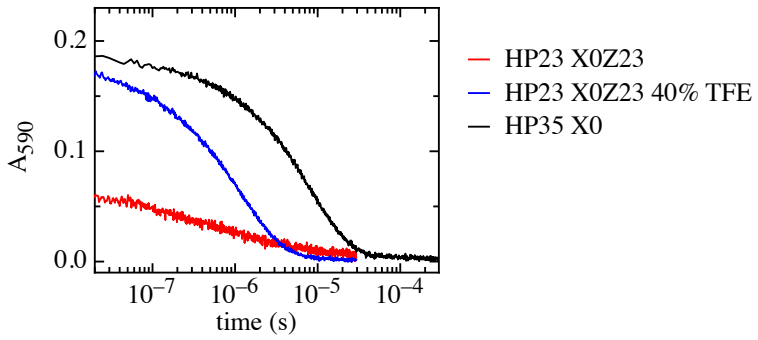

Figure 4.39: TTET kinetics of HP23 Xan0Z2 and the donor only reference HP35 Xan0 (Data taken from[53]). Transient absorbance decay was measured at 590 nm.

The results from CD spectroscopy are confirmed by the TTET measurements. In buffer the HP23 Xan0Nal23 variant shows a very small signal of the TTET traces with only 25 % of the donor only amplitude (Fig. 4.39). As donor only reference serves the full length variant HP35 Xan0 with $4.8{\cdot}10{-}6\ s^{-1}$ half-life and hence no quenching of the xanthone triplet state is visible. One explanation of the amplitude loss is that HP23 Xan0Nal23 oligomerizes in a conformation that brings the TTET labels in close proximity. In this case the triplet transfer occurs within the dead-time of the instrument. In the presence of TFE the amplitude is regained and TTET kinetics look as expected. This is in agreement with the data from CD measurements, that also indicate that TFE is able to stabilize HP23 Xan0Nal23 in a monomeric from.

The data for this variant shows that the TTET labelled fragment containing only helix 1 and 2 is not stably folded in isolation in a monomeric from and further characterization of this variant would not give further insight into the folding mechanism of HP35.

4.4.6 Discussion on the dynamics in HP35 variants

Different variants of the C-terminal domain of villin headpiece HP35 have been characterized by TTET. Previous results showed a equilibrium between two alternative states N and N′ on the native side of the major unfolding barrier[53]. These show different kinetics in the variant HP35 Nal23Xan35 which has the TTET labels located around helix 3 so this helix has to partially unfold to allow loop formation and consequent energy transfer. Prior to global unfolding the structure unlocks to the N′ state. The unlocked state N′ is characterized by weakened interaction but a higher structural flexibility[53].

The coupling of TTET to the unlocking/relocking equilibrium can be described by a three-state system (Fig. 4.26). It was possible to quantify the unlocking and the relocking rate constants as well as the rate constant for unfolding of helix3/TTET by the fitting the three-state model to TTET kinetics of HP35 Nal23Xan35 to k_{-l}=1.7 · 10^6 s^{-1}, k_l=1.6 · 10^6 s^{-1} and k_T=3.7 · 10^6 s^{-1} (Tab. 4.5). All three rate constants are in the same order of magnitude which gives a equilibrium constant $K_{eq} = k_{-l}/k_l$ close to 1, meaning that N and N′ are equally populated. To test for salt effects a urea and a $NaCl$ dependence has been recorded and showed only minor contributions of the salt on the unlocking /relocking dynamics in HP35 Nal23Xan35. In addition, the GdmCl dependence of the TTET kinetics in the presence of 0.5 M Na_2SO_4 could by evaluated with the three-state model (Tab. 4.5). The rate constants for unlocking and relocking do not change significantly compared to the values in the absence of Na_2SO_4. The rate constant for unfolding of helix3/TTET is reduced which might be due to a deceleration of the partial unfolding or undocking of helix 3 in Na_2SO_4 as this stabilizes compact structures,.

The leucine 28 is located in helix 3 and the side chain takes part in the hydrophobic core. In HP35 L28A Nal23Xan35 is was substituted with alanine. The unfolding transitions recorded by CD spectroscopy confirmed that the leucine 28 contributes to the stability as replacement with alanine leads to a global destabilization by 5 kJ/mol. Due to the presence of a significant amount of unfolded protein in the absence of denaturant reliable values for the microscopic rate constants could only be obtained in the presence of Na_2SO_4. Compared to HP35 Nal23Xan35 all rate constants are slowed down but mainly the relocking rate constant is affected (Tab. 4.5). This results in a higher equilibrium constant of 1.6. The L28A mutation slows

down relocking to N and therefore the equilibrium is shifted to the unlocked state N′. In addition, the rate constant for unfolding of helix3/TTET is reduced which might be due to a increased stability of helix 3 as alanine has a higher helix propensity than leucine.

HP35 variant	solvent additive	λ_1	λ_2	k_{-l}	k_l	k_T	K_{eq}
HP35 Nal23Xan35	-	1.1	5.9	1.7	1.6	3.7	1.1
	0.5 M Na_2SO_4	0.9	4.7	1.6	1.7	3.2	0.9
HP35 L28A Nal23Xan35	-	1.3	12.2	(1.6)	(2.4)	(9.5)	(0.7)
	0.5 M Na_2SO_4	0.9	3.9	1.2	0.8	2.8	1.6

Table 4.5: Apparent and microscopic rate constants and the equilibrium constant K_{eq} = N′/N = k_{-l}/k_l of HP35 variants in 10 mM potassium phosphate, pH 7, in the presence and absence of Na_2SO_4. All rate constants are given in 10^6 s^{-1}. The values HP35 L28A Nal23Xan35 in the absence of Na_2SO_4 were calculated with extrapolated rate constants and the sum of the amplitudes of λ_1 and λ_2 normalized to 1.

In the variant HP35 Xan0Nal12 I examined if a partial unfolding intermediate after global unlocking of N to N′ can also be formed by unfolding of helix 1. CD measurements revealed that it is folded even though with a low stability. The ^{1}H NMR spectrum was disturbed compared to the spectrum of the WT or HP35 N23Xan35 and pointed to a not completely folded structure in HP35 Xan0Nal12. Although the labels should be separated based on the NMR and X-ray structures in the native state TTET experiments show that they are in close contact and the triplet state is quenched.

Further I tested wether a part of the HP35 folds in independently and therefore even a smaller folding unit would be accessible as suggested by Tang *et al.*[158,160]. The TTET labelled fragment HP23 Xan0Nal23 containing only helix 1 and 2 was not stably folded as a monomer as CD and TTET measurements revealed but could be stabilized by addition of TFE.

5 Summary

Dynamics in proteins do not only govern the folding reaction but are also involved in function and regulation of proteins. To get further insight into protein dynamics I characterized two small model systems, isolated α-helices and the small protein domains HP35, in which it is possible to address individual questions.

Folding and unfolding dynamics of alanine-based helical peptides

Ala-based helical peptides are widely used to examine α-helix stability and dynamics in the absence of long range interactions and tertiary structure[96]. In a previous study local folding and unfolding rate constants were determined with triplet-triplet energy transfer (TTET)[90]. The TTET donor xanthone and the acceptor naphthalene were inserted with i,i+6 spacing into helical peptides. Energy transfer via van der Waals contact only occurs upon partial unfolding between the labels and was be monitored by the absorbance change at 590 nm[28,29]. Previous results revealed a position independent helix formation rate constant whereas helix unfolding is faster in the peptide center compared to the termini, yielding a higher local stability in the center. The experimental results were reproduced by Monte Carlo simulations using a kinetic linear Ising model, which showed that the dynamics of helix formation and opening are governed by a diffusion of boundary mechanism where the helix-coil boundary moves along the polypeptide chain[90].

Here the effect of helix length of the rate constants of helix formation and unfolding was investigated to test this mechanism. The model predicts a length-independent folding rate constant and a length-dependent unfolding rate constant in the peptide center as well as unaffected rate constants in the terminal regions. TTET measurements of Ala-based helical peptides between 16 and 41 amino acids length with the labels in the center and at the N-terminus confirmed these predictions. The length dependence was also simulated with the kinetic linear Ising model and could quantitatively reproduce the experimental data. The boundary diffusion in helical peptides

can be described by a classical Einstein-type, one-dimensional diffusion process with a diffusion coefficient, D, of $2.7 \cdot 10^7$ (amino acids)^2/s and $6.1 \cdot 10^{-9}$ cm^2/s for the helix-coil boundary. Additional contributions from coil nucleation accelerates the unfolding rate constant in long helical peptides above 40 amino acids, which is observed both in experiment and simulations.

The end-capping of α-helices influences helix stability and helix-coil dynamics to a great extent [116]. To investigate this effect, TTET kinetics were measured in centrally labelled Ala-based helical peptides with different N- and C-terminal caps. The folding and unfolding rate constants were evaluated with the Leffler relationship (Φ_f-value analysis) and yield a Φ_f-value of 0.03±0.16 and the corresponding Φ_u-value of 0.97±0.08. The linear Ising model reproduced the Φ_f-value of 0.03 showing that boundary diffusion is slowed down by stabilizing capping motifs, whereas refolding is not affected.

Local effects of stabilizing caps were investigated in helical peptides with the TTET labels at the N-terminus. The Φ-value analysis yielded a Φ_f of 0.35±0.11, showing that helix formation as well as unfolding are affected. Likewise, the dynamics in the helix center were investigated with amino acid replacements between the labels in a host/guest study. Similar to the local effect of caps, a Φ_f-value of 0.33±0.13 is observed for amino acid replacements with linear side chains between the labels in the central region of the peptide. If branched amino acids are incorporated into the central region between the labels both the folding and the unfolding rate constant decrease compared to the Leffler plot for linear side chains. Thus the branched amino acids interfere with helix formation as well as unfolding. Φ_f-values of about 0.3 agree well with Φ-values that are commonly found in small, single-domain proteins [183,186].

To gain additional information on the ground and transitions states of the helix-coil transition the effect of pressure was measured in alanine-based helical peptides. Most proteins unfold under increasing pressure as the native state has a larger volume than the unfolded state. This volume change is the result of opposing contributions from solvent and packing effects during the folding process. In isolated α-helices all side chains remain solvent accessible and no void volumes are formed. Thus it is possible to separate the contribution from secondary structure formation. We measured TTET kinetics in a centrally labelled 21 amino acid Ala-based helical peptide between 0.1 to 390 MPa. The measurements revealed increased helicity with increasing pressure. Comparison of the experimental results with Monte-Carlo simulations based on the

kinetic linear Ising model yielded a negative reaction volume ΔV^0 of -0.23 cm^3/mol (-0.38 $Å^3$/molecule) for the addition of a single helical residue. Residual helical structure has been detected in in the pressure unfolded state of several proteins[194,207–209]. These observations can be explained by the increase in helix stability with increasing pressure. Thus increasing pressure destabilizes the native tertiary structure but locally stabilizes helical structure. Large activation volumes for addition and removal of a single helical residue of 2.2 cm^3/mol (3.7 $Å^3$/molecule) and 2.4 cm^3/mol (4.0 $Å^3$/molecule), respectively, show that the transition state has a larger volume than either the helical or the coil state. The main difference between the helical and the coil state are intramolecular i,i+4 hydrogen bonds in contrast to intermolecular backbone to solvent hydrogen bonds. The small reaction volumes shows that both have similar volumes but the opening of a hydrogen bond in the transition state significantly increases the volume.

Dynamics in the villin headpiece subdomain

The villin headpiece subdomain HP35 is a stably folded[152] with folding/unfolding kinetics in the µs time range as determined in T-Jump experiments and MD simulations[153,154,157]. It thus represents a good model system to study fast folding processes. Previously, different variants of HP35 were studied by TTET[53]. Two alternative native states, the locked state N and the unlocked state N′, were found on the native side of the major unfolding barrier. Mechanistic insight into the dynamics of these two states was gained in the HP35 Nal23Xan35 variant with the TTET labels spanning helix 3. The unlocking reaction to N′ involves a positive change in ΔH as well as ΔS which reveals that the unlocking weakens the interactions but facilitates more structural flexibility. From the unlocked state helix 3 can partially unfold to a high energy intermediate[53].

The data showed that N′ has increased flexibility and a dry core which are characteristic of the dry molten globule (DMG) predicted by Shaknovich and Finkelstein[45]. This DMG should have an increased volume compared to the native state. To test wether the unlocked state of HP35 represents a DMG, we determined the reaction volume, ΔV^0, and the activation volumes, $\Delta V^{0‡}$, of the N to N′ transition with high pressure TTET experiments on the HP35 Nal23Xan35 variant. Experiments between 0.1 MPa and 390 MPa revealed a small and negative reaction volume of

ΔV^0=-1.8 cm^3/mol (3.0 Å^3/molecule), which shows that the unlocked state has a slightly larger volume than the locked state. Thus N′ is a compact folded state, not the proposed DMG state. In contrast, the activation volumes were large and positive with $\Delta V_{-l}^{0\ddagger}$=6.8 cm^3/mol (11.3 Å^3/molecule) and $\Delta V_l^{0\ddagger}$=8.6±1.3 cm^3/mol (14.3 Å^3/molecule), pointing to a transitions state with a larger volume than either the locked state N or the unlocked state N′. This indicates that structural re-arrangements during the locking/unlocking transition leads to an expanded transition state, which shows the characteristics of a DMG state.

Furthermore, the properties of the N′ state were characterized under different solvent conditions and for serveral HP35 variants. To test for salt effects on the N/N′ equilibrium, the effect of urea and $NaCl$ on the TTET kinetics was investigated. The results did not show any significant effect on the dynamics or the equilibrium of the N to N′ transition. Addition of sodium sulfate is known to stabilize compact structures. However 0.5 M Na_2SO_4 has no effect on the unlocking and relocking rate constants of the N to N′ transition. Only the rate constant for unfolding of helix3/TTET is slowed down maybe due to a deceleration of the partial unfolding or undocking of helix 3 by Na_2SO_4.

To test the effect of amino acid replacement in the core of HP35 on the N to N′ transition a Leu28Ala variant was investigated. In the HP35 L28A Nal23Xan35 variant leucine 28 was replaced by alanine to reduce the hydrophobic interactions in the core and at the same time to stabilize helix 3. The L28A mutation leads to a global destabilization of HP35 by 5 kJ/mol. Therefore, the native state dynamics and the N/N′ equilibrium is characterized in presence of 0.5 M Na_2SO_4. The results show a decrease of all rate constants compared to HP35 Nal23Xan35 with the greatest effect on the relocking rate constant (Tab. 4.5). Thus in the L28A variant the relocking to N is slowed down with a ensuing shift of the equilibrium to the unlocked state N′. In addition, the rate constant for unfolding of helix3/TTET is reduced perhaps due to increased stability of helix 3.

We further investigated whether in the N′ state helix 1 can also unfold independently similar to helix 3. Therefore, a variant with the TTET labels in position 0 and 12 (HP35 Xan0Nal12) was synthesized. It was strongly destabilized with only little N formed and no meaningful results could be gained. Finally, we characterized an even smaller folding unit, consisting of the first 23 amino acids of HP35, which has been proposed to fold independently[158,160]. This fragment consists of helix 1 and

helix 2 and the TTET labels are placed at the termini in position 0 and 23. The results showed that HP23 Xan0Nal23 is not stably folded as a monomer but tends to aggregate into helical oligomers.

Acknowledgment

I am most grateful to Prof. Dr. Thomas Kiefhaber for his guidance and support throughout my thesis. His deep understanding of the underlying mechanisms and his patience in the data analysis taught me to look one level below the obvious. I am also thankful for the many chances to present my research. And I like to thank Prof. Dr. George Rose for valuable discussions.

Many thanks to Andreas Reiner, who got me very smoothly started on the project and answered uncountable questions. And I thank Andreas Reiner and Beat Fierz for discussions and very organized data I could go back to. I also want to thank Maren Büttner who performed most of the simulations in this thesis. I enjoyed our collaboration very much.

I like to thank all my current and former colleagues of the Kiefhaber lab, in particular Tobias Aumüller, Annett Bachmann, Susanne Halbritter, Michael Hösl, Kristine Steen Jensen, Peter Kämmerer, Richard Kil, Sabine Kullick, Natalie Merk, Christian Nyffenegger, Alexander Ogrodnik, Andreas Reiner, Tobias Schümmer, Lena Schwarzer, Ursula Seidel, Jeremy Sloan, Karin Stecher, Matthias Stecher, Traudl Wenger, Daniel Winter and Ursula Zinth for discussions, support and a good time working together. Thank you to my students Philipp Wortmann, Angela Ibler, Dominik Alterauge, Marcal Stangier, Yvonne Köhler and Haruko Miura, I enjoyed working together with during their internship.

I also want thank to Harald Wunder from the technical workshop, with whom I designed and constructed the adaptation of the high-pressure cell to the TTET setup. For synthesis on xanthonic acid I thank Joseph Wey.

In addition, I thank Tanja Peterlin-Neumaier, Annett Bachmann and Nikolaus Neumaier for proofreading parts of this thesis and I like to thank Prof. Dr. Sevil Weinkauf for guidance and support throughout my study.

And a very special thanks to my family and friends, especially to Nikolaus, for support, a sympathetic ear during my thesis and all the valuable time together. This dissertation is dedicated to my mum, who cordially supported me throughout my whole life.

List of Abbreviations

CD	circular dichroism
DBU	1,8-diazabicyclo[5.4.0]undec-7-en
DCM	dichlormethan
DHFR	dihydrofolate reductase
DIPEA	N,N-diisopropylethylamine
DMF	dimethylformamid
DMG	dry molten globule
DMSO	dimethylsulfoxid
Dpr	α, β-diaminopropionic acid
Fmoc	fluorenylmethoxycarbonyl
FRET	Förster resonance energy transfer
FTIR	Fourier transform infrared spectroscopy
GdmCl	guanidinium chloride
GS	poly-glycine-serine peptide
HATU	O-(7-azabenzotriazol-1-yl)-N,N,N′,N′-tetramethyluronium hexafluorophosphate
HBTU	O-(benzotriazol-1-yl)-N,N,N′,N′-tetramethyluronium hexafluorophosphate
HP35	villin headpiece subdomain
HPLC	high-performance liquid chromatography
I	intermediate
IR	infrared spectroscopy
MABA	4-(methylamino)benzoic acid
MALDI-TOF-MS	matrix-assisted laser desorption/ionization time of flight mass spectrometry
MD	molecular dynamics
MFPT	mean first passage times
N	native state
N′	unlocked native state
Nal	naphthalene

NMM	4-methylmorpholine
NMP	1-methyl-2-pyrrolidinone
NMR	nuclear magnetic resonance
PPII	polyproline II
PyBOP	benzotriazol-1-yloxy)tripyrrolidinophosphonium hexafluorophosphate
REFERs	rate equilibrium free energy relationships
SASA	solvent accessible surface area
TES	triethylsilan
TFA	trifluoroacetic acid
TMAO	trimethylamine N-oxide
TFE	2,2,2-trifluorethanol
T-jump	temperature jump
TTET	triplet-triplet energy transfer
U	unfolded state
WT	wild type

Bibliography

[1] Anfinsen, C. B. (1973) Principles that govern the folding of protein chains. *Science*, **181**, 223–230.

[2] Ramachandran, G. N., Ramakrishnan, C., and Sasisekharan, V. (1963) Stereochemistry of polypeptide chain configurations. *J. Mol. Biol.*, **7**, 95–99.

[3] Ramachandran, G. N. and Sasisekharan, V. (1968) Conformation of polypeptides and proteins. *Advan. Protein Chem.*, **23**, 283–437.

[4] Porter, L. L. and Rose, G. D. (2011) Redrawing the ramachandran plot after inclusion of hydrogen-bonding constraints. *Proc. Natl. Acad. Sci. USA*, **108**, 109–13.

[5] Fierz, B. and Kiefhaber, T. (2005) Dynamics of unfolded polypeptide chains. *Protein Folding Handbook (Buchner, J. and Kiefhaber, T. eds.)*, pp. 805–851.

[6] Tanford, C. (1968) Protein denaturation. *Advan. Prot. Chem.*, **23**, 121–282.

[7] Tanford, C. (1970) Protein denaturation. Part C. theoretical models for the mechanism of denaturation. *Adv. Prot. Chem.*, **24**, 1–95.

[8] Uversky, V. N. (2013) A decade and a half of protein intrinsic disorder: Biology still waits for physics. *Protein Sci.*, **22**, 693–724.

[9] Sánchez, I. and Kiefhaber, T. (2003) Hammond behavior versus ground state effects in protein folding: evidence for narrow free energy barriers and residual structure in unfolded states. *J. Mol. Biol.*, **327**, 867–884.

[10] Fleming, P. J. and Rose, G. D. (2005) Conformational properties of unfolded proteins. *Protein Folding Handbook (Buchner, J. and Kiefhaber, T. eds.)*, **2**, 710–736.

[11] Anderson, D., Becktel, W., and Dahlquist, F. (1990) pH-induced denaturation of proteins: a single salt bridge contributes 4-5 kcal/mol to the free energy of folding of T4 lysozyme. *Biochemistry*, **29**, 2403–2408.

[12] Vogel, D. and Jaenicke, R. (1976) Circular-dichroism and absorption spectroscopic studies on specific aromatic residues involved in the different modes of aggregation of tobacco-mosaic-virus protein. *Eur. J. Biochem.*, **61**, 423–431.

[13] Kauzmann, W. (1959) Some factors in the interpretation of protein denaturation. *Adv. Prot. Chem.*, **14**, 1–63.

[14] Baldwin, R. L. (2007) Energetics of protein folding. *J. Mol. Biol.*, **371**, 283–301.

[15] Wetlaufer, D. B. (1973) Nucleation, rapid folding, and globular intrachain regions in proteins. *Proc. Natl. Acad. Sci. USA*, **70**, 697–701.

[16] Rose, G. D. (1979) Hierarchic organization of domains in globular proteins. *J. Mol. Biol.*, **134**, 447–470.

[17] Karplus, M. and Weaver, D. L. (1976) Protein-folding dynamics. *Nature*, **260**, 404–406.

[18] Bachmann, A. and Kiefhaber, T. (2002) Test for cooperativity in the early kinetic intermediate in lysozyme folding. *Biophys. Chem.*, **96**, 141–151.

[19] Anson, M. L. and Mirsky, A. E. (1931) The reversibility of protein coagulation. *J. Phys. Chem.*, **35**, 185–193.

[20] Jackson, S. (1998) How do small single-domain proteins fold? *Folding and Design*, **3**, R81–R91.

[21] Kiefhaber, T., Sánchez, I., and Bachmann, A. (2005) Characterization of protein folding barriers with rate-equilibrium free-energy relationships. *Protein Folding Handbook (Buchner, J. and Kiefhaber, T. eds.)*, **1**, 411–453.

[22] Greene, R. F. J. and Pace, C. N. (1974) Urea and guanidine-hydrochloride denaturation of ribonuclease, lysozyme, alpha-chymotrypsin and beta-lactoglobulin. *J. Biol. Chem.*, **249**, 5388–5393.

[23] Bolen, D. W. and Rose, G. D. (2008) Structure and energetics of the hydrogen-bonded backbone in protein folding. *Annu Rev Biochem*, **77**, 339–362.

[24] Myers, J. K., Pace, C. N., and Scholtz, J. M. (1995) Denaturant m-values and heat capacity changes: relation to changes in accessible surface areas of protein unfolding. *Protein Sci.*, **4**, 2138–2148.

[25] Kubelka, J., Chiu, T. K., Davies, D. R., Eaton, W. A., and Hofrichter, J. (2006) Sub-microsecond protein folding. *J. Mol. Biol.*, **359**, 546–553.

[26] Jaenicke, R. (1987) Folding and association of proteins. *Progr. Biophys. Mol. Biol.*, **49**, 117–237.

[27] Kiefhaber, T., Quaas, R., Hahn, U., and Schmid, F. X. (1990) Folding of ribonuclease T1. 1. Existence of multiple unfolded states created by proline isomerization. *Biochemistry*, **29**, 3053–3061.

[28] Bieri, O., Wirz, J., Hellrung, B., Schutkowski, M., Drewello, M., and Kiefhaber, T. (1999) The speed limit for protein folding measured by triplet-triplet energy transfer. *Proc. Natl. Acad. Sci. USA*, **96**, 9597–9601.

[29] Krieger, F., Fierz, B., Bieri, O., Drewello, M., and Kiefhaber, T. (2003) Dynamics of unfolded polypeptide chains as model for the earliest steps in protein folding. *J. Mol. Biol.*, **332**, 265–274.

[30] Fierz, B. and Kiefhaber, T. (2007) End-to-end vs interior loop formation kinetics in unfolded polypeptide chains. *J. Am. Chem. Soc.*, **129**, 672–679.

[31] Jaenicke, R. (1999) Stability and folding of domain proteins. *Progr. Biophys. Mol. Biol.*, **71**, 155–241.

[32] Bachmann, A. and Kiefhaber, T. (2005) Kinetic mechanisms in protein folding. *Protein Folding Handbook (Buchner, J. and Kiefhaber, T. eds.)*, **1**, 379–410.

[33] Lang, K., Schmid, F., and Fischer, G. (1987) Catalysis of protein folding by prolyl isomerase. *Nature*, **329**, 268–270.

[34] Creighton, T. (1997) Protein folding coupled to disulphide bond formation. *Biol. Chem.*, **378**, 731–744.

[35] Eyring, H. (1935) The activated complex in chemical reactions. *J. Chem. Phys.*, **3**, 107–115.

[36] Leffler, J. (1953) Parameters for the description of transition states. *Science*, **117**, 340–341.

[37] Bachmann, A. and Kiefhaber, T. (2001) Apparent two-state tendamistat folding is a sequential process along a defined route. *J. Mol. Biol.*, **306**, 375–386.

[38] Sánchez, I. E. and Kiefhaber, T. (2003) Evidence for sequential barriers and obligatory intermediates in apparent two-state protein folding. *J. Mol. Biol.*, **325**, 367–376.

[39] Baldwin, R. and Rose, G. (1999) Is protein folding hierarchic? II. Folding intermediates and transition states. *Trends Biochem. Sci.*, **24**, 77–83.

[40] Kim, P. S. and Baldwin, R. L. (1990) Intermediates in the folding reactions of small proteins. *Annu. Rev. Biochem.*, **59**, 631–660.

[41] Griko, Y. V., Privalov, P. L., Venyaminov, S. Y., and Kutyshenko, V. P. (1988) Thermodynamic study of the apomyoglobin structure. *J. Mol. Biol.*, **202**, 127–138.

[42] Oliveberg, M. and Wolynes, P. G. (2005) The experimental survey of protein-folding energy landscapes. *Q Rev Biophys*, **38**, 245–288.

[43] Bryngelson, J. and Wolynes, P. (1989) Intermediates and barrier crossing in a random model (with applications to protein folding). *J. Phys. Chem.*, **93**, 6902–6915.

[44] Kim, P. and Baldwin, R. (1982) Specific intermediates in the folding reactions of small proteins and the mechanism of protein folding. *Annu. Rev. Biochem.*, **51**, 459–489.

[45] Shaknovich, E. and Finkelstein, A. (1989) Theory of cooperative transition in protein folding. I. Why denaturation of globular protein is a first-order phase transition. *Biopolymers*, **28**, 1667–1680.

[46] Shaknovich, E. and Finkelstein, A. (1989) Theory of cooperative transition in protein folding. II. Phase diagram for a protein molecule in solution. *Biopolymers*, **28**, 1681–1694.

[47] Baldwin, R. L., Frieden, C., and Rose, G. D. (2010) Dry molten globule intermediates and the mechanism of protein unfolding. *Proteins Struct. Funct. Bioinf.*, **78**, 2725–2737.

[48] Kiefhaber, T. and Baldwin, R. L. (1996) Hydrogen exchange and the unfolding pathway of ribonuclease A. *Biophys. Chem.*, **59**, 351–356.

[49] Kiefhaber, T., Labhardt, A., and Baldwin, R. (1995) Direct NMR evidence for an intermediate preceeding the rate-limiting step in the unfolding of ribonuclease A. *Nature*, **375**, 513–515.

[50] Kiefhaber, T. and Baldwin, R. L. (1995) Kinetics of hydrogen bond breakage in the process of unfolding of ribonuclease A measured by pulsed hydrogen exchange. *Proc. Natl. Acad. Sci. USA.*, **92**, 2657–2661.

[51] Hoeltzli, S. and Frieden, C. (1995) Stopped-flow NMR spectroscopy: Real-time unfolding studies of 6-19f-tryptophan-labeled escherichia coli dihydrofolate reductase. *Proc. Natl. Acad. Sci. USA*, **92**, 9318–9322.

[52] Jha, S. K. and Udgaonkar, J. B. (2009) Direct evidence for a dry molten globule intermediate during the unfolding of a small protein. *Proc. Natl. Acad. Sci. USA*, **106**, 12289–94.

[53] Reiner, A., Henklein, P., and Kiefhaber, T. (2010) An unlocking/relocking barrier in conformational fluctuations of villin headpiece subdomain. *Proc. Natl. Acad. Sci. USA*, **107**, 4955–4960.

[54] Kauzmann, W. (1987) Thermodynamics of unfolding. *Nature*, **325**, 763–764.

[55] Bridgman, P. W. (1914) The coagutation of albumen by pressure. *J. Biol. Chem.*, **19**, 511–512.

[56] Meersman, F., Smeller, L., and Heremans, K. (2006) Protein stability and dynamics in the pressure-temperature plane. *Biochim. Biophys. Acta*, **1764**, 346–354.

[57] Royer, C. A. (2002) Revisiting volume changes in pressure-induced protein unfolding. *Biochim. Biophys. Acta*, **1595**, 201–209.

[58] Silva, J. L., Foguel, D., and Royer, C. A. (2001) Pressure provides new insights into protein folding, dynamics and structure. *Trends Biochem Sci*, **26**, 612–618.

[59] Doster, W. and Friedrich, J. (2005) Pressure-temperature phase diagrams of protein. *Protein Folding Handbook (Buchner, J. and Kiefhaber, T. eds.)*, **1**, 99–126.

[60] Nash, D. P. and Jonas, J. (1997) Structure of pressure-assisted cold denatured lysozyme and comparison with lysozyme folding intermediates. *Biochemistry*, **36**, 14375–14383.

[61] Panick, G., Malessa, R., Winter, R., Rapp, G., Frye, K. J., and Royer, C. A. (1998) Structural characterization of the pressure-denatured state and unfolding/refolding kinetics of staphylococcal nuclease by synchrotron small-angle X-ray scattering and fourier-transform infrared spectroscopy. *J. Mol. Biol.*, **275**, 389–402.

[62] Herberhold, H., Marchal, S., Lange, R., Scheyhing, C. H., Vogel, R. F., and Winter, R. (2003) Characterization of the pressure-induced intermediate and unfolded state of red-shifted green fluorescent protein-a static and kinetic FTIR, UV/VIS and fluorescence spectroscopy study. *J. Mol. Biol.*, **330**, 1153–1164.

[63] Hawley, S. (1971) Reversible pressure-temperature denaturation of chymotrypsinogen. *Biochemistry*, **10**, 2436–2442.

[64] Smeller, L. (2002) Pressure-temperature phase diagrams of biomolecules. *Biochim. Biophys. Acta*, **1595**, 11–29.

[65] Roche, J., Caro, J. A., Norberto, D. R., Barthe, P., Roumestand, C., Schlessman, J. L., Garcia, A. E., García-Moreno, B. E., and Royer, C. A. (2012) Cavities determine the pressure unfolding of proteins. *Proc. Natl. Acad. Sci. USA*, **109**, 6945–6950.

[66] Gerstein, M. and Chothia, C. (1996) Packing at the protein-water interface. *Proc. Natl. Acad. Sci. USA*, **93**, 10167–10172.

[67] Grigera, J. R. and McCarthy, A. N. (2010) The behavior of the hydrophobic effect under pressure and protein denaturation. *Biophys. J.*, **98**, 1626–1631.

[68] Chalikian, T. V. and Macgregor, R. B., Jr (2009) Origins of pressure-induced protein transitions. *J. Mol. Biol.*, **394**, 834–842.

[69] Rasper, J. and Kauzmann, W. (1962) Volume changes in protein reactions. I. Ionization reactions of proteins. *J. Am. Chem. Soc.*, **84**, 1771–1777.

[70] Pappenberger, G., Saudan, C., Becker, M., Merbach, A., and Kiefhaber, T. (2000) Denaturant-induced movement of the transition state of protein folding revealed by high pressure stopped-flow measurements. *Proc. Natl. Acad. Sci. USA*, **97**, 17–22.

[71] Jacob, M., Holtermann, G., Perl, D., Reinstein, J., Schindler, T., Geeves, M. A., and Schmid, F. X. (1999) Microsecond folding of the cold shock protein measured by a pressure-jump technique. *Biochemistry*, **38**, 2882–2891.

[72] Jacob, M. H., Saudan, C., Holtermann, G., Martin, A., Perl, D., Merbach, A. E., and Schmid, F. X. (2002) Water contributes actively to the rapid crossing of a protein unfolding barrier. *J. Mol. Biol.*, **318**, 837–845.

[73] Vidugiris, G. J., Markley, J. L., and Royer, C. A. (1995) Evidence for a molten globule-like transition state in protein folding from determination of activation volumes. *Biochemistry*, **34**, 4909–4912.

[74] Rouget, J.-B., Aksel, T., Roche, J., Saldana, J.-L., Garcia, A. E., Barrick, D., and Royer, C. A. (2011) Size and sequence and the volume change of protein folding. *J. Am. Chem. Soc.*, **133**, 6020–6027.

[75] Krieger, F., Fierz, B., Axthelm, F., Joder, K., Meyer, D., and Kiefhaber, T. (2004) Intrachain diffusion in a protein loop fragment from carp parvalbumin. *Chem. Phys.*, **307**, 209–215.

[76] Satzger, H., Schmidt, B., Root, C., Zinth, W., Fierz, B., Krieger, F., Kiefhaber, T., and Gilch, P. (2004) Ultrafast quenching of the xanthone triplet by energy transfer: new insight into the intersystem crossing kinetics. *J. Phys. Chem. A*, **108**, 10072–10079.

[77] Heinz, B., Schmidt, B., Root, C., Satzger, H., Milota, F., Fierz, B., Kiefhaber, T., Zinth, W., and Gilch, P. (2006) On the unusual fluorescence properties of xanthone in water. *Phys. Chem. Chem. Phys.*, **8**, 3432 – 3439.

[78] Rauch, S. (2009) *Side chain effects on helix dynamic*. Master's thesis, Technical University Munich.

[79] Dexter, D. L. (1953) A theory of sensitized luminescence in solids. *J. Chem. Phys.*, **21**, 836–850.

[80] Closs, G., Johnson, M., Miller, J., and Piotrowiak, P. (1989) A connection between intramolecular long-range electron, hole and triplet energy transfer. *J. Am. Chem. Soc.*, **111**, 3751–3753.

[81] Wagner, P. and Klán, P. (1999) Intramolecular triplet energy transfer in flexible molecules: electronic, dynamic, and structural aspects. *J. Am. Chem. Soc.*, **121**, 9626–9635.

[82] Fierz, B., Satzger, H., Root, C., Gilch, P., Zinth, W., and Kiefhaber, T. (2007) Loop formation in unfolded polypeptide chains on the picoseconds to microseconds time scale. *Proc. Natl. Acad. Sci. USA*, **104**, 2163–2168.

[83] Möglich, A., Krieger, F., and Kiefhaber, T. (2005) Molecular basis for the effect of urea and guanidinium chloride on the dynamics of unfolded polypeptide chains. *J. Mol. Biol.*, **345**, 153–162.

[84] Krieger, F., Möglich, A., and Kiefhaber, T. (2005) Effect of proline and glycine residues on dynamics and barriers of loop formation in polypeptide chains. *J. Am. Chem. Soc.*, **127**, 3346–3352.

[85] Krieger, F. (2004) *Dynamics in Unfolded Polypeptide Chains as Model for Elementary Steps in Protein Folding*. Ph.D. thesis, Biozentrum, University of Basel, Switzerland.

[86] Munoz, V., Thompson, P. A., Hofrichter, J., and Eaton, W. A. (1997) Folding dynamics and mechanism of beta-hairpin formation. *Nature*, **390**, 196–199.

[87] Williams, S., Causgrove, T. P., Gilmanshin, R., Fang, K. S., Callender, R. H., Woodruff, W. H., and Dyer, R. B. (1996) Fast events in protein folding: helix melting and formation in a small peptide. *Biochemistry*, **35**, 691–697.

[88] Lednev, I. K., Karnoup, A. S., Sparrow, M. C., and Asher, S. A. (1999) Alpha-helix peptide folding and unfolding activation barriers: A nanosecond UV resonance raman study. *J. Am. Chem. Soc.*, **121**, 8074–8086.

[89] Thompson, P., Munoz, V., Gouri, S. J., Henry, E., Eaton, W. A., and Hofrichter, J. (2000) The helix-coil kinetics of a heteropeptide. *J. Phys. Chem. B*, **104**, 378–389.

[90] Fierz, B., Reiner, A., and Kiefhaber, T. (2009) Local conformational fluctuations in alpha-helices measured by fast triplet transfer. *Proc. Natl. Acad. Sci. USA*, **106**, 1057–1062.

[91] Pauling, L., Corey, R. B., and Branson, H. R. (1951) The structure of proteins: two hydrogen-bonded helical configurations of the polypeptide chain. *Proc. Natl. Acad. Sci. USA*, **37**, 205–211.

[92] Barlow, D. J. and Thornton, J. M. (1988) Helix geometry in proteins. *J. Mol. Biol.*, **201**, 601–619.

[93] Schellman, J. (1955) The stability of hydrogen-bonded peptide structures in aqueous solutions. *Compt. rend. Carlsberg Lab. (Ser. Chim.)*, **29**, 230–259.

[94] Doig, A. J., Errington, N., and Iqbalsyah, T. M. (2005) Stability and design of alpha-helices. *Protein Folding Handbook (Buchner, J. and Kiefhaber, T. eds.)*, **1**, 247–313.

[95] Bolin, K. A. and Millhauser, G. L. (1999) Alpha and 3-10: the split personality of polypeptide helices. *Acc. Chem. Res.*, **32**, 1027–1033.

[96] Marqusee, S. and Baldwin, R. L. (1987) Helix stabilization by Glu-...Lys+ salt bridges in short peptides of de novo design. *Proc. Natl. Acad. Sci. USA*, **84**, 8898–8902.

[97] Marqusee, S., Robbins, V. H., and Baldwin, R. L. (1989) Unusually stable helix formation in short alanine-based peptides. *Proc. Natl. Acad. Sci. USA*, **86**, 5286–5290.

[98] Chakrabartty, A., Schellman, J. A., and Baldwin, R. L. (1991) Large differences in the helix propensities of alanine and glycine. *Nature*, **351**, 586–588.

[99] Chakrabartty, A., Kortemme, T., and Baldwin, R. L. (1994) Helix propensities of the amino acids measured in alanine-based peptides without helix-stabilizing side-chain interactions. *Protein Sci.*, **3**, 843–852.

[100] Baldwin, R. L. (1995) Alpha-helix formation by peptides of defined sequence. *Biophys. Chem.*, **55**, 127–135.

[101] Doig, A. J., Chakrabartty, A., Klingler, T. M., and Baldwin, R. L. (1994) Determination of free energies of N-capping in alpha-helices by modification of the Lifson-Roig helix-coil therapy to include N- and C-capping. *Biochemistry*, **33**, 3396–3403.

[102] Scholtz, J. M., Barrick, D., York, E. J., Stewart, J. M., and Baldwin, R. L. (1995) Urea unfolding of peptide helices as a model for interpreting protein unfolding. *Proc. Natl. Acad. Sci. USA*, **92**, 185–189.

[103] Smith, J. S. and Scholtz, J. M. (1996) Guanidine hydrochloride unfolding of peptide helices: separation of denaturant and salt effects. *Biochemistry*, **35**, 7292–7297.

[104] Rohl, C. A., Chakrabartty, A., and Baldwin, R. L. (1996) Helix propagation and N-cap propensities of the amino acids measured in alanine-based peptides in 40 volume percent trifluoroethanol. *Protein Sci.*, **5**, 2623–2637.

[105] Nelson, J. and Kallenbach, N. (1986) Stabilization of the ribonuclease S-peptide alpha-helix by trifluorethanol. *Proteins*, **1**, 211–217.

[106] Jasanoff, A. and Fersht, A. R. (1994) Quantitative determination of helical propensities from trifluoroethanol titration curves. *Biochemistry*, **33**, 2129–2135.

[107] Vila, J. A., Ripoll, D. R., and Scheraga, H. A. (2000) Physical reasons for the unusual alpha-helix stabilization afforded by charged or neutral polar residues in alanine-rich peptides. *Proc. Natl. Acad. Sci. USA*, **97**, 13075–13079.

[108] Luo, P. and Baldwin, R. L. (1999) Interaction between water and polar groups of the helix backbone: an important determinant of helix propensities. *Proc. Natl. Acad. Sci. USA*, **96**, 4930–4935.

[109] Armstrong, K. M., Fairman, R., and Baldwin, R. L. (1993) The (i, i + 4) Phe-His interaction studied in an alanine-based alpha-helix. *J. Mol. Biol.*, **230**, 284–291.

[110] Shoemaker, K. R., Fairman, R., Schultz, D. A., Robertson, A. D., York, E. J., Stewart, J. M., and Baldwin, R. L. (1990) Side-chain interactions in the C-peptide helix: Phe 8 ... His 12+. *Biopolymers*, **29**, 1–11.

[111] Padmanabhan, S. and Baldwin, R. L. (1994) Helix-stabilizing interaction between tyrosine and leucine or valine when the spacing is i, i + 4. *J. Mol. Biol.*, **241**, 706–713.

[112] Padmanabhan, S. and Baldwin, R. (1995) Tests for helix-stabilizing interactions between various nonpolar side chains in alanine-based peptides. *Prot. Sci.*, **3**, 1992–1997.

[113] Huyghues-Despointes, B., Klingler, T., and Baldwin, R. (1995) Mesuring the strength of side-chain hydrogen bonds in peptide helices: the Gln-Asp (i, i+4) interaction. *Biochemistry*, **34**, 13267–13271.

[114] Stapley, B. J. and Doig, A. J. (1997) Hydrogen bonding interactions between glutamine and asparagine in alpha-helical peptides. *J. Mol. Biol.*, **272**, 465–473.

[115] Errington, N. and Doig, A. J. (2005) A phosphoserine-lysine salt bridge within an alpha-helical peptide, the strongest alpha-helix side-chain interaction measured to date. *Biochemistry*, **44**, 7553–7558.

[116] Doig, A. J. and Baldwin, R. L. (1995) N- and C-capping preferences for all 20 amino acids in alpha-helical peptides. *Protein Sci.*, **4**, 1325–1336.

[117] Harper, E. T. and Rose, G. D. (1993) Helix stop signals in proteins and peptides: the capping box. *Biochemistry*, **32**, 7605–7609.

[118] Schellman, C. (1980) The alphaL conformation at the ends of helices. *Protein Folding*, pp. 53–61.

[119] Aurora, R. and Rose, G. D. (1998) Helix capping. *Protein Sci.*, **7**, 21–38.

[120] Prieto, J. and Serrano, L. (1997) C-capping and helix stability: the pro C-capping motif. *J. Mol. Biol.*, **274**, 276–288.

[121] Chakrabartty, A., Doig, A. J., and Baldwin, R. L. (1993) Helix capping propensities in peptides parallel those in proteins. *Proc. Natl. Acad. Sci USA*, **90**, 11332–11336.

[122] Decatur, S. M. (2000) IR spectroscopy of isotope-labeled helical peptides: probing the effect of N-acetylation on helix stability. *Biopolymers*, **54**, 180–185.

[123] Shoemaker, K., Kim, Brems, Marqusee, York, Chaiken, Stewart, and Baldwin, R. L. (1985) Nature of the charged group effect on the stability of the C-peptide helix. *Proc. Natl. Acad. Sci. USA*, **82**, 2349–2353.

[124] Zimm, B. H. and Bragg, J. K. (1959) Theory of phase transition between helix and random coil in polypeptide chains. *J. Chem. Phys.*, **31**, 526–535.

[125] Lifson, S. and Roig, A. (1961) On the theory of helix-coil transition in polypeptides. *J. Chem. Phys.*, **34**, 1963–1974.

[126] Stapley, B. J., Rohl, C. A., and Doig, A. J. (1995) Addition of side chain interactions to modified Lifson-Roig helix-coil theory: application to energetics of phenylalanine-methionine interactions. *Protein Sci.*, **4**, 2383–2391.

[127] Munoz, V. and Serrano, L. (1994) Elucidating the folding problem of helical peptides using empirical parameters. *Nature Struct. Biol.*, **1**, 399–409.

[128] Munoz, V. and Serrano, L. (1997) Development of the multiple sequence approximation within the AGADIR model of alpha-helix formation: comparison of Zimm-Bragg and Lifson-Roig formalism. *Biopolymers*, **41**, 495–509.

[129] Qian, H. and Schellman, J. (1992) Helix-coil theories: A comparative study for finite length polypeptides. *J. Phys. Chem.*, **96**, 3978–3994.

[130] Gruenewald, B., Nicola, C., Lustig, A., Schwarz, G., and Klump, H. (1979) Kinetics of the helix-coil transition of a polypeptide with non-ionic side groups, derived from ultrasonic relaxation measurements. *Biophys. Chem.*, **9**, 137–147.

[131] Scholtz, J. M., Qian, H., York, E. J., Stewart, J. M., and Baldwin, R. L. (1991) Parameters of helix-coil transition theory for alanine-based peptides of varying chain lengths in water. *Biopolymers*, **31**, 1463–1470.

[132] Rohl, C. A., Scholtz, J. M., York, E. J., Stewart, J. M., and Baldwin, R. L. (1992) Kinetics of amide proton exchange in helical peptides of varying chain lengths. interpretation by the Lifson-Roig equation. *Biochemistry*, **31**, 1263–1269.

[133] Wang, T., Zhu, Y., Getahun, Z., Du, D., Huang, C.-Y., DeGrado, W. F., and Gai, F. (2004) Length dependent helix-coil transition kinetics of nine alanine-based peptides. *J. Phys. Chem. B*, **108**, 15301–15310.

[134] Ising, E. (1925) Beitrag zur Theorie des Ferromagnetismus. *Zeitschrift für Physik*, **31**, 253–258.

[135] Schwarz, G. (1965) On the kinetics of the helix-coil transition of polypeptides in solution. *J. Mol. Biol.*, **11**, 64–77.

[136] Schwarz, G. and Seelig, J. (1968) Kinetic properties and the electric field effect of the helix-coil transition of poly(gamma-benzyl l-glutamate) determined from dielectric relaxation measurements. *Biopolymers*, **6**, 1263–1277.

[137] Thompson, P. A., Eaton, W. A., and Hofrichter, J. (1997) Laser temperature jump study of the helix-coil kinetics of an alanine peptide interpreted with a 'kinetic zipper' model. *Biochemistry*, **36**, 9200–9210.

[138] Huang, C. Y., Klemke, J. W., Getahun, Z., DeGrado, W. F., and Gai, F. (2001) Temperature-dependent helix-coil transition of an alanine based peptide. *J. Am. Chem. Soc.*, **123**, 9235–9238.

[139] Huang, C. Y., Getahun, Z., Zhu, Y., Klemke, J. W., DeGrado, W. F., and Gai, F. (2002) Helix formation via conformation diffusion search. *Proc. Natl. Acad. Sci. USA*, **99**, 2788–2793.

[140] Lapidus, L. J., Eaton, W. A., and Hofrichter, J. (2002) Measuring dynamic flexibility of the coil state of a helix-forming peptide. *J. Mol. Biol.*, **319**, 19–25.

[141] Takekiyo, T., Shimizu, A., Kato, M., and Taniguchi, Y. (2005) Pressure-tuning FT-IR spectroscopic study on the helix-coil transition of Ala-rich oligopeptide in aqueous solution. *Biochim. Biophys. Acta*, **1750**, 1–4.

[142] Imamura, H. and Kato, M. (2008) Effect of pressure on helix-coil transition of an alanine-based peptide: An FTIR study. *Proteins Struct. Funct. Bioinf.*, **75**, 911–918.

[143] Paschek, D., Gnanakaran, S., and Garcia, A. E. (2005) Simulations of the pressure and temperature unfolding of an alpha-helical peptide. *Proc. Natl. Acad. Sci. USA*, **102**, 6765–6770.

[144] Friederich, E., Vancompernolle, K., Louvard, D., and Vandekerckhove, J. (1999) Villin function in the organization of the actin cytoskeleton. correlation of in vivo effects to its biochemical activities in vitro. *J. Biol. Chem.*, **274**, 26751–26760.

[145] McKnight, C. J., Doering, D. S., Matsudaira, P. T., and Kim, P. S. (1996) A thermostable 35-residue subdomain within villin headpiece. *J. Mol. Biol.*, **260**, 126–134.

[146] McKnight, C., Doering, D., and Kim, P. (1997) NMR structure of the 35-residue villin headpiece subdomain. *Nat. Struct. Biol.*, **4**, 180–184.

[147] Chiu, T. K., Kubelka, J., Herbst-Irmer, R., Eaton, W. A., Hofrichter, J., and Davies, D. R. (2005) High-resolution X-ray crystal structures of the villin headpiece subdomain, an ultrafast folding protein. *Proc. Natl. Acad. Sci. USA*, **102**, 7517–7522.

[148] Frank, B. S., Vardar, D., Buckley, D. A., and McKnight, C. J. (2002) The role of aromatic residues in the hydrophobic core of the villin headpiece subdomain. *Protein Sci.*, **11**, 680–687.

[149] Xiao, S., Bi, Y., Shan, B., and Raleigh, D. P. (2009) Analysis of core packing in a cooperatively folded miniature protein: the ultrafast folding villin headpiece helical subdomain. *Biochemistry*, **48**, 4607–4616.

[150] Brown, J. W., Farelli, J. D., and McKnight, C. J. (2012) On the unyielding hydrophobic core of villin headpiece. *Protein Sci.*, **21**, 647–654.

[151] Vermeulen, W., Van Troys, M., Bourry, D., Dewitte, D., Rossenu, S., Goethals, M., Borremans, F. A. M., Vandekerckhove, J., Martins, J. C., and Ampe, C.

(2006) Identification of the PXW sequence as a structural gatekeeper of the headpiece C-terminal subdomain fold. *J. Mol. Biol.*, **359**, 1277–1292.

[152] Bi, Y., Cho, J.-H., Kim, E.-Y., Shan, B., Schindelin, H., and Raleigh, D. P. (2007) Rational design, structural and thermodynamic characterization of a hyperstable variant of the villin headpiece helical subdomain. *Biochemistry*, **46**, 7497–7505.

[153] Kubelka, J., Eaton, W., and Hofrichter, J. (2003) Experimental tests of villin subdomain folding simulations. *J. Mol. Biol.*, **329**, 625–630.

[154] Buscaglia, M., Kubelka, J., Eaton, W. A., and Hofrichter, J. (2005) Determination of ultrafast protein folding rates from loop formation dynamics. *J. Mol. Biol.*, **347**, 657–664.

[155] Brewer, S. H., Vu, D. M., Tang, Y., Li, Y., Franzen, S., Raleigh, D. P., and Dyer, R. B. (2005) Effect of modulating unfolded state structure on the folding kinetics of the villin headpiece subdomain. *Proc. Natl. Acad. Sci. USA*, **102**, 16662–16667.

[156] Wang, M., Tang, Y., Sato, S., Vugmeyster, L., McKnight, C., and Raleigh, D. (2003) Dynamic NMR line-shape analysis demonstrates that the villin headpiece subdomain folds on the microseconds time scale. *J. Am. Chem. Soc.*, **125**, 6032–6033.

[157] Zagrovic, B., Snow, C. D., Khaliq, S., Shirts, M. R., and Pande, V. S. (2002) Native-like mean structure in the unfolded ensemble of small proteins. *J. Mol. Biol.*, **323**, 153–164.

[158] Tang, Y., Goger, M. J., and Raleigh, D. P. (2006) NMR characterization of a peptide model provides evidence for significant structure in the unfolded state of the villin headpiece helical subdomain. *Biochemistry*, **45**, 6940–6946.

[159] Meng, W., Shan, B., Tang, Y., and Raleigh, D. P. (2009) Native like structure in the unfolded state of the villin headpiece helical subdomain, an ultrafast folding protein. *Protein Sci.*, **18**, 1692–1701.

[160] Tang, Y., Rigotti, D. J., Fairman, R., and Raleigh, D. P. (2004) Peptide models provide evidence for significant structure in the denatured state of a rapidly folding protein: the villin headpiece subdomain. *Biochemistry*, **43**, 3264–3272.

[161] Duan, Y. and Kollman, P. (1998) Pathways to a protein folding intermediate observed in a 1-microsecond simulations in aqueous solution. *Science*, **282**, 740–744.

[162] Lei, H., Wu, C., Liu, H., and Duan, Y. (2007) Folding free-energy landscape of villin headpiece subdomain from molecular dynamics simulations. *Proc. Natl. Acad. Sci. USA*, **104**, 4925–4930.

[163] Ensign, D. L., Kasson, P. M., and Pande, V. S. (2007) Heterogeneity even at the speed limit of folding: large-scale molecular dynamics study of a fast-folding variant of the villin headpiece. *J. Mol. Biol.*, **374**, 806–816.

[164] Beauchamp, K. A., Ensign, D. L., Das, R., and Pande, V. S. (2011) Quantitative comparison of villin headpiece subdomain simulations and triplet-triplet energy transfer experiments. *Proc. Natl. Acad. Sci. USA*, **108**, 12734–9.

[165] Chodera, J. D., Singhal, N., Pande, V. S., Dill, K. A., and Swope, W. C. (2007) Automatic discovery of metastable states for the construction of Markov models of macromolecular conformational dynamics. *J Chem Phys*, **126**, 155101.

[166] Serrano, A. L., Bilsel, O., and Gai, F. (2012) Native state conformational heterogeneity of HP35 revealed by time-resolved FRET. *J. Phys. Chem. B*, **116**, 10631–10638.

[167] Graham, R. and Lewis, J. (1978) Synthesis of 9-oxoxanthen-2-carboxylic acids. *J. Chem. Soc.*, pp. 876–881.

[168] Pace, C. (1986) Determination and analysis of urea and guanidine hydrochloride denaturation curves. *Meth. Enzymol.*, **131**, 266–280.

[169] Kiefhaber, T., Kohler, H. H., and Schmid, F. X. (1992) Kinetic coupling between protein folding and prolyl isomerization. I. theoretical models. *J. Mol. Biol.*, **224**, 217–229.

[170] Lagrias, J., Reeds, J., Wright, M., and Wright, P. (1998) Convergence properties of the nelder-mead simplex method in low dimensions. *SIAM Journal of Optimization*, **9**, 112–147.

[171] Neumaier, S., Reiner, A., Büttner, M., Fierz, B., and Kiefhaber, T. (2013) Testing the diffusing boundary model for the helix-coil transition in peptides. *Proc. Natl. Acad. Sci. USA*, **110**, 12905–12910.

[172] van Holde, K. E. (1971) Biophysical chemistry. *(Prentice-Hall, London)*.

[173] Granéli, A., Yeykal, C. C., Robertson, R. B., and Greene, E. C. (2006) Long-distance lateral diffusion of human Rad51 on double-stranded DNA. *Proc. Natl. Acad. Sci. USA*, **103**, 1221–1226.

[174] Wang, Y. M., Austin, R. H., and Cox, E. C. (2006) Single molecule measurements of repressor protein 1D diffusion on DNA. *Phys Rev Lett*, **97**, 48302.

[175] Blainey, P. C., Graziano, V., Pérez-Berná, A. J., McGrath, W. J., Flint, S. J., San Martín, C., Xie, X. S., and Mangel, W. F. (2013) Regulation of a viral proteinase by a peptide and DNA in one-dimensional space: IV. viral proteinase slides along DNA to locate and process its substrates. *J. Biol. Chem.*, **288**, 2092–2102.

[176] Presta, L. G. and Rose, G. D. (1988) Helix signals in proteins. *Science*, **240**, 1632–41.

[177] Richardson, J. S. and Richardson, D. C. (1988) Amino acid preferences for specific locations at the ends of alpha helices. *Science*, **240**, 1648–52.

[178] Hol, W. G. (1985) The role of the alpha-helix dipole in protein function and structure. *Prog Biophys Mol Biol*, **45**, 149–95.

[179] Shoemaker, K. R., Kim, P. S., York, E. J., Stewart, J. M., and Baldwin, R. L. (1987) Tests of the helix dipole model for stabilization of alpha-helices. *Nature*, **326**, 563–7.

[180] Sali, D., Bycroft, M., and Fersht, A. R. (1988) Stabilization of protein structure by interaction of alpha-helix dipole with a charged side chain. *Nature*, **335**, 740–743.

[181] Matouschek, A., Kellis, J. J., Serrano, L., and Fersht, A. R. (1989) Mapping the transition state and pathway of protein folding by protein engineering. *Nature*, **340**, 122–126.

[182] Northey, J., Maxwell, K., and Davidson, A. (2002) Protein folding kinetics beyond the phi value: using multiple amino acid substitutions to investigate the structure of the SH3 domain folding transition state. *J. Mol. Biol.*, **320**, 389–402.

[183] Sánchez, I. and Kiefhaber, T. (2003) Origin of unusual phi-values in protein folding: Evidence against specific nucleation sites. *J. Mol. Biol.*, **334**, 1077–1085.

[184] Scholtz, J. M. and Baldwin, R. L. (1992) The mechanism of alpha-helix formation by peptides. *Ann. Rev. Biophys. Biomol. Struct.*, **21**, 95–118.

[185] Lin, M. M., Mohammed, O. F., Jas, G. S., and Zewail, A. H. (2011) Speed limit of protein folding evidenced in secondary structure dynamics. *Proc. Natl. Acad. Soc. USA*, **108**, 16622–16627.

[186] Naganathan, A. and Munoz, V. (2010) Insights into protein folding mechanisms from large scale analysis of mutational effects. *Proc. Natl. Acad. Sci. USA*, **107**, 8611–8616.

[187] Gans, P. J., Lyu, P. C., Manning, M. C., Woody, R. W., and Kallenbach, N. R. (1991) The helix-coil transition in heterogeneous peptides with specific side-chain interactions: theory and comparison with CD spectral data. *Biopolymers*, **31**, 1605–1614.

[188] Neumaier, S., Büttner, M., Bachmann, A., and Kiefhaber, T. (2013) Transition state and ground state properties of the helix-coil transition in peptides deduced from high-pressure studies. *Proc. Natl. Acad. Sci. USA*, **110**, 20988–20993.

[189] Panick, G. and Winter, R. (2000) Pressure-induced unfolding/refolding of ribonuclease A: static and kinetic fourier transform infrared spectroscopy study. *Biochemistry*, **39**, 1862–1869.

[190] Brandts, J., Halvorson, H., and Brennan, M. (1975) Consideration of the possibility that the slow step in protein denaturation reactions is due to cis-trans isomerism of proline residues. *Biochemistry*, **14**, 4953–4963.

[191] Schmid, F. X. (1983) Mechanism of folding of ribonuclease A. Slow refolding is a sequential reaction via structural intermediates. *Biochemistry*, **22**, 4690–4696.

[192] Kiefhaber, T. and Schmid, F. X. (1992) Kinetic coupling between protein folding and prolyl isomerization. II. Folding of ribonuclease A and ribonuclease T1. *J. Mol. Biol.*, **224**, 231–240.

[193] Houry, W., Rothwarf, D., and Scheraga, H. (1995) The nature of the initial step in the conformational folding of disulfide intact ribonuclease A. *Nature struct. Biol.*, **2**, 495–503.

[194] Vajpai, N., Nisius, L., Wiktor, M., and Grzesiek, S. (2013) High-pressure NMR reveals close similarity between cold and alcohol protein denaturation in ubiquitin. *Proc. Natl. Acad. Sci. USA*, **110**, 368–376.

[195] Fierz, B., Joder, K., Krieger, F., and Kiefhaber, T. (2007) Using triplet-triplet energy transfer to measure conformational dynamics in polypeptide chains. *Methods Mol. Biol.*, **350**, 169–187.

[196] Rohl, C. A. and Baldwin, R. L. (1994) Exchange kinetics of individual amide protons in 15N-labeled helical peptides measured by isotope-edited NMR. *Biochemistry*, **33**, 7760–7767.

[197] Neumann, C. and Kauzmann, A., W.and Zipp (1973) Pressure-dependence of weak acid ionization in aqueous buffers. *J. Phys. Chem.*, **77**, 2687–2691.

[198] Chakrabartty, A., Kortemme, T., Padmanabhan, S., and Baldwin, R. L. (1993) Aromatic side-chain contribution to far-ultraviolet circular dichroism of helical

peptides and its effect on measurement of helix propensities. *Biochemistry*, **32**, 5560–5565.

[199] Scholtz, J. M., Marqusee, S., Baldwin, R. L., York, E. J., Stewart, J. M., Santoro, M., and Bolen, D. W. (1991) Calorimetric determination of the enthalpy change for the alpha-helix to coil transition of an alanine peptide in water. *Proc. Natl. Acad. Sci. USA*, **88**, 2854–2858.

[200] Christensen, R. G. and Cassel, J. M. (1967) Volume changes accompanying collagen denaturation. *Biopolymers*, **5**, 685–689.

[201] Luo, P. and Baldwin, R. L. (1997) Mechanism of helix induction by trifluoroethanol: a framework for extrapolating the helix-forming properties of peptides from trifluoroethanol/water mixtures back to water. *Biochemistry*, **36**, 8413–8421.

[202] Reiner, A., Wildemann, D., Fischer, G., and Kiefhaber, T. (2008) Effect of thioxopeptide bonds on alpha-helix structure and stability. *J. Am. Chem. Soc.*, **130**, 8079–8084.

[203] Bachmann, A., Wildemann, D., Praetorius, F., Fischer, G., and Kiefhaber, T. (2011) Mapping backbone and side-chain interactions in the transition state of a coupled protein folding and binding reaction. *Proc. Natl. Acad. Sci. USA*, **108**, 3952–3957.

[204] Tiffany, M. L. and Krimm, S. (1973) Extended conformations of polypeptides and proteins in urea and guanidine hydrochloride. *Biopolymers*, **12**, 575–587.

[205] Shi, Z., Olson, C. A., Rose, G. D., Baldwin, R. L., and Kallenbach, N. R. (2002) Polyproline II structure in a sequence of seven alanine residues. *Proc. Natl. Acad. Sci. USA*, **99**, 9190–9195.

[206] Roche, J., Dellarole, M., Caro, J. A., Guca, E., Norberto, D. R., Yang, Y., Garcia, A. E., Roumestand, C., García-Moreno, B., and Royer, C. A. (2012) Remodeling of the folding free energy landscape of staphylococcal nuclease by cavity-creating mutations. *Biochemistry*, **51**, 9535–9546.

[207] Rouget, J.-B., Schroer, M. A., Jeworrek, C., Pühse, M., Saldana, J.-L., Bessin, Y., Tolan, M., Barrick, D., Winter, R., and Royer, C. A. (2010) Unique features of the folding landscape of a repeat protein revealed by pressure perturbation. *Biophys. J.*, **98**, 2712–21.

[208] Narayanan, S. P., Maeno, A., Matsuo, H., Oda, M., Morii, H., and Akasaka, K. (2012) Extensively hydrated but folded: a novel state of globular proteins stabilized at high pressure and low temperature. *Biophys. J.*, **102**, L8–10.

[209] Prigozhin, M. B., Liu, Y., Wirth, A. J., Kapoor, S., Winter, R., Schulten, K., and Gruebele, M. (2013) Misplaced helix slows down ultrafast pressure-jump protein folding. *Proc. Natl. Acad. Sci. USA*, **110**, 8087–8092.

[210] Frauenfelder, H., Sligar, S. G., and Wolynes, P. G. (1991) The energy landscapes and motions of proteins. *Science*, **254**, 1598–603.

[211] Eisenmesser, E., Bosco, D., Akke, M., and Kern, D. (2002) Enzyme dynamics during catalysis. *Science*, **295**, 1520–1523.

[212] Eisenmesser, E. Z., Millet, O., Labeikovsky, W., Korzhnev, D. M., Wolf-Watz, M., Bosco, D. A., Skalicky, J. J., Kay, L. E., and Kern, D. (2005) Intrinsic dynamics of an enzyme underlies catalysis. *Nature*, **438**, 117–21.

[213] Hvidt, A. and Nielsen, S. (1966) Hydrogen exchange in proteins. *Advan. Prot. Chem.*, **21**, 287–386.

[214] Vugmeyster, L. and McKnight, C. J. (2008) Slow motions in chicken villin headpiece subdomain probed by cross-correlated NMR relaxation of amide NH bonds in successive residues. *Biophys J.*, **95**, 5941–5950.

[215] Kalbitzer, H. R., Görler, A., Li, H., Dubovskii, P. V., Hengstenberg, W., Kowolik, C., Yamada, H., and Akasaka, K. (2000) 15N and 1H NMR study of histidine containing protein (HPr) from staphylococcus carnosus at high pressure. *Protein Sci*, **9**, 693–703.